Fall 2014

Machinability improvement during high-speed end-milling of Inconel 718 alloy

Chukwujekwu Nnadi

Department:

MACHINABILITY IMPROVEMENT DURING HIGH-SPEED END-MILLING OF INCONEL 718 ALLOY

by

CHUKWUJEKWU IKWY NNADI

A THESIS

Presented to the Faculty of the Graduate School of the

MISSOURI UNIVERSITY OF SCIENCE AND TECHNOLOGY

In Partial Fulfillment of the Requirements for the Degree

MASTER OF SCIENCE IN MECHANICAL ENGINEERING

2014

Approved by

Anthony Okafor, Advisor

K. Chandrashekhara

V. Samaranayake

PUBLICATION THESIS OPTION

This thesis is presented in publication format and is divided into two separate papers. The first paper comprising pages 4 to 106 is to be submitted for publication in the International Journal for Advanced Machine tools and Manufacture, with the title, "Investigating the effects of machining parameters and cooling strategies on cutting force, tool wear and cutting temperature in high-speed end-milling of Inconel 718 alloy". The second Paper comprises pages 107 to 162 and is to be submitted for publication in the Journal of Materials Processing Technology, under the title, "Evaluation of the effects of machining parameters and cooling strategies on surface roughness and a comparative evaluation of cooling strategies on residual stresses in high-speed end-milling of Inconel 718 alloy"

ABSTRACT

This thesis presents the results of the experimental investigation of the effects of machining parameters (spindle speed and feedrate) and cooling strategies [Minimum Quantity Lubrication (MQL), Cryogenic Liquid Nitrogen (LN_2), and combined ($MQL+LN_2$)] on cutting force components, cutting temperature, tool wear and surface roughness during high-speed slot end-milling of Inconel 718 alloy. In addition, a comparative evaluation of the three cooling strategies was conducted for cutting force components, surface roughness and residual stresses. All end-milling experiments were conducted on a Cincinnati Milacron Vertical Machining center (VMC), using a 0.5 inch (12.7 mm) diameter, 0.03 inch (0.762 mm) corner radius four-flute uncoated carbide end-mill. A one-third fractional factorial design of experiments was constructed (nine experimental runs) and used in analyzing all experimental results. Cutting force components were acquired using a Kistler type 9272 4-component dynamometer, which was connected to an amplifier and a junction box. Cutting temperature was measured using a 0.125 inch (3.175 mm) diameter ungrounded k-type thermocouple, while tool wear was investigated indirectly by analyzing the maximum cutting force components of the last two passes (19 and 20). Surface roughness and residual stresses were measured using a profilometer and X-ray diffraction respectively. The results showed that high spindle speed (750 rpm) and medium feed rate (2 ipm) gave the lowest cutting force components, while low spindle speed (250 rpm) gave the lowest cutting temperature and tool wear. Furthermore, a low spindle speed (250 rpm) and feed rate (1 ipm) gave the least surface roughness, while MQL cooling strategy induced the highest compressive stresses.

ACKNOWLEDGMENT

I want to express my profound gratitude to my advisor, Professor A. C. Okafor for his guidance, financial and moral support throughout this research. I want to thank him for the Graduate Research Assistantship support from his National Science Foundation (NSF) grant without which it would have been impossible to bring this work to a completion. I also gratefully acknowledge the financial assistance provided by the Department of Mechanical and Aerospace Engineering in the form of Graduate Teaching Assistantship.

I would also like to thank Dr. K. Chandrashekhara and Dr. V. Samaranayake for serving as my committee members, and for finding time to review my thesis. I am also grateful to my colleague Mahmood Shaman Ameen for our collaboration and cooperation at various stages of this research. Furthermore, I want to thank the workshop staff especially Mitch Contrell and Randal Lewis for the help they rendered in various capacities.

Lastly, I would love to thank my immediate family, my parents Sir, Engr C. O. Nnadi (KSJ) and Lady Nkeiruka Nnadi (KSJ), my siblings Ejiofor Chukwuzoba Nnadi and Njideka Chinasa Nnadi. Without their unflinching moral support and prayers, I wouldn't have completed this work.

TABLE OF CONTENTS

LIST OF ILLUSTRATIONS

PAPER 2

LIST OF TABLES

1. INTRODUCTION

Nickel alloy (Inconel 718) is widely used in the aerospace, petroleum, automotive, and medical industries. It is predominantly made up of nickel, chromium, and molybdenum. Common applications of this alloy include: gas turbine blades, space craft, nuclear reactors, pumps, pressure vessels, and heat exchanger tubing etc. It is mainly used in harsh environments such as those subject to excessive corrosion, high temperatures and pressures. Nickel alloys and a host of other alloys like Ti-6Al-4V, Hastelloy are classified as difficult-to-cut metals. They are highly desired in such harsh conditions because of an excellent combination of peculiar properties like: high capacity to resist fracture, high resistance to corrosion, and high strength-to-weight ratio etc. However, they are characterized as "difficult-to-cut" because of the inherent problems they pose during machining. Some of these problems include: low thermal conductivity, work hardening tendencies, high chemical affinity with cutting tools, formation of burrs and built up edges (BUE), high cutting temperatures and high cutting forces. Inconel 718 alloy has a uniquely low thermal conductivity and as such, the enormous amount of heat generated during its machining is not removed as fast as it is generated. In other words, much of the heat generated during machining remains in the cutting zone, and is mostly concentrated on the cutting flutes of the tool. The extreme heat generated adversely affects the tool by causing severe wear. The presence of hard carbide in Inconel 718 also makes the tool susceptible to abrasion wear during machining. Inconel 718 alloy also displays a high reactivity with cutting tool materials, because the high temperatures generated during machining causes some particles from the workpiece material to be welded on the cutting edges of the tool, which invariably leads to more wear of the tool.

Massive tool wear leads to an increase in cutting forces. As temperature continues to rise and more tool wear is induced, the tool will reach a point of complete plastic deformation, which may lead to breakage. As a result, sufficient cooling and lubrication is needed to reduce the enormous amount of heat generated in the cutting zone, as well as reducing the coefficient of friction. Furthermore, appropriate machining parameters must be chosen in order to increase the feasibility of working with difficult-to-cut metals like Inconel 718.

The first paper presents the results of the investigations of the effects of machining parameters (speeds and feeds) and cooling strategies: [Minimum Quantity Lubrication (MQL), Cryogenic Liquid Nitrogen (LN_2) and a combination of Minimum Quantity Lubrication and Cryogenic Liquid Nitrogen ($MQL+LN_2$)] on cutting force components, tool wear, and cutting temperature in high-speed end-milling of Inconel 718 alloy. Cutting force components were acquired using a Kistler type 9272 4-component dynamometer. The dynamometer was connected to an amplifier to help boost the acquired voltage signals. Furthermore, the amplifier was connected to a junction box to help separate the cutting force acquired into three cutting force components F_X, F_Y, and F_Z. The maximum cutting force for each cutting force component was obtained and plotted. Cutting temperature was measured by inserting a 0.125 inch (3.175 mm) diameter ungrounded k-type thermocouple into the center of the slot, while tool wear was investigated indirectly by analyzing the maximum cutting force components of the last two passes (19 and 20). An increase in tool wear leads to a corresponding increase in cutting force components. Therefore, analysis of cutting force components at final machining lengths can give a measure of how much the tool has worn. A one-third

fractional factorial design of experiments was constructed and used in analyzing the experimental results. Various combinations of speeds, feeds and cooling strategies were combined according to the treatment combinations derived from the one-third fractional factorial design of experiments, and its effect on cutting force components, cutting temperature, and tool wear was studies.

The second paper presents the evaluation of the effects of machining parameters (speeds and feeds) and cooling strategies (MQL, LN_2, MQL+LN_2) on surface roughness, and a comparative evaluation of three cooling strategies on residual stresses in high-speed end-milling of Inconel 718 alloy. Surface roughness was measured using a pocket surf profilometer having a piezoelectric probe, while residual stresses were measured using the X-ray diffraction technique. The effects of machining parameters and cooling strategies on surface roughness were investigated by constructing a one-third fractional factorial design of experiments. Furthermore, a comparative investigation of the 3 cooling strategies was conducted for surface roughness and residual stresses.

PAPER

I. INVESTIGATING THE EFFECTS OF MACHINING PARAMETERS AND COOLING STRATEGIES ON CUTTING FORCES, TOOL WEAR, AND CUTTING TEMPERATURE IN HIGH-SPEED SLOT END-MILLING OF INCONEL 718

A. Chukwujekwu Okafor*, Chukwujekwu Nnadi
Computer Numerical Control and Virtual Manufacturing Laboratory
Department of Mechanical and Aerospace Engineering
Missouri University of Science and Technology
327 Toomey Hall, Rolla, MO-65409-0050, USA
Email:okafor@mst.edu

*Corresponding Author: Tel: 1-(573) 341-4695, Fax: 1-(573) 341-6899

ABSTRACT

This paper presents the results of experimental investigation of the effects of machining parameters (spindle speed and feed rate) and cooling strategies: Minimum Quantity Lubrication (MQL), cryogenic Liquid Nitrogen (LN_2), and a combination of Minimum Quantity Lubrication and cryogenic Liquid Nitrogen (MQL+LN_2) on cutting force components (F_x, F_y, and F_z), tool wear, and cutting temperature during high-speed slot end-milling of Inconel 718 alloy. A one-third fractional factorial design of experiment having three factors at three levels was generated and used in conducting and analyzing the experimental results. All machining experiments were conducted on a Cincinnati Milacron Vertical Machining center (VMC), with acramatic 2100 controller, using a four-flute, 0.5 inch (12.7 mm) diameter, 0.03 inch (0.762 mm) corner radius uncoated solid carbide bull-nosed helical end-mill. A kistler 9272 four-component

dynamometer was used to acquire cutting force components, while an ungrounded K-type thermocouple probe having a diameter of 0.125 inches (3.175 mm) was used in measuring temperature at the cutting zone. Tool wear was measured indirectly by comparing the maximum cutting force variation from the 1^{st} pass to the 20^{th} pass. Results obtained from Analysis of Variance (ANOVA) show that MQL cooling strategy, high spindle speed of 750 rpm (30 m/min), and medium feed rate of 2 ipm (50.8 mm/min) gave the lowest cutting force components. A comparative evaluation of the 3 cooling strategies at recommended optimum machining parameters of 750 rpm (30 m/min) and 1 ipm (25.4 mm/min) shows that combined (MQL+LN_2) cooling strategy reduced the resultant cutting force by 11.81% and 21% compared with LN_2 and MQL respectively for initial machining length of 76.2 mm, while MQL reduced resultant force by 73.6% compared to combined (MQL+LN_2) at final cutting length. Furthermore, it was observed that the use of cryogenic cooling strategy (LN_2) at -15 ˚C, low spindle speed of 250 rpm (10 m/min), and a high feed rate of 3 ipm (76.2 mm/min) gave the lowest cutting temperature. Also, the cutting force in the feed direction (F_y) and axial direction (F_z) increased more rapidly compared to F_x during severe tool wear and up to the point of complete plastic deformation. Therefore, both can be used for indirect monitoring of tool wear. The use of combined (MQL+LN_2) cooling strategy, low spindle speed of 250 rpm (10 m/min), and low feed rate of 1 ipm (25.4 mm/min) resulted in the lowest tool wear. Lastly, a comparative evaluation of the 3 cooling strategies showed that combined (MQL+ LN_2) gave the least cutting force during moderate tool wear, while MQL gave the lowest cutting force during extreme tool wear. LN_2 cooling strategy consistently gave the highest cutting force for all machining lengths. The results show that the use of

combined (MQL+LN_2) and MQL cooling strategy increase tool life by 25 % compared to LN_2 cooling strategy.

Key words: High-Speed end-milling, Inconel-718, Cryogenic Machining, Minimum Quantity Lubrication, cutting force components, tool wear.

1. INTRODUCTION

Nickel alloy (Inconel 718) is widely used in the aerospace, petroleum, automotive, and biomedical industries. It is predominantly made up of nickel, chromium, and molybdenum. Common applications of this alloy include: gas turbine blades, space craft, nuclear reactors, pumps, pressure vessels, and heat exchanger tubing etc. It is mainly used in harsh environments such as those subject to excessive corrosion, high temperatures and pressures. Nickel alloys and a host of other alloys like Ti-6Al-4V, Hastelloy are classified as difficult-to-cut metals. They are highly desired in such harsh conditions because of their excellent combination of peculiar properties like: high capacity to resist fracture, high resistance to corrosion, and high strength-to-weight ratio. However, they are characterized as "difficult-to-cut" because of the inherent problems they pose during machining. Some of these problems include: low thermal conductivity, work hardening tendencies, high chemical affinity with cutting tools, formation of burrs and built up edges (BUE), high cutting temperatures and high cutting forces. Inconel 718 alloy has a uniquely low thermal conductivity and as such, the enormous amount of heat generated during its machining is not removed as fast as it is generated. In other words, much of the heat generated during machining remains in the cutting zone, and is mostly concentrated on the cutting edges of the tool. The extreme heat generated adversely affects the tool by causing severe wear. The presence of hard carbide particles in Inconel 718 also makes the tool susceptible to abrasion wear during machining. Inconel 718 alloy also displays a high reactivity with cutting tool materials, because the high temperatures generated during machining causes some particles from the workpiece material to be

welded on the cutting edges of the tool, which eventually breaks off causing more wear of the tool. Massive tool wear leads to an increase in cutting forces. As temperature continues to rise and more tool wear is induced, the tool will reach a point of complete plastic deformation, which may lead to tool breakage.

Therefore, in order to circumvent these inherent problems, a number of factors must be considered when machining Inconel 718 alloy. Care must be taken that appropriate machining parameters (speeds, feeds, and depths of cut) suitable for the machining of this alloy are chosen before machining. Also, appropriate tools made from materials with high melting point, which can withstand the heat generated during machining of Inconel 718 must be used. It is pertinent that a cutting tool with good combination of tool geometry, tool material, and coatings is used. Cutting tools required for Inconel 718 must have excellent wear resistance, high hot hardness, good thermal shock resistance, high strength and toughness, and good chemical stability [1]. Common types of tool materials used in machining Inconel 718 include: carbide (coated and uncoated), ceramic, and cobalt high speed steel tools. Chipping is a major failure mode in the machining of difficult-to-cut metals with carbide tools, and is a result of high temperature, thermal, cyclical and mechanical stresses, as well as adhesion of the work material onto the tool faces [2]. The resulting high cutting temperatures strongly affect cutting forces, tool wear, tool life, chip formation mechanism and contribute to the thermal deformation of the cutting tool during machining of difficult-to-cut alloys [3]. As a result of these adverse effects of high cutting temperature generated at the cutting zone, it is imperative to employ efficient techniques that can reduce the coefficient of friction, and thus the high cutting temperatures generated during machining of Inconel 718. End-

milling operations are performed in many aerospace and automotive industries in the form of profile milling, face milling, slot milling etc. Contemporary industrial slot end-milling parameters for Inconel 718 using uncoated carbide tools are approximately 267 rpm and 1 ipm (25.4 mm/min) for speed and feed rate respectively. Therefore, spindle speed values above this range can be referred to as high-speed end-milling for Inconel 718. High-speed machining is used in many aerospace and automotive industries for the manufacture of thin-walled monolithic components. It has the potential to increase material removal rate, thereby reducing machining time and increasing productivity. Some published works regarding high-speed machining of various metals like aluminum and other difficult-to-cut alloys have reported it to be advantageous in terms of reducing cutting forces. High-speed milling of difficult-to-cut metals like Inconel 718 may have the potential of reducing cutting forces compared to using conventional machining speeds. Abele and Frohlich [4] presented a review of several researches that have been conducted on high-speed milling of titanium alloys. They concluded that high-speed milling of titanium alloy (Ti-6Al-4V) reduces cutting forces compared to conventional machining of titanium, and that the main advantage of high speed end-milling is that it improves performance by increasing the material removal rate. Safari et al [5] investigated the effects of high-speed end-milling on cutting force in cryogenic machining of Ti-6Al-4V using coated and uncoated carbide tools. They compared 3 cutting speeds at 0.2, 0.25, and 0.3 m/min. They reported that lowest cutting force components were obtained when machining at the highest cutting speed of 0.3 m/min. Balaji et al [6] also lent credence to the idea that high-speed machining of difficult-to-cut metals reduces cutting force by conducting an investigation on high-speed orthogonal

turning of titanium alloys. They reported that higher cutting speeds with a positive tool rake angle was best at minimizing cutting force, tool wear, and cutting temperature compared to lower cutting speeds and a negative rake angle. They explained that this was due to the fact that at higher cutting speeds, thermo-mechanical instability is intense and less work is needed for shear failure. In spite of the numerous advantages that have been achieved in high-speed machining of difficult-to-cut metals, many authors also report some problems. Liao et al [7] reported high cutting temperature and difficult chip disposal to be the two major problems encountered during high-speed slot end-milling of Inconel 718. They investigated spindle speed ranges from 10 – 170 m/min, and feed rates of 0.02 and 0.05 mm/tooth. They explained that the rise of temperature was due to the difficulty of chips to be disposed as fast as they were produced. As a result, they recommended appropriate speed ranges of 90 – 110 m/min in which high-speed milling of Inconel 718 was most viable. However, they did not recommend appropriate feed ranges, and likewise the depth of cut.

Another factor that can also help increase the efficiency in machining of Inconel 718 alloy and other difficult-to-cut metals is the use of suitable and viable cooling and lubrication techniques. Coolants are necessary in removing the heat generated at the cutting zone thereby reducing the cutting temperature, while lubricants are used in reducing the coefficient of friction at the cutting zone, and hence cutting forces. Presently in many industries, water based emulsion is used as a source of conventional cooling and lubrication during machining. This coolant is flooded on the cutting zone usually under high pressure with the aid of a nozzle, thereby removing the heat generated and also carrying out chips produced. This high pressure coolant impinging on the cutting zone

leads to the reduction of cutting temperature, cutting forces and tool wear. The effects of a high pressure coolant were investigated by Ezugwu and Bonny [8] during machining of nickel base Inconel 718 alloy with coated carbide tools. The authors reported that a longer tool life was achieved when using coolants at high pressure of 203 bars compared with coolants at a low pressure of 110 bars. Furthermore, they stated that the higher the cutting speed (> 20 m/min), the more effective the high pressure coolant will be in increasing tool life. They attributed the increase in tool life to a decrease in nose wear, which was made possible because of the better cooling and lubricating effect of coolant at high pressure. However, these coolants must be disposed after usage, and this disposal could adversely affect the environment as the fluids can readily become pollutants if not well handled. In addition, the cost of disposal of these conventional coolants adds up to the total over head cost to the manufacturer. Due to the environmental effects, many industries are coming under increased pressure to jettison the use of emulsion coolant in favor of more environmentally friendly methods of cooling during machining, which could be termed green machining.

Cryogenic machining offers a good alternative and a step in the direction of green machining. It involves applying liquid nitrogen to the cutting zone and allowing it to evaporate, releasing nitrogen gas which is non-green house, and non flammable. Few researches have been conducted on cryogenic machining for both regular metals and difficult-to-cut metals alike. Su et al [9] investigated the effects of various cooling and lubrication conditions during high-speed end-milling of titanium alloy (Ti-6Al-4V) using coated carbide inserts, and discovered that the use of cryogenic coolant at -10˚C decreased tool wear and increased tool life compared to dry machining and flood coolant.

They explained that this was due to the fact that the cryogenic fluid at -10˚C reduced the cutting temperature, and thus the diffusion rate of tool material atoms, which consequently led to lower flank wear rates. Ahsan and Mirghani [10] reported that cryogenic turning of stainless steel to have improved tool life up to 4 times compared to conventional emulsion cooling. Yusuf [11] presented an evaluation of machining performance in cryogenic turning of Inconel 718, and made comparisons with dry turning. He reported that cryogenic turning of Inconel 718 using un-coated carbide inserts reduced all three cutting force components, when compared to dry turning at high cutting speeds of120 m/min. Shane et al [12] proposed a new cooling approach in a bid to improve tool life in the cryogenic machining of titanium alloy Ti-6Al-4V. They employed a specially designed micro-nozzle to focus liquid nitrogen between a chip breaker and the tool rake face, and another auxiliary nozzle to spray LN_2 to the flank at the cutting edge. They reported that the combination of these 2 micro-nozzles provided the most effective way of cooling, while also using the lowest LN_2 flow rate. Some of the merits of using liquid nitrogen as a cryogenic fluid during machining are that it helps in preventing the adhesion between the chips and the cutting edge, which improves the abrasion condition of the tool, and also the integrity of the machined surface [13]. Additionally, liquid nitrogen prevents chips from burning by virtue of it being an inert gas, and its application to the cutting zone prevents the entrance of oxygen to a large extent which is a necessary ingredient for burning [13]. The most important is that cryogenic machining makes use of liquid nitrogen which is safe, non-combustible, evaporates and returns to the atmosphere leaving no residue to contaminate the part, machine tool or operator, thus eliminating disposal costs [14]. Zhao and Hong [15]

investigated cryogenic properties of various engineering materials, including titanium alloy Ti-6AL-4V. He reported that the hardness of annealed titanium increased by 8.5 HRC when it was cooled from room temperature beyond -50 ˚C. He therefore stated that Ti-6Al-4V can maintain its toughness and hardness at low temperatures of liquid nitrogen. This means using extremely low temperatures of liquid nitrogen could be detrimental while machining difficult-to-cut metals, as hardening the work-piece would lead to increased tool wear, cutting temperature and cutting forces. Therefore, it is pertinent that the cryogenic fluid is directed and focused properly as much as possible at the cutting zone, so as to avoid a needless cooling of the workpiece material. To solve this problem, Shane et al [16] proposed a new economical cryogenic approach, while investigating the effects of cryogenic machining (turning) on friction and cutting forces in machining Ti-6Al-4V alloy. This approach uses a minimum amount of LN_2 injected through a micro-nozzle formed between the chip breaker and the tool rake and assisted by the secondary nozzle for flank cooling in turning. The authors stated that in this manner, LN_2 is not wasted by cooling unnecessary areas and this reduces the negative impact of increasing the cutting force, decreasing tool life and the abrasion of pre-cooling the work-piece material.

The use of minimum quantity lubrication (MQL) in place of conventional emulsion cooling also eliminates the costs and adverse environmental effects of disposing conventional coolants, and does not contaminate the part or operator. MQL systems spray tiny mists of oil and air mixture on the cutting zone. The oil contained in the mist acts as the lubricant, while the air acts as the coolant. Therefore, it does a simultaneous job of cooling and lubricating the cutting tool and cutting zone, thereby reducing the coefficient

of friction and cutting temperature, and consequently reducing cutting forces and tool wear. A number of researches have been conducted on various difficult-to-cut metals and other regular metals using MQL cooling strategy. Zhao et al [17] compared MQL and dry machining during high-speed peripheral milling of Ti-6Al-4V alloy. They reported tool wear in dry machining to be 0.37 mm at a machining length of 4.8 m, while that of MQL was 0.12 mm for the same machining length. They attributed this difference in tool wear to be due to the fact that during dry machining, the workpiece material easily adheres to the tool surface because of mechanical, thermal, and chemical loads in the contact zone. They therefore concluded that MQL was better at reducing cutting forces and improving tool life in high-speed milling of titanium alloy compared with dry machining. Also, Ezugwu [18] further extolled the advantages of minimum quantity lubrication in high-speed machining of aero engine alloys by explaining that the reduction in cutting forces and tool wear by MQL was as a result of the lubricating oil and air being able to get into the tool-workpiece and tool-chip interfaces under pressure, thereby reducing the temperature generated during machining and also reducing the coefficient of friction**.** This is possible because when MQL jets hit the workpiece and tool at high speed and pressure, the cutting oil gets much more fragmented into more tiny micro-droplets which improve its penetration into the tool/chip and tool/work-piece interfaces, and the smaller the size of the micro-droplets, the easier it is for the oil droplets to get into the tool/work-piece and tool chip interfaces, and thus the better its lubricating effect. [19]. Thamizhmani et al [20] experimentally investigated the effects of minimum quantity lubrication on tool flank wear during end-milling of Inconel 718 using super hard cobalt end-mill. The authors investigated 3 flow rates: 12.5, 25, and 37.5 ml/hr, and 3 cutting

speeds of 10, 20 and 30 m/min at a constant federate of 0.15 mm/tooth and depth of cut of 0.4 mm. They reported that the highest flow rate of 37.5 ml/hr produced the least wear on the tool's cutting edge as well as contributing most to the cooling and lubrication of the tool-chip interface. Lastly, they concluded that MQL increased the life of a super cobalt tool, compared to dry machining. Liao et al [21] reported that in machining of hardened steel, flood coolants gave the shorter tool life due to thermal cracks generated, while MQL gave a longer tool life due to its efficiency in reducing thermal cracks and delaying the welding of chips onto the tool flutes. Despite these numerous benefits in using minimum quantity lubrication, there are also some reported demerits in the use of minimum quantity lubrication. Boubekri and Shaikh [22] reported a major problem with the use of MQL as it pertains to environmental and health issues. They reported that MQL cooling strategy generates significant amount of mist compared to flood cooling which could be detrimental to the operators. Therefore, they emphasized the need for the installation of a mist collection or filtering equipment in the work area where MQL is used.

As seen from the above review of published works, little or no work has been done in high-speed slot end-milling of Inconel 718. Most of the published works have been more in turning. Furthermore, the few that have been published in milling did not investigate high-speed milling of this alloy, and particularly slot end-milling. Also, only a few studies of the individual viability and potentials of minimum quantity lubrication and cryogenic cooling have been investigated. There has been no total comprehensive study of the effects of machining parameters, cryogenic cooling, and minimum quantity lubrication on cutting force components, tool wear, and cutting temperature. Furthermore,

the potential benefits of combining the use of minimum quantity lubrication and liquid nitrogen simultaneously have not been investigated in previous works. Also, in previous published works, it is not clear how liquid nitrogen (LN_2) was increased from a temperature of -196˚C to a suitable cold temperature range to be used in the cutting zone, that would not adversely increase the workpiece hardness. Therefore, the aim of this research is to investigate the main and interaction effects of three cooling strategies [(MQL, LN_2, and combined (MQL+LN_2)] and machining parameters (feed and speed) on cutting forces, tool wear and cutting temperature during high-speed slot end-milling of Inconel 718. A novel cooling approach of combining MQL and LN_2 simultaneously is investigated. The objective is to find optimum machining parameters and cooling strategy, which would give the lowest cutting forces, cutting temperature and tool wear. Lastly, a comparative study of the 3 cooling strategies was conducted using the recommended optimum machining parameters obtained from the analysis of variance. analysis was done using a one-third fractional factorial design of experiments.

2. EXPERIMENTAL DESIGN

A three-factor at three-level design of experiment was chosen for this analysis. A one-third fractional factorial experimental design requiring 9 experimental runs was generated to reduce the number of experimental runs and cost. Each run was replicated once resulting in 18 experimental runs. A full factorial design would have resulted in 54 runs with replication, which is time consuming and costly.

2.1. EXPERIMENTAL PARAMETERS AND LEVELS

The 3 factors selected for this experiment were: spindle speed, feed rate, and cooling strategy. The aim of this experiment is to investigate the effects of these factors (cooling strategies, speed and feed) on cutting force components (F_x, F_y, F_z), cutting temperature, and tool wear in slot end-milling of Inconel 718 and to determine optimum cutting parameters and cooling strategy that will give the lowest cutting force components, tool wear, and cutting temperature. Spindle speed at 3 levels 250, 500, and 750 rpm corresponding to 10, 20, and 30 m/min, and feed rate at 3 levels 1, 2, and 3 ipm corresponding to 25.4, 50.8, and 76.2 mm/min were chosen. The cooling strategies at 3 levels chosen are: Minimum Quantity Lubrication (MQL), Liquid Nitrogen (LN_2) and a combination of Minimum Quantity Lubrication and Liquid Nitrogen (MQL+LN_2). The speed ranges were chosen to encompass low, medium, and high spindle speed after extensive review of published literature and consultation with cutting tool manufacturers. Other factors that were not investigated were kept constant throughout the experiment, like the axial depth of cut at 0.05 inch (1.27 mm) and a radial depth of cut at 0.5 inch (12.7 mm). Table 1 shows the factors and their respective levels.

Table 1. Factors and levels

Factors			
Level	Cooling Methods	Speed rpm (m/min)	Feed rate ipm (mm/min)
0	MQL	250 (10)	1 (25.4)
1	LN_2 (-15 ˚C)	500 (20)	2 (50.8)
2	MQL+LN_2 (-15 ˚C)	750 (30)	3 (76.2)

2.2. SELECTION OF TREATMENT COMBINATIONS/METHOD OF STATISTICAL ANALYSIS

For a full factorial experiment, there will be a total of 27 experimental runs for 3 factors at 3 levels. A one-third fractional factorial design was constructed in order to reduce the total number of experimental runs to 9. To do this, higher order interactions were aliased with the mean, and 3 blocks with 9 experimental runs in each of them were constructed. After performing some analysis and applying modulo 3 arithmetic, the block that contained the principal fraction (0, 0, 0,) was chosen for this experiment. Table 2 shows the 9 treatment combinations that were generated and used.

Table 2. One-third fractional factorial design of experiment

Experimental Runs	Treatment Combinations	3 factors at 3 levels Cooling Method	Speed rpm (m/min)	Feed ipm (mm/min)
1	(0,0,0)	MQL	250 (10)	1 (25.4)
2	(0,1,2)	MQL	500 (20)	3 (76.2)
3	(1,0,1)	LN_2 (-15˚C)	250 (10)	2 (50.8)
4	(2,0,2)	MQL+LN_2(-15˚C)	250 (10)	3 (76.2)
5	(0,2,1)	MQL	750 (30)	2 (50.8)
6	(1,1,0)	LN_2 (-15˚C)	500 (20)	1 (25.4)
7	(1,2,2)	LN_2 (-15˚C)	750 (30)	3 (76.2)
8	(2,1,1)	MQL+LN_2(-15˚C)	500 (20)	2 (50.8)
9	(2,2,0)	MQL+LN_2(-15˚C)	750 (30)	1 (25.4)

2.2.1. Analysis of Variance (ANOVA)

Analysis of Variance (ANOVA) is used to test the significant difference between the means of each factor. It can determine if the variation in the results of the dependent variable is due to the change of one factor level to another, and not just due to random chance. In other words, ANOVA provides the statistical test of whether or not the means of several groups are equal. In this experiment, results from ANOVA were used to test whether or not there was significant difference between the means of the factors. The ANOVA uses an F-test with a p-value to test for significance. The F- test uses an F ratio (variance ratio) which is the ratio of the mean square effect to the mean square error. The larger the F-ratio for a given factor, the more likely the test for significance is not due to random chance. Also, the p-value gives the probability of the test for significance of the

effects on the dependent variable. The p-value is compared with a significance level ($\alpha = 0.05$), and if the p-value given in the ANOVA result is less than the significance level then the difference between means of that effect is said to be significantly different from zero.

2.2.2. Pareto Chart of Effects

A Pareto chart is a visual representation of all effects (both main and interaction) in the form of bar charts in relation with how they significantly affect the dependent variable. A dashed red line running across any of the bar charts shows the magnitude required for that effect to be statistically significant. It lists each effect in the order of significance. The Pareto chart is very useful in reviewing a large number of factors, and for presenting the results of an experiment to an audience that is not familiar with standard statistical terminologies.

2.2.3. Marginal Means

Marginal means plots were used in this experiment to pictorially show the effects of each factor (spindle speed, feed rate, and cooling strategy) on the dependent variables (cutting force components, indirect tool wear, and cutting temperature)

2.2.4. Desirability Surface/contour Plot

The desirability surface/contour plots were used in this experiment to show a 3-D figure of the statistical relationship between the factors (spindle speed, feed rate and cooling strategy) and the dependent variables (cutting force, tool wear, and cutting temperature). The plots are partitioned in areas marked by distinct colors (green, yellow, and red). These colors help in the interpretation of the relationship between the factors

and the dependent variable in a given region of the plot. More green color means that the factor is more desirable, and more red means it is less desirable.

2.3. SETTING UP OF COOLING STRATEGIES

One of the aims of this experiment is to investigate the effects of cooling strategies on cutting force components, tool wear and cutting temperature. The cooling strategies that were investigated are: MQL, LN_2, and combined (MQL+LN_2). Each of these cooling strategies was set up independently for this experiment.

2.3.1. Minimum Quantity Lubrication Set up

MQL is a mixture of mineral oil and air that is sprayed on the cutting zone in the form of mists. For this experiment, an Acculube MQL precision pump applicator was used to spray lubricant mist on the cutting zone. The precision pump applicator uses a positive displacement system to spray the lubricant, and it can be regulated to control the amount of lubricant applied to the cutting zone and on the tool flutes. For this experiment, shop air supplied at 85 psi to the CNC machine is stepped down at the input to the MQL precision pump applicator to 65 psi. Thus, the air pressure used by the precision pump applicator is 65 psi. It also has a valve that can be used to regulate the volume of air that is mixed with the droplets of oil. Due to the extreme hardness of Inconel 718 super alloy, it is pertinent that sufficient volume of air is used to transport the lubricant. This would be more efficient in cooling the cutting zone and removing chips. To this end, the air valve was increased by turning it counter clock wisely two and a half times. This ensured that sufficient volume of air was available to transport the lubricant to the cutting zone. Furthermore, the volume of oil that gets mixed up with the air to form

the lubricant can also be regulated. The precision pump applicator has a valve, which is graduated from 0 to 7, and this valve can be controlled to regulate the amount of oil going to the cutting zone depending on the machining operation involved. For this end-milling experiment, the precision pump applicator manual was consulted and the recommendation was for the valve to be set at 7, between 0 and 6. Also, the precision pump has a frequency generator which is used to regulate the number of times the lubricant is applied to the cutting zone per second, which is the pump cycle. For this experiment, various pump cycles were investigated to see which was more efficient in milling Inconel 718 without wasting so much lubricant. A pump cycle of 3 strokes per second was chosen for this work. Lastly, a loc-line adjustable nozzle was connected to the precision pump applicator so the lubricant can flow through it to the cutting zone.

2.3.2. Cryogenic Liquid Nitrogen set up

The use of cryogenic Liquid Nitrogen (LN_2) in milling involves the application of sub zero temperature liquid nitrogen to the cutting zone. This method of cooling is very efficient in removing the enormous amount of heat generated during the milling of Inconel 718 alloy. A 160 liters cylinder with a pressure relief valve of 230 psi containing liquid nitrogen was used for these experiments. Transportation of liquid nitrogen from the cylinder to the milling zone was done using pipe couplings, valves, nozzles, and a flexible cryogenic flow line. The cryogenic flow line had a pressure gauge fitted to it to measure the pressure of liquid nitrogen flowing through it to the cutting zone. The pressure gauge had a 0.25" (6.35 mm) Swagelok pipe fitted to it, which was also connected to a 0.25" (6.35 mm) Tee, and in turn linked up to a 0.25" (6.35 mm) pig tail pipe. This was in order to prevent liquid nitrogen from getting in contact with the

pressure gauge so as not to damage it. The temperature of liquid nitrogen in the tank was extremely cold at -196˚C. This extremely cold temperature of liquid nitrogen if used this way, would negatively affect the milling of Inconel 718 alloy. Very cold temperatures have the tendency to increase the hardness of the already difficult to cut metals and this would increase the cutting forces drastically, which will lead to severe wear of the cutting flutes and consequently tool breakage. To this end, it was pertinent to increase the temperature of liquid nitrogen before applying it on the cutting zone. As a result, a 1.5 inches (38.1 mm) outer diameter and 1.375 " (34.93 mm) inner diameter nozzle with an orifice of 1/16 " (1.59 mm) was designed to help increase LN_2 temperature from -196˚C. Also, liquid nitrogen was mixed with shop air to help increase the cold air temperature to a more acceptable working temperature to avoid work-hardening of the workpiece. For these experiments, a temperature of -15˚C was chosen for the mixture of LN_2 and shop air as the optimum milling temperature for Inconel 718 super alloy based on published literature data [23]. The challenge therefore, was how to increase the temperature OF LN_2 from -196˚C to -15˚C in the output nozzle.

2.4. CALIBRATION OF CRYOGENIC SET UP

The calibration of the cryogenic liquid nitrogen set up was necessary in order to ensure repeatability in getting a fixed optimum temperature of -15˚C at the output nozzle. To ensure a fixed temperature at the output nozzle, it is pertinent to determine a fixed amount of liquid nitrogen pressure and air pressure combination that will yield the desired temperature. The calibration was done by recording different values of LN_2 and air pressures and their corresponding temperatures at the nozzle outlet. A total number of 11 different combinations of LN_2 pressure, air pressure and their corresponding

temperatures were made. To perform the calibration, a multiple regression model was developed using Statistica software 7 from Stat Soft. The multiple regression model has 2 factors namely: LN_2 pressure and shop air pressure, and one dependent variable which is the temperature at the nozzle outlet. The aim of the regression model is to establish a relationship between the factors LN_2 pressure and air pressure and the dependent variable output temperature. Thus, fixed values of LN_2 pressure and shop air pressure can be obtained, which when combined will give a nozzle output temperature of -15˚C. A 0.125" (3.175 mm) diameter ungrounded k-type thermocouple was taped around the nozzle output to record the temperature of LN_2 and air mixture, as well as the lab room temperature. The multiple regression model is of the form:

$$Y = Bo + B_1X_1 + B_2X_2 + Є \quad (1)$$

Where Y represents the dependent variable output temperature, X_1 represents LN_2 pressure, and X_2 represents shop air pressure. Bo represents the intercept of the equation, B_1 represents the coefficient of LN_2 pressure, B_2 represents the coefficient of shop air pressure, and Є represents the error. The multiple regression analysis was performed using a significance level of 0.05. To begin calibrating, the cryogenic flow line was turned on for the LN_2 to gush out of the nozzle outlet. To ensure the pressure of LN_2 in the flow line was steady as seen from the gauge, LN_2 was allowed to flow out for about 20 minutes until the whole length of the flow line was completely frozen and ice became visible throughout the length of the flow line. This was important in order to prevent the fluctuation of LN_2 pressure in the flow line. Once the LN_2 pressure in the flow line became constant, shop air was turned on to mix with the LN_2 to form a mixture. Then, different values of LN_2 pressure and air pressure were selected and their output

temperature was measured and recorded. The range of values of LN_2 pressure chosen was from 40 psi to 75 psi, while the range of values for shop air pressure chosen was from 15 to 45 psi. These ranges of values were chosen arbitrarily, however, consideration was taken to avoid high air pressure so as to prevent excessive whistling noise made by air at high pressure. Firstly, LN_2 pressure at 40 psi was chosen together with air pressure of 15 psi. The temperature measured by the thermocouple was 2.41268 ˚C. Secondly, LN_2 pressure of 50 psi and air pressure of 20 psi were chosen, and the recorded temperature was 1.02068 ˚C. This procedure was repeated until 11 different combinations of LN_2 pressures and air pressures with their corresponding output temperatures were recorded. For each combination of LN_2 and air pressure, the reading of the thermocouple was recorded. Table 3 gives 11 cryogenic temperature calibration data

Table 3. Cryogenic Temperature calibration data

LN_2 Pressure Psi (MPa)	Air Pressure Psi (MPa)	Temperature (˚C)
40 (0.276)	15 (0.103)	2.41268
50 (0.344)	20 (0.138)	1.02068
55 (0.379)	30 (0.207)	-0.33645
60 (0.414)	15 (0.103)	-25.9122
60 (0.414)	30 (0.207)	-13.7055
60 (0.414)	25 (0.172)	-15.8007
65 (0.448)	30 (0.207)	-17.3153
65 (0.448)	35 (0.241)	-15.1913
70 (0.483)	35 (0.241)	-24.6755
70 (0.483)	40 (0.276)	-20.2317
75 (0.517)	45 (0.310)	-24.6572

The above data were entered into Statistica Software 7 and Analysis of Variance (ANOVA) was conducted on the observations to see if the treatment combination mean was significantly different from zero or not. In simple terms, to find out if the results obtained were significant. Table 4 shows the results obtained from the Analysis of Variance (ANOVA).

Table 4. ANOVA for Calibration of Cryogenic set-up

Effect	Analysis of Variance; DV: Temperature				
	Sums of Squares	df	Mean Squares	F	P-level
Regress.	1023.510	2	511.7551	49.81684	0.000031
Residual	82.182	8	10.2727		
Total	1105.692				

From the ANOVA table above, it can be seen that the treatment combination has a p-value of 0.000031. This p-value is the probability that the observations made were due to random chance and not because of an actual variation of the effects. This p-value is compared with the significance level ($\alpha = 0.05$), and since the p-value is much less than 0.05 it shows there is sufficient evidence to conclude that the test for the treatment combination means is significant. In other words the result of the calibration is significant at the given significance level of 0.05.

Next, a model was fitted to the observations made by conducting a multiple regression analysis. The aim of the model is to generate an equation which best approximates the relationship between the independent variables (LN_2 and air pressures) and the dependent variable (temperature). A forward step wise multiple regression method was used, and Table 5 below gives the results of the multiple regression model.

Table 5. Multiple regression model for calibration data

	Regression Summary for Dependent Variable: Temperature					
	R = 0.96211945 R^2 = 0.92567383 Adjusted R^2 = 0.90709228					
N = 11	F (2,8) = 49.817 P<0.00003 Std. Error of estimate: 3.2051					
	Beta	Std. Err. of Beta	B	Std. Err. of Beta	t(8)	p-level
Intercept			59.01976	7.417012	7.95735	0.000045
LN_2 Pressure	-1.52675	0.176607	-1.61276	0.186555	-8.64493	0.000025
Air Pressure	0.79834	0.176607	0.86543	0.191448	4.52045	0.001949

From the table, the p-values of the intercept, LN_2 pressure, and air pressure are 0.000045, 0.000025, and 0.001949 respectively. They are all less than the significance level of 0.05, and thus, their effect is not due to random chance and so they have significant effect on temperature. Therefore, the 3 can be left in the model equation. Furthermore, the coefficients of the intercept, LN_2 pressure and air pressure are 59.01976, -1.61276, and 0.86543 respectively. Thus, the multiple regression equation becomes:

$$Y = 59.02 - 1.613\ X_1 + 0.865\ X_2 \quad (2)$$

Where Y represents temperature, X_1 represents LN_2 pressure and X_2 represents air pressure. The above equation can be used to predict values of shop air, when LN_2 pressure and temperature are known, and also values for LN_2 pressure when shop air pressure and temperature are known. Also, the R^2 value of the model is 0.9257, which is the value that measures the validity of the model. For this calibration, it means that 92.57 percent of the observed values can be accounted for by the model equation**.** Table 6

presents different predicted values of shop air pressure which will give temperatures of -10˚C, -15˚C, and -20˚C when LN_2 pressures are fixed.

Table 6. Pressure predicted values from calibration equation

Temperature(˚C)	LN_2 Pressure Psi (MPa)	Air Pressure Psi (MPa)
-10˚ C	55 (0.379)	22.77 (0.157)
	60 (0.414)	32.09 (0.221)
	65 (0.448)	41.42 (0.286)
-15˚C	**55 (0.379)**	**16.99 (0.117)**
	60 (0.414)	26.31 (0.181)
	65 (0.448)	35.64 (0.246)
-20˚C	55 (0.379)	11.21 (0.077)
	60 (0.414)	20.53 (0.142)
	65 (0.448)	29.86 (0.206)

These predicted values for shop air were obtained by substituting the fixed values of LN_2 pressures and the desired output temperatures into the model equation, and solving for X_2 which represents air pressure. Therefore, the table above presents calibrated values of various possible combinations of LN_2 pressure and air pressure, and their corresponding output temperature. For this experiment, a combination of LN_2 pressure at 55 psi and air pressure at 16.99 psi was chosen to give the optimum desired cooling temperature of -15˚C. The chosen parameters are highlighted in bold in the Table.

3. EXPERIMENTAL SET UP AND PROCEDURE

3.1. PREPARING THE WORK-PIECES

Before conducting the slot end-milling experiments, 2 rectangular workpieces of inconel 718 with dimensions 3" (76.2 mm) × 6" (152.4 mm) × 1.5" (38.1 mm) each were prepared. Firstly, 2 holes 1.5" (38.1 mm) deep and 2.3622" (60 mm) apart were drilled on the workpieces. These holes were used in fastening the workpieces to the dynamometer, which was used for cutting force acquisition. Next, 2 counter bores of Ø 0.55" (13.97 mm) × 0.312" (7.92 mm) and Ø 0.4" (10.16 mm) × 0.712" (18.1 mm) were performed on the 2 drilled holes in order to accommodate the dimensions of the clamping bolts. Thirdly, the 2 holes were tapped so that a bolt could be threaded through from the work-piece and fastened to the dynamometer. Lastly, 9 holes of 0.125" (3.175 mm) diameter and 1" (25.4 mm) deep were drilled in the workpieces, and a K-type ungrounded thermocouple was inserted for temperature measurement. Each of the 9 holes was drilled to correspond with the center of each slot.

3.2. EXPERIMENTAL SET UP

The workpiece was fastened on the dynamometer by screwing a bolt through the drilled and tapped holes of the work-piece, and cutting force was acquired during machining and separated into its components. Also, a thermocouple was inserted into the 0.125 in. (3.175 mm) diameter holes on workpiece and used to measure the temperature of the slot during machining.

3.3. CUTTING FORCE ACQUISITION

A Kistler type 9272 4-component dynamometer was used to measure cutting force components for these milling experiments. The workpiece was fastened on the dynamometer, and both were tightened on the CNC machine's vice. The dynamometer was connected to a Kistler type 5405 A break out junction box, where force signals from the dynamometer were separated into the constituent force components F_x, F_y, and F_z. Also, cutting force components from the junction box were passed through 3 separate channels of Kistler type 5010 B dual mode amplifiers, where the acquired signals were amplified. The amplified signals were passed through low pass filters with a set frequency of 680 Hz. The aim of the low pass filters was to get rid of unwanted noise and extraneous vibrations from the end-milling process. These filtered signals were passed to a Tektronix TDS 420A digitizing oscilloscope where the signals were saved and later transferred to a Pentium PC for processing. In the oscilloscope, the signals were digitized at a sampling frequency of 1 Ks/s, with number of sampling points of 5000 per signal. This resulted in a record length of 5 seconds. This is the total length of time it took to acquire cutting force signals. The digitized signals were saved and later transferred to a PC for processing.

3.4. TEMPERATURE MEASUREMENTS

An ungrounded K-type 0.125 in. diameter thermocouple probe was inserted into the drilled holes, and used in measuring the cutting temperature at the center of each slot during machining. The thermocouple probe was connected to a PC on which the software Labview 2013 from National Instrument was downloaded. The Pentium PC displayed the

temperature reading of the slot. Figure 1 shows a schematic and photograph of the complete experimental set up.

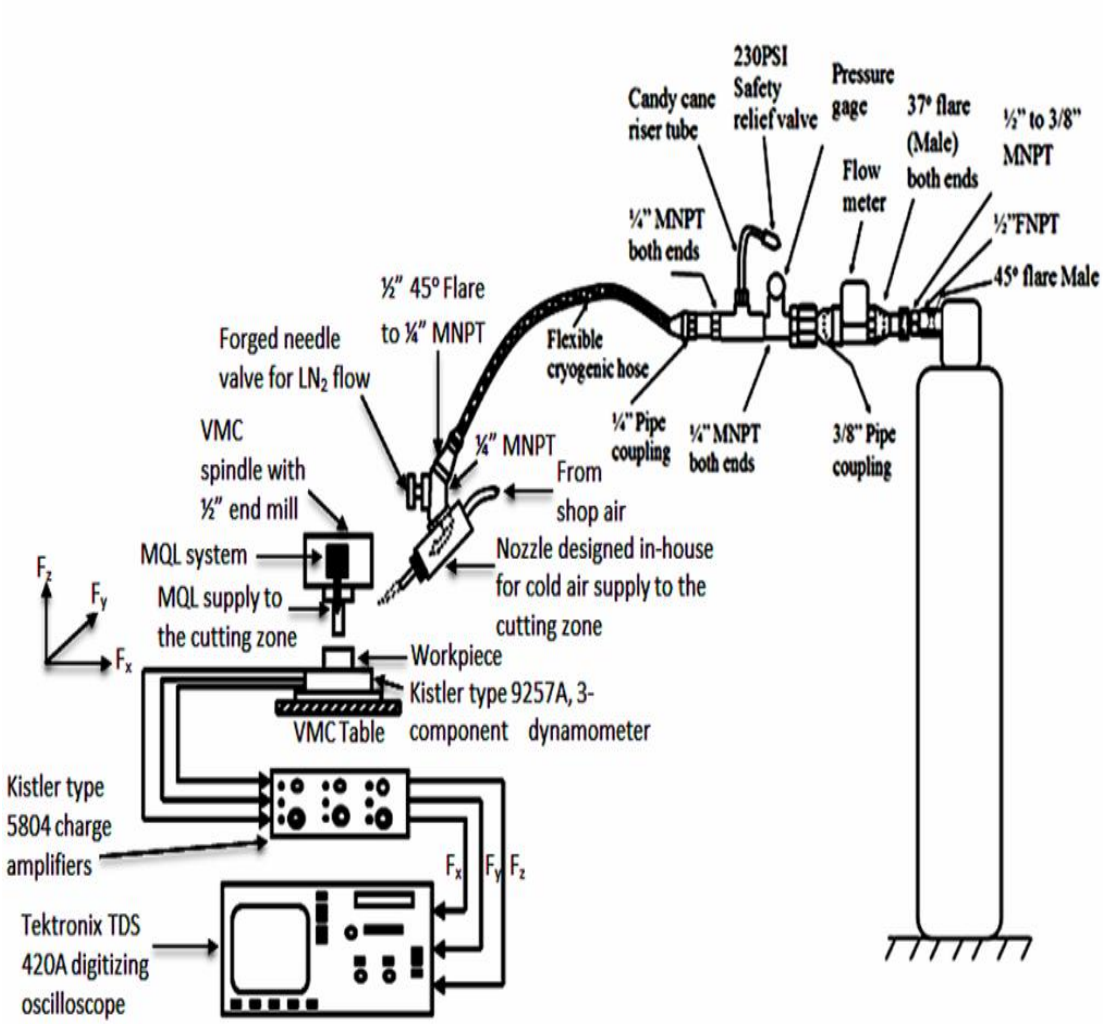

Figure 1. Schematic/Picture of experimental set-up with cryogenic flow line and data acquisition system

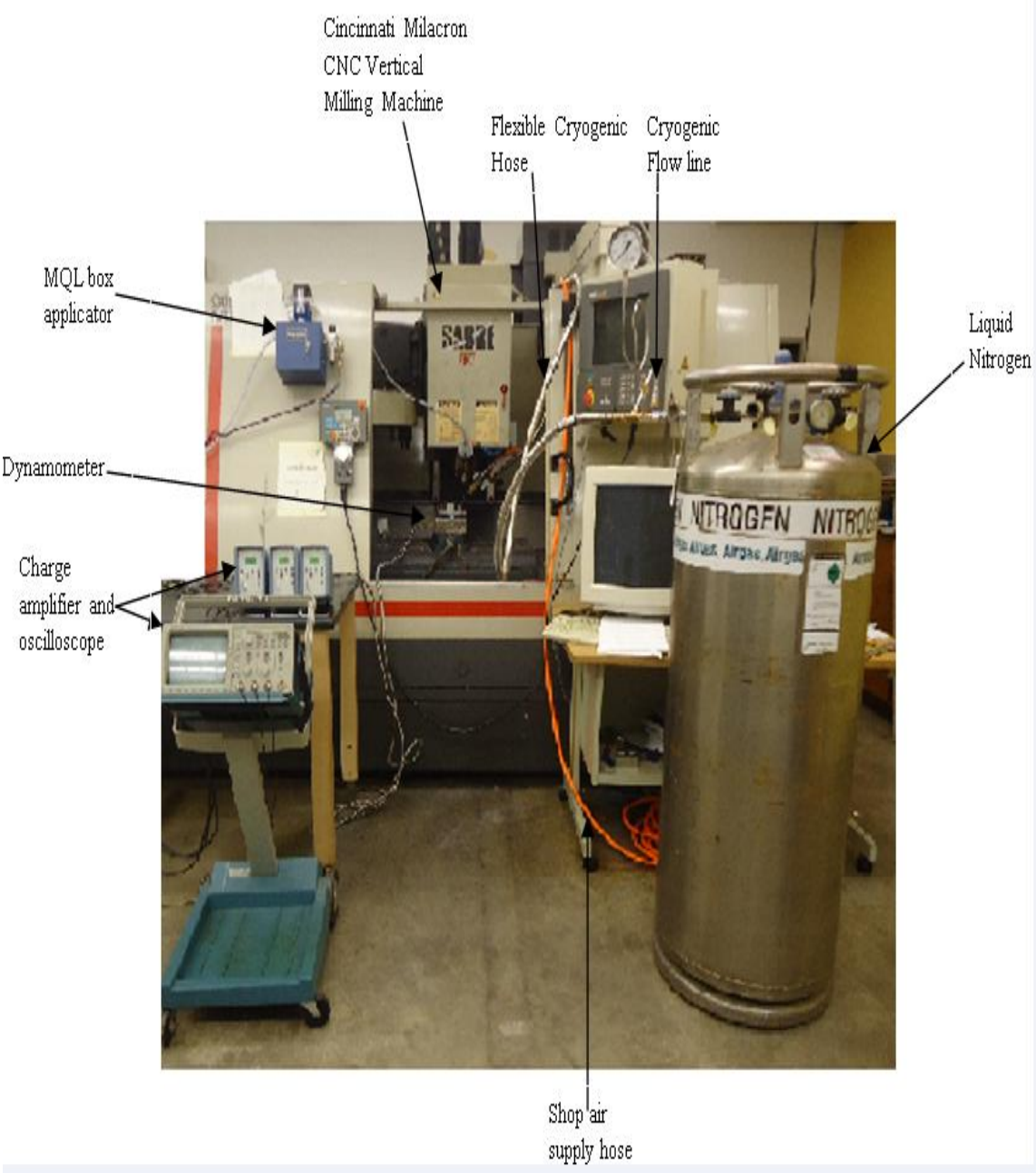

Figure 1. Schematic/Picture of experimental set-up with cryogenic flow line and data acquisition system (cont.)

3.5. PROCEDURE

Slot end-milling experiments were conducted on Cincinnati Milacron Vertical Machining Center (VMC), Sabre 750 equipped with acramatic 2100 controller. Two rectangular blocks of Inconel 718 alloy each measuring 3 inches (76.2 mm) × 6 inches (152.4 mm) × 1.5 inches (38.1 mm) were used for the slot end-milling experiments. Four-flute uncoated solid carbide bullnose helical end-mills of 0.5 inch (12.7 mm) shank diameter, 3 inches (76.2 mm) overall length and 1inch (25.4 mm) flute length were used for all experimental runs. The end-mills have a corner radius of 0.03" (0.762 mm), which was chosen to give minimum cutting force values during machining [24]. Two sets of machining tests were conducted in this experiment using the two blocks of Inconel 718 alloy. Each block is designed to contain a maximum of 8 slots, and the slots were separated by a rib of width 0.125 inch (3.175 mm). For the first part of the experiment, 9 slots each having a depth and width of 1inch (25.4 mm) and 0.5 inch (12.7 mm) respectively were made and used to investigate the effects of machining parameters and cooling strategies on cutting force components, cutting temperature and tool wear, and also to obtain optimum machining parameters and cooling strategy. The machining parameters investigated are: spindle speed at 250, 500, and 750 rpm, feed rates at 1, 2, and 3 ipm. While the cooling strategies investigated were: MQL, LN_2 and a combined (MQL+LN_2). An axial depth-of-cut of 0.05 inch (1.27 mm) was chosen and held constant for all experimental runs. Also, the radial depth of cut was kept constant at 0.5 inch (12.7 mm). The machining parameters used were specific to the carbide tool used for this experiment, and were chosen based on reviewed literature and after consultations with cutting tool manufacturers. Also, before arriving at these parameters, various spindle speeds and feed rates were investigated and lots of issues were encountered. Speeds of

900, 1000, 1500, and 2000 rpm were first investigated; however, the cutting forces generated were so high thereby causing tool breakage along the shank with just a little impact on the work-piece. Likewise, feed rates of 6 (152.4 mm/min), 9 (228.6 mm/min) and 12 ipm (304.8 mm/min) were investigated. These also generated extremely high cutting forces and led to tool breakages within a short machining duration. This is because machining Inconel 718 with very high speeds and feeds generates an enormously high amount of temperature at the cutting zone and also induces high cutting forces, which results in an extreme wear of the cutting edges, and consequently tool breakage. Also, various axial depths-of-cut were investigated such as: 0.125 inch (3.175 mm), 0.1 inch (2.54 mm), and 0.0625 inch (1.59 mm). These axial depths-of-cut induced very high cutting forces, which led to complete plastic deformation of the cutting edges and tool breakage. For this experiment, an axial depth-of-cut of 0.05 inch (1.27 mm) was found to be suitable and was used for all experimental runs conducted. This resulted in a total of 20 passes made for each slot in order to achieve a slot depth of 1 inch (25.4 mm/min). A new end-mill was used for each slot bringing the total to 9 end-mills used for the first part of this experiment. For the second part of this experiment, the optimum machining parameters obtained were used in conducting a comparative evaluation of the 3 cooling strategies, MQL, LN_2, and combined (MQL+LN_2), with regards to their effectiveness to reduce cutting force components, cutting temperature and tool wear. For the second part of the experiment, additional 2 end-mills were used bringing the total number of end-mills used for all slot end-milling tests to 11.

For each machining pass, the direction of feed for all machining passes was along the positive Y axis**.** The appropriate speed, feed and cooling strategy were used and

acquisition of the cutting force components were made when the tool was at approximately the center of each slot. The cutting force components were saved in the oscilloscope and analyzed. Also, the reading of the thermocouple inserted at the center of each slot was displayed by the PC and recorded during each cutting force acquisition. Not all machining passes were acquired. Cutting forces were acquired pass numbers 1, 2, 10, 15, 19, and 20 as well as their corresponding temperature values. This corresponds to machining lengths of 76.2, 152.4, 762, 1143, 1447.8, and 1524 mm respectively. Also for each cutting force component acquisition made, the chips were collected and studied as well as the tool used. Figure 2 shows a 2D and 3D workpiece design with the slots.

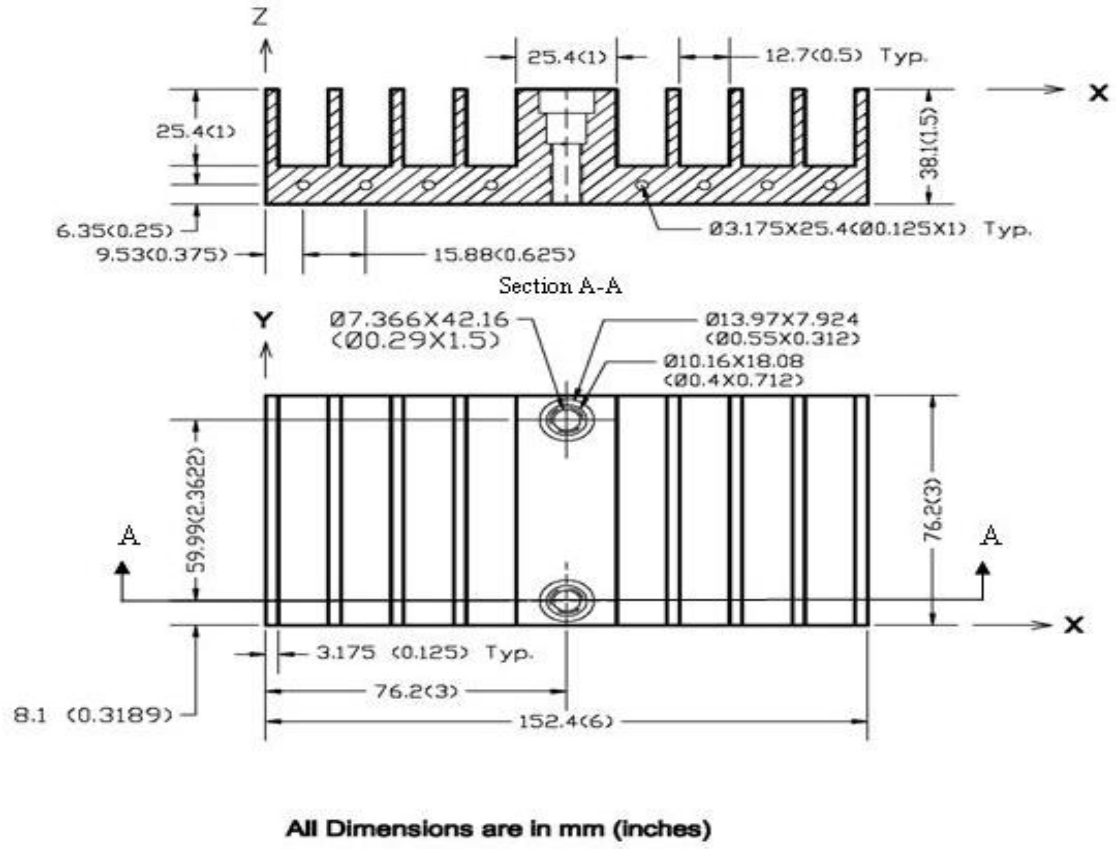

Figure 2. Workpiece design for slot end-milling experiments

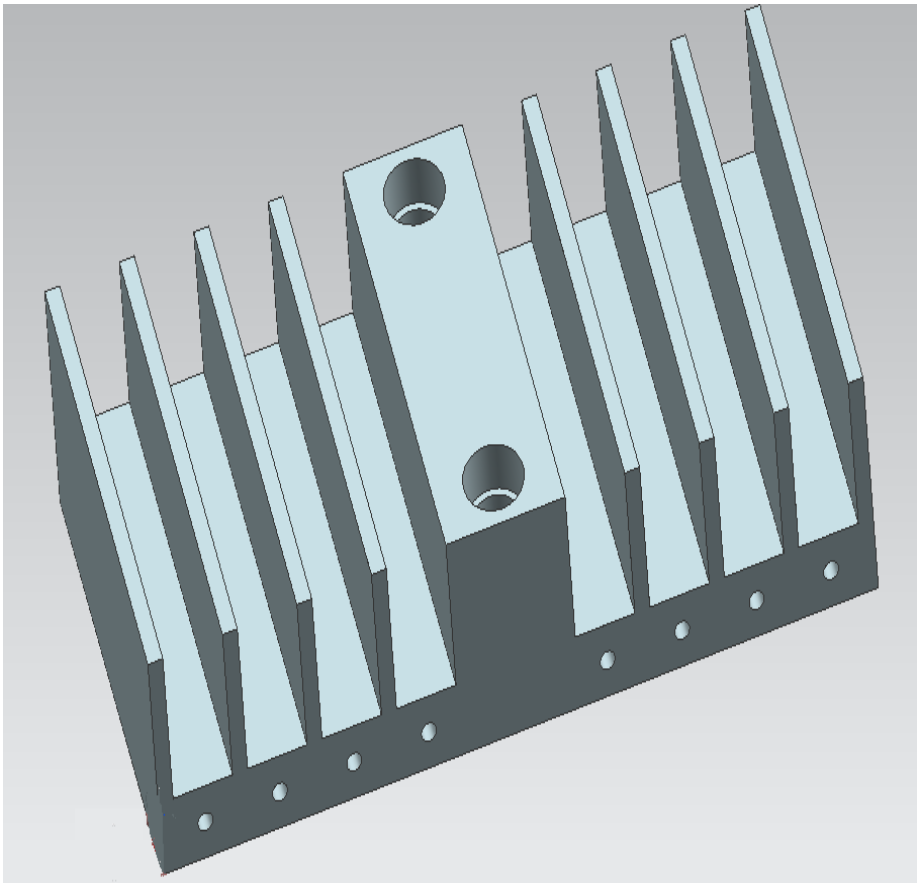

Figure 2. Workpiece design for slot end-milling experiments (cont.)

The CNC program containing the G & M codes for machining run #1 (slot #1) in inch unit is given below

: T1 M6;

N10 G01 X0.375 Y-1 Z1 F50;

N20 G01 Z-0.05 F10; (Pass #1)

N30 S250 M03

N40 G01 Y3.7 F1

N50 G01 Z1 F50

N60 G01 X0.375 Y-1 F50

N70 G01 Z-0.1; (Pass # 2)

N80 G01 Y3.7 F1

N90 G01 Z1 F50

N100 G01 X0.375 Y-1 F50

N110 G01 Z-0.15; PASS # 3

N120 G01 Y3.7 F1

N130: G01 Z1 F50

N140: G01 X0.375 Y-1 F50

N150: G01 Z-0.2 F10; PASS # 4

N160: G01 Y3.7 F1

N170: G01 Z1 F50

N180: G01 X0.375 Y-1 F50

N190: G01 Z-0.25 F10; PASS # 5

N200: G01 Y3.7 F1

N210: G01 Z1 F50

N220: G01 X0.375 Y-1 F50

N230: G01 Z-0.3 F10; PASS # 6

N240: G01 Y3.7 F1

N250: G01 Z1 F50

N260: G01 X0.375 Y-1 F50

N270: G01 Z-0.35 F20; PASS # 7

N280: G01 Y3.7 F1

N290: G01 Z1 F50

N300: G01 X0.375 Y-1 F50

N310 G01 Z-0.4 F10

N320 G01 Y3.7 F1

N330 G01 Z1 F4

N340 G01 X0.375 Y-1 Z-0.45 PASS #9

N350 G01 Y3.7 F1

N360 G01 Z1 F50

N370 G01 X0.375 Y-1 Z-0.5 PASS #10

N380 G01 Y3.7 F1

N390 G01 Z1 F4

This process of increasing the axial depth of cut incrementally was continued until a slot depth of 1 inch was attained.

4. RESULTS, ANALYSIS AND DISCUSSIONS

For each experimental run, the acquired cutting force components (F_x, F_y, F_z) for passes 1, 2, 10, 15, 19, and 20 were acquired, which corresponds to machining lengths of 76.2, 152.4, 762, 1143, 1447.8, and 1524 mm respectively. The signals obtained were filtered using an 8-point moving average to remove extraneous noises and bring out the major signal patterns in the time domain. The maximum value for each cutting force component was also determined. The maximum cutting force data for pass numbers 1 and 2 were used as first and second replicates in conducting ANOVA to analyze the effects of machining parameters and cooling strategies on cutting force components. Additionally, the maximum cutting force data for the 19^{th} and 20^{th} passes were used as first and second replicates in conducting ANOVA to analyze tool wear indirectly. The 10^{th} and 15^{th} passes were used for plotting purposes in order to see the overall progression of cutting forces from the first pass to the twentieth pass.

4.1. MAXIMUM CUTTING FORCE COMPONENTS VERSUS LENGTH OF CUT FOR EACH EXPERIMENTAL RUN

Figure 3 shows a representative sample of acquired cutting force components signals, for the 15^{th} pass (1143 mm length of cut) using medium speed of 500 rpm and low feed rate of 1 ipm (25.4 mm/min) with LN_2 cooling strategy.

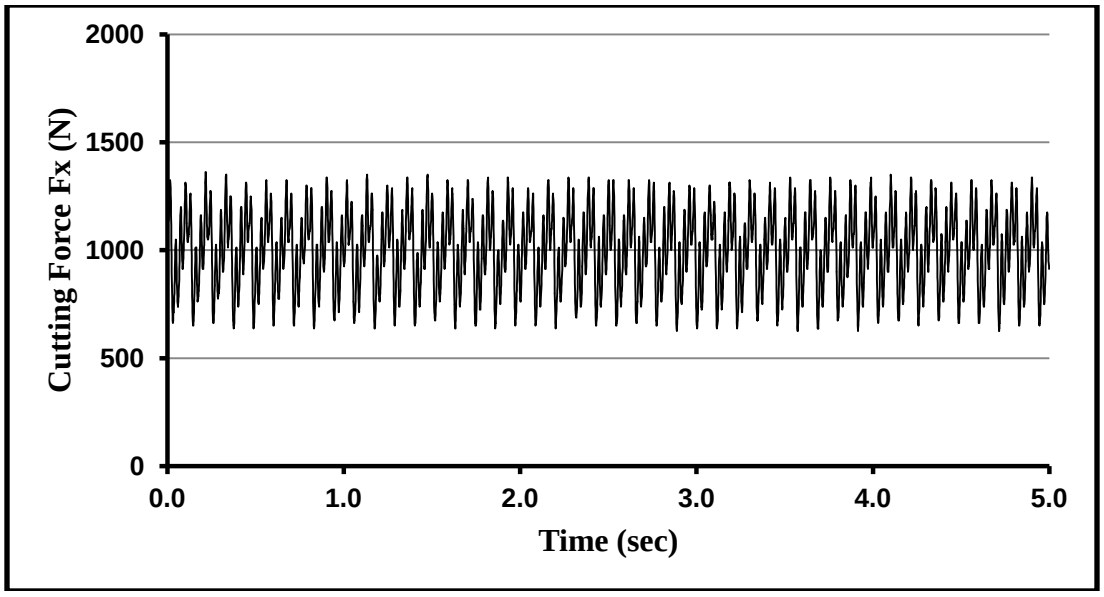

a. Signal of cutting force component F_x (LN2, n = 500 rpm, F = 1 ipm)

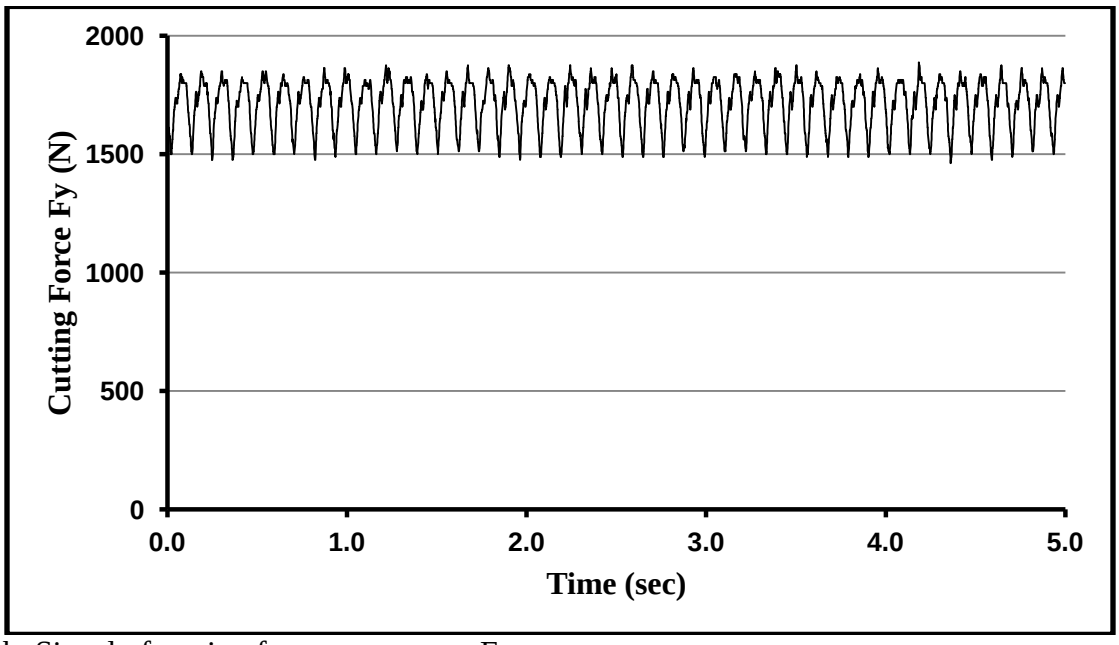

b. Signal of cutting force component F_y

Figure 3. Cutting force components for LN_2, 500 rpm and 1 ipm

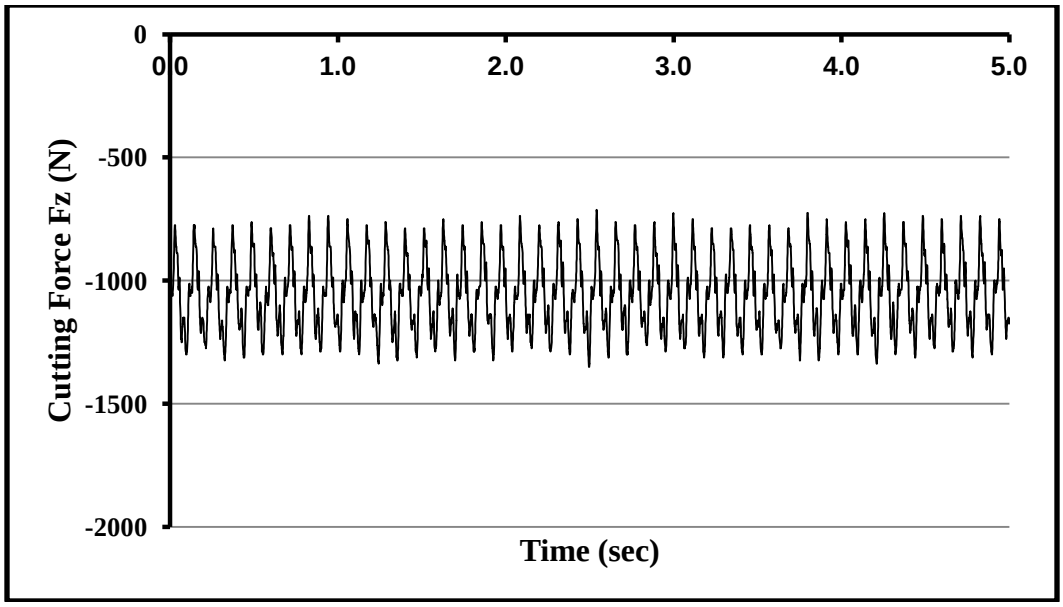

c. Signal of cutting force component F_z

Figure 3. Cutting Force components for LN_2, 500 rpm and 1 ipm. (cont.)

The acquired cutting force signals for each experimental run was processed for each cutting force component, and the maximum cutting force was obtained for each machining length/pass acquired. The maximum force was plotted against machining lengths for each of the 3 force components. For each experimental run, the 3 cutting force components were superimposed and analyzed.

4.2. LN_2 COOLING STRATEGY

Figure 4, 5, and 6 show the plots of the maximum cutting force component versus length of cut for all experimental runs using LN_2 cooling strategy.

4.2.1. Maximum Cutting Force Components Variation for LN_2 cooling at Low Spindle Speed (250 rpm) & Medium Feed rate (2 ipm)

Figure 4 shows the plot of maximum cutting force components (F_x, F_y, and F_z) for LN_2 cooling strategy at spindle speed of 250 rpm and feed rate of 2 ipm,

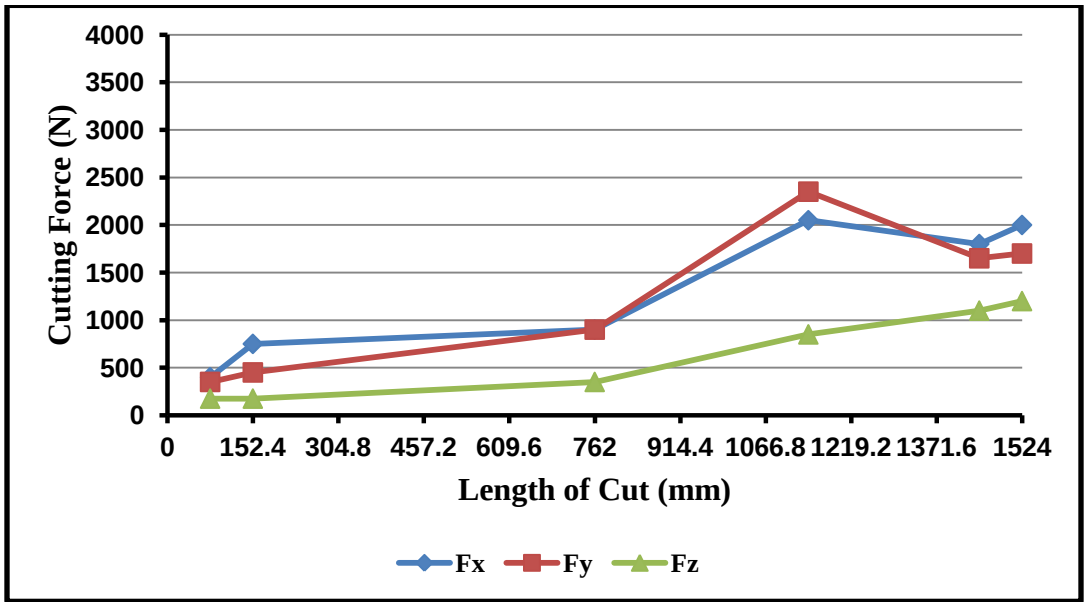

Figure 4. Plot of maximum cutting force components for LN_2 cooling at 250 rpm and 2 ipm

The plot shows the force component F_x (400 N) to be higher than F_y (350 N) with F_z (175 N) being the least for most of the length of cut. For the last pass (20th pass), corresponding to 1524 mm length of cut, the maximum cutting force components are 2000, 1700, 1200 and 2886.2 N for F_x, F_y, F_z and F_r respectively. Sparks and tool wear were minimal for most of the cutting lengths, and the chips produced were shinny for the entire machining length. The low speed of 250 rpm was responsible for the very low wear on the cutting edges, as well as for the absence of sparks for most of the machining length. Sparks became more visible from 1143 mm length of cut, and increased steadily but was not large enough to cause a drastic chipping of the cutting edges. This is because LN_2 was very effective in removing the heat generated while machining with a low speed

of 250 rpm. However, this experimental run was marked by lots of vibrations, which caused the acquired signals to increase drastically from the 10^{th} pass (762 mm length of cut). The reason for the vibration may be due to the fact that the medium feed of 2 ipm was too fast for the low speed of 250 rpm. Lastly, it was observed that cutting force F_x was highest for a majority of the entire machining length. This is because the speed of 250 rpm was low enough to prevent severe wear, which would have caused a drastic jump in F_y and F_z.

4.2.2. Maximum Cutting Force Components Variation for LN_2 cooling at Medium Spindle Speed (500rpm) and Low feed rate (1ipm)

Figure 5 shows the plot of maximum cutting force components for LN2 at medium spindle speed of 500 rpm and low feed rate 1 ipm.

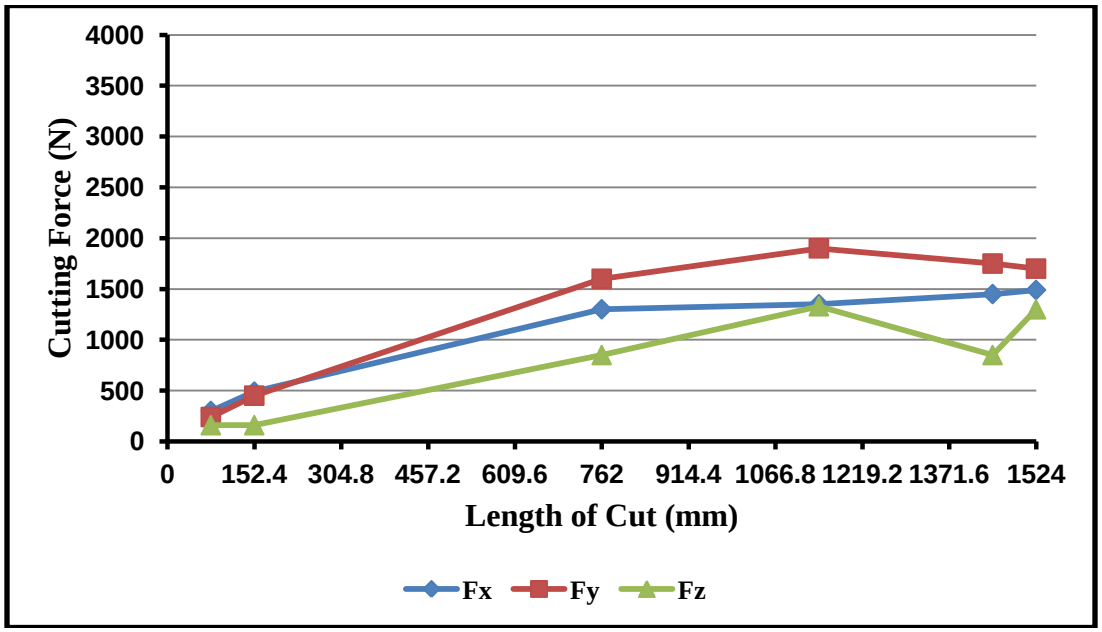

Figure 5. Plot of maximum cutting force components for LN_2 cooling at 500 rpm and 1 ipm

The plot shows the feed force F_y to be higher than the other 2 force components F_x and F_z for all the lengths of cut. At 76.2 mm and 152.4 mm lengths of cut, F_x was higher than F_y with F_z being the least. However, with an increase in length of cut up to

762 mm and with greater tool wear, F_y gradually overtook F_x and F_z also rising sharply but still being the least. This follows that with an increase in tool wear, F_y and F_z tend to increase drastically with F_y overtaking F_x. This experimental run was characterized by formation of burrs at the end of the slot, and high cutting temperature which was evident with bright sparks, especially beginning from 609.6 mm length of cut. Furthermore, chipping of the cutting edges was drastically increased compared to machining with at spindle speed of 250 rpm. This is because cutting speed is a major determinant of tool life, and an increase in cutting speed leads to more tool wear, and thus a reduction in tool life. The maximum cutting force components F_x, F_y, F_z and F_r varied from 300, 240, 160, and 416.2 N for the first pass to 1490, 1700, 1300 and 2607.7 N for the 20th pass.

4.2.3. Maximum Cutting Force Components Variation for LN_2 cooling High Spindle Speed (750rpm) and High feed rate (3ipm)

Figure 6 shows the plot of cutting force components for LN_2 cooling at high spindle speed (750 rpm) (30 m/min) and high feed rate of (3 ipm) (76.2 mm/min).

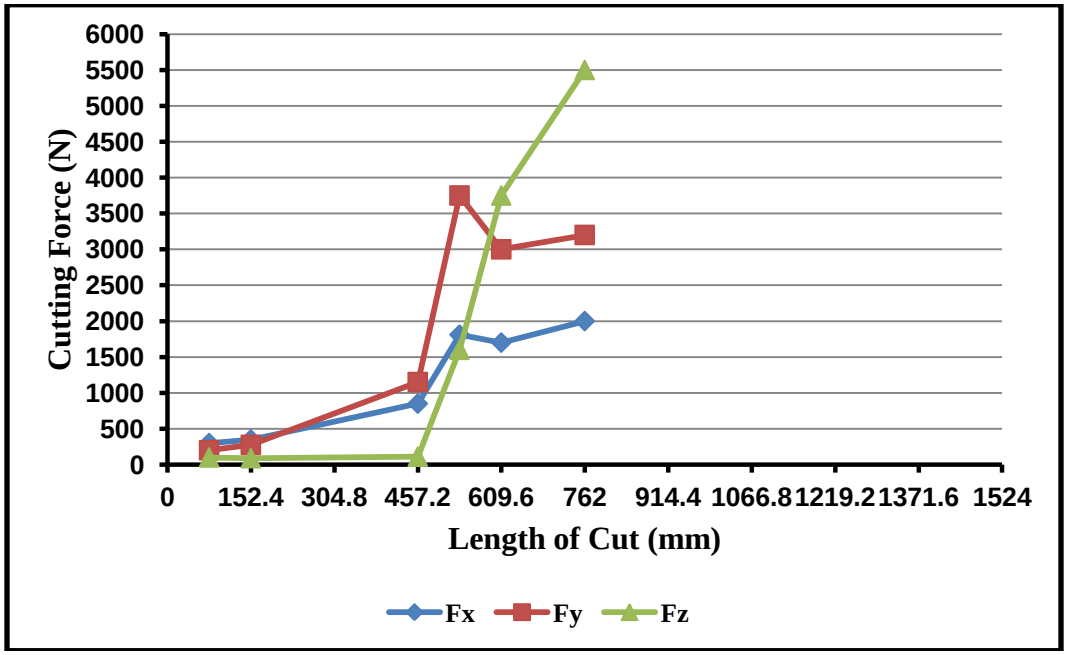

Figure 6. Plot of maximum cutting force components for LN_2 cooling strategy at 750 rpm and 3 ipm

This experimental run generated the highest cutting forces among the 3 LN_2 cooling conditions. These extreme machining parameters had the most adverse effects on the cutting tool. At initial lengths of cut 76.2 mm and 152.4 mm, F_x was higher than F_y with F_z being the least as is usually the case when the cutting edges hasn't suffered severe wear. However, beyond 152.4 mm and up to 457.2 mm lengths of cut, F_y overtook F_x and F_z to become the most dominant cutting force component. This is because a drastic increase in tool wear causes F_y to rise sharply and surpass F_x to become the dominant force component. At this length of cut, burrs were produced in the slot and the chips were burnt in brownish-black coloration. Also, with increase in machining length up to 609.6 mm and with more severe wear of the cutting edges, the chips produced became shorter and burnt in completely black coloration and F_z surpassed F_y and F_x to be the most sensitive to tool wear. This is the only case among the 3 LN_2 cooling conditions where F_z overtook F_x and F_y. This means that while an increase in tool wear causes F_Y to rise above F_X, severe tool wear triggered by extreme machining parameters can cause F_z to rise even higher, above F_x and F_y to become the most dominant force component. In this experimental run, high speed of 750 rpm (30 m/min) and high feed rate of 3 ipm (76.2 mm/min) led to massive chipping of the tool's cutting edges and generated an enormous amount of heat. This caused particles from the work-piece to be welded to the cutting flutes, and started acting like a part of the cutting flute, which in turn led to more abrasive wear, increase in coefficient of friction, and consequently a drastic increase in cutting forces. By the time the tool reached 762 mm length of cut (10^{th} pass), all the cutting flutes were burnt completely and the flutes had undergone complete plastic deformation at the cutting edges. At this stage, the tool was no longer cutting but just rubbing on the slot

producing thick curly peels of burnt metal instead of chips. The tool had obviously exceeded its life, and machining was terminated. This again reaffirms the fact that cutting speed is the major determinant of tool life and that LN_2 cooling strategy was not efficient in removing the amount of heat generated in the cutting zone while machining Inconel 718 at a high speed of 750 rpm. This machining condition therefore, is not recommended for performing slot end-milling Inconel 718 using uncoated carbide tools. The cutting force components F_x, F_y, F_z, varied from 300, 200, 100 N for the first pass to approximately 2000, 3000, 5500 N respectively for the 10^{th} pass before the tool broke.

4.3. MQL COOLING STRATEGY

Figure 7, 8, and 9 show the plots of maximum cutting force components versus length of cut for all experimental runs using MQL cooling strategy.

4.3.1. Maximum Cutting Force Components Variation for MQL cooling at Low Spindle speed (250 rpm) and Low Feed rate (1ipm)

Figure 7 shows the plot of maximum cutting force components (F_x, F_y, & F_z) during machining with low spindle 250 rpm (10 m/min) speed and low feed rate 1ipm.

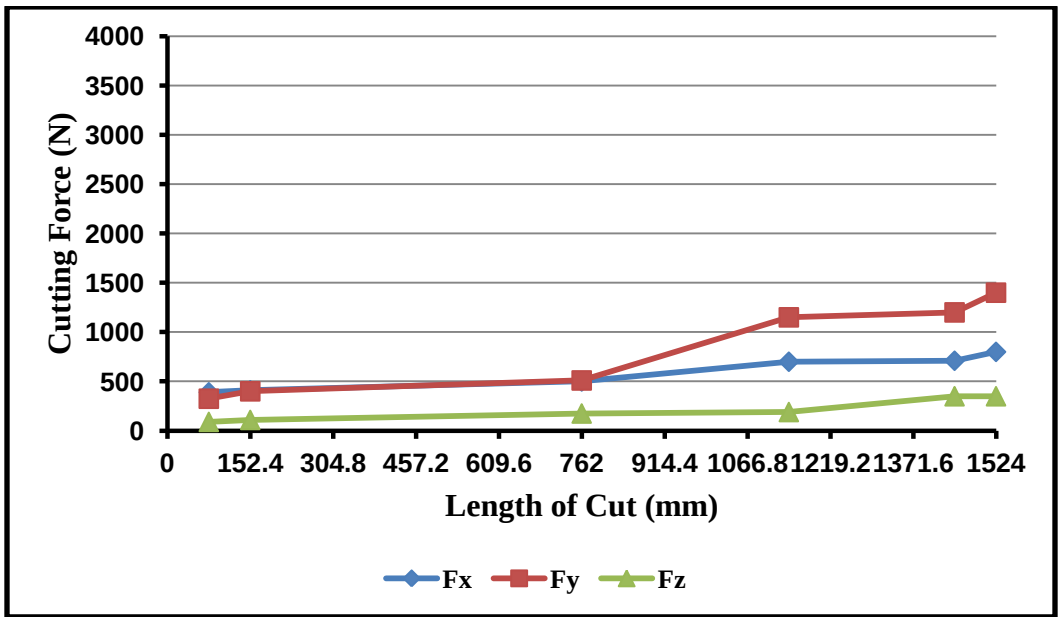

Figure 7. Plot of maximum cutting force components for MQL cooling strategy at 250 rpm and 1 ipm

The plot shows that F_x starts out higher than F_y with F_z being the least force component. However, as the length of cut increased up to 762 mm with a corresponding increase in tool wear, F_y caught up with F_x, while F_z was still the least force component. Beyond 762 mm, F_y surpassed F_x to become the most dominant cutting force component, with F_z rising but still lagging behind F_x. The machining length where F_y overtook F_x was marked by an increase in tool wear; however, tool wear was not severe enough to cause a drastic increase in F_z as has been observed when machining with extreme machining parameters. Tool wear in this experimental run was minimal for all machining passes, and there wasn't any formation of burrs and Built up Edges (BUE). However, beyond the machining length of 762 mm, the cutting flutes wore faster, with an accompanying rise in cutting temperature which was evident in increased sparks. This corresponds to the point where F_y remarkably rose higher than F_x and F_z. Also, during the initial stages of machining, the chips produced were shinny and curled in a distinctive C-shape. However, as the cutting temperature increased due to tool wear, this C-shape became less pronounced and eventually led to the chips being straightened out, in addition to being slightly burnt. The reason is that with sustained machining time, MQL was no longer efficient in removing the enormous amount of heat generated in the cutting zone. MQL's ability to improve machining is more due to its excellent lubricating qualities than its cooling qualities. Therefore, with severe wearing of the cutting edges, and an increase in coefficient of friction, MQL was not able to keep up with the massive heat generated. However, the low machining parameters ensured that the tool was still in good condition after reaching a machining length of 1524 mm with no built up edge and chipping along the flute. It was also responsible for the relatively low cutting force components

generated. This was one of the best machining conditions and is very highly recommended. The cutting force components F_x, F_y, F_z and F_r varied from 390, 325, 90, and 515.6 N for the first pass to 800, 1400, 350, and 1650 N respectivelt at the 20th pass.

4.3.2. Maximum Cutting Force Components Variation for MQL cooling at Medium Spindle Speed (500 rpm) and High Feed rate (3 ipm)

Figure 8 shows the plot of maximum cutting force components (F_x, F_y, & F_z) for medium and high spindle speed and feed respectively.

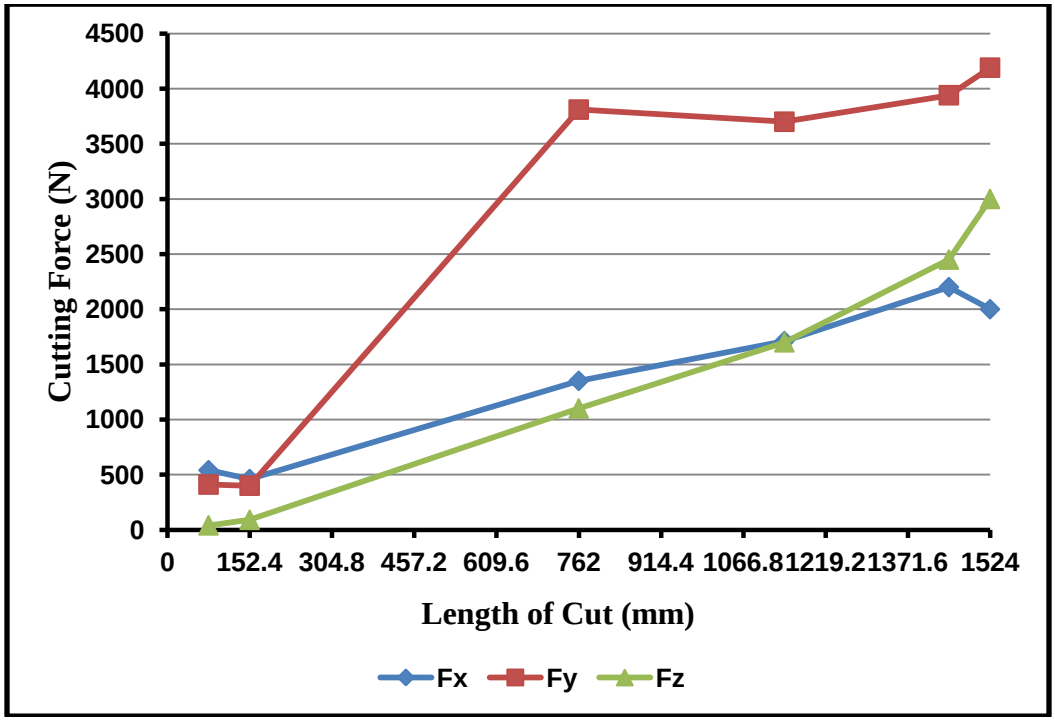

Figure 8. Plot of maximum cutting force components for MQL, 500 rpm and 3 ipm

The plot shows F_x to be higher than F_y at initial length of cut of 76.2mm, with F_z being the least. However, after length of cut of 152.4 mm, there was a significant increase in tool wear, which was responsible for F_y surpassing F_x to become the most dominant force component. In addition, F_z rose sharply and tried to catch up with F_x. Furthermore, at 1143 mm length of cut, F_z finally caught up with F_x and overtook it to become the

second most dominant cutting force component. This observation is consistent with previous observations made and shows that severe tool wear has significant effect on F_y, and causes it to be the most dominant cutting force component with F_z rising also to become the 2^{nd} most dominant and sensitive to tool wear. However, with more increase in machining length of cut, and a corresponding increase in tool wear, F_z will rise and surpass F_x and may even catch up with F_y and overtake it if more wear is induced. The chips produced during this experimental run were long in the early passes, but gradually became shorter and burnt in bluish coloration leading up to a machining length of cut of 762 mm. Also, from 762 mm to 1143 mm length of cut, the tool was no longer machining but peeling out material from the right rib of the slot. This caused the right rib of the slot to be rough and enlarged a little, and resulted in it being cut like a ramp. This anomaly corrected itself subsequently from pass 15 (1143 mm length of cut) and beyond. The reason for this anomaly may be due to the possibility that during the lengths of cut leading up to 762 mm length of cut where there was a drastic increase in F_y; there was an accompanying rise in temperature which caused some of the chips to be temporarily welded on the cutting edges. These chips caused the size of the cutting flutes to be increased slightly and this may have caused the cutting flutes to enlarge the slot during machining as a result. Then beyond 1143 mm length of cut, the chips may have fallen off the tool edges and the tool returned to its normal size, which resulted in the slot returning to its normal width. Secondly, it could be that the heat produced from 762 mm to 1143 mm length of cut was high enough to have caused a little expansion of the tool, which resulted in the increase of the width of the slot during machining. This anomaly needs further investigation. Lastly, beyond 1143 mm and up to 1524 mm length of cut, chips

produced were very short and completely burnt in black coloration. The cutting force components F_x, F_y, F_z and F_r varied from 540, 410, 40 and 679.2 N for the first pass to 2000, 4190, 3000, and 5527.8 N respectively for the 20th pass.

4.3.3. Maximum Cutting Force Components Variation for MQL cooling at High Spindle (750 rpm) and Medium Feed rate (2 ipm)

Figure 9 shows the plot of maximum cutting force components while machining in high speed (750 rpm) medium feed rate (2 ipm) and MQL cooling strategy.

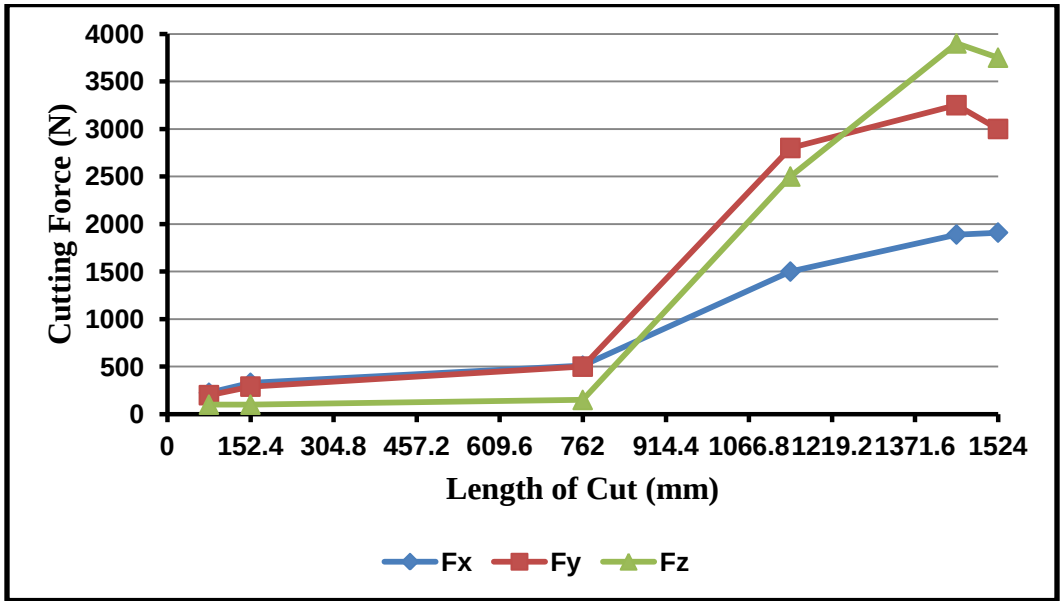

Figure 9. Plot of maximum cutting force components for MQL, 750 rpm and 2 ipm

The plot shows F_x to be slightly higher than F_y and F_z for machining lengths of 76.2 mm and 152.4 mm and up to 762 mm. It shows the 3 cutting force components having a gradual increase from a machining length of 76.2 mm to 762 mm. This gradual increase signifies a gradual tool wear as against a more drastic or severe one. Beyond the cutting length of 762 mm, the 3 cutting force components show a more drastic increase with F_y surpassing F_x, and F_z also overtaking F_x. The drastic increase in F_y and F_z was as a result of an increase in tool wear due to severe chipping of the tool flutes. At a machining length of 1219.2 mm, F_z rose sharply and surpassed F_y to be the most dominant force component, and was so for the rest of the machining length. The steep

rise of the slope of F_z to become the dominant cutting force component was as a result of extreme tool wear due to excessive chipping of the tool flutes. This once again is consistent with previous observations made for extreme machining conditions. The result shows that F_x will usually be higher than F_y with F_z being the least as long as the tool flutes are not severely worn. However, with more machining time and accompanying tool wear, F_y will rise above F_x to become the most dominant cutting force component, with F_Z also rising sharply and approaching F_x. Furthermore, with even more machining time and severe tool wear, F_z tends to increase drastically until it surpasses F_x and F_y to be the most dominant cutting force component. The tool used was heavily burnt in black coloration and had the presence of built up edges (BUE) around the four flutes. Also, the chips produced were very black and slightly elongated. This was because of the enormous amount of temperature generated. Lastly, the effect of speed on tool life was evident in this experimental run. It was observed that tool wear was more drastic for a high speed of 750 rpm, compared to low and medium speeds of 250 rpm and 500 rpm respectively. There was more massive chipping of the cutting edges for a high speed of 750 rpm, compared to the previous low and medium speeds. This means that the tool wore faster when machining in high speed, which reaffirms the effect of cutting speed on tool life. An increase in cutting speed when machining Inconel 718 will adversely affect tool life. MQL cooling strategy was not very effective in reducing the amount of heat generated when machining Inconel 718 at a high speed of 750 rpm.

4.4. MQL+LN_2 COOLING STRATEGY

Figure 10, 11, and 12 give the plots for maximum cutting force component for all experimental runs using combined (MQL+LN_2) cooling strategy.

4.4.1. Maximum Cutting Force Components Variation For combined (MQL+LN_2) cooling at Low Spindle Speed (250 rpm) and High Feed Rate (3 ipm)

Figure 10 shows the plot of maximum cutting force components for combined (MQL+LN_2) cooling at low spindle speed of 250 rpm and high feed rate of 3 ipm.

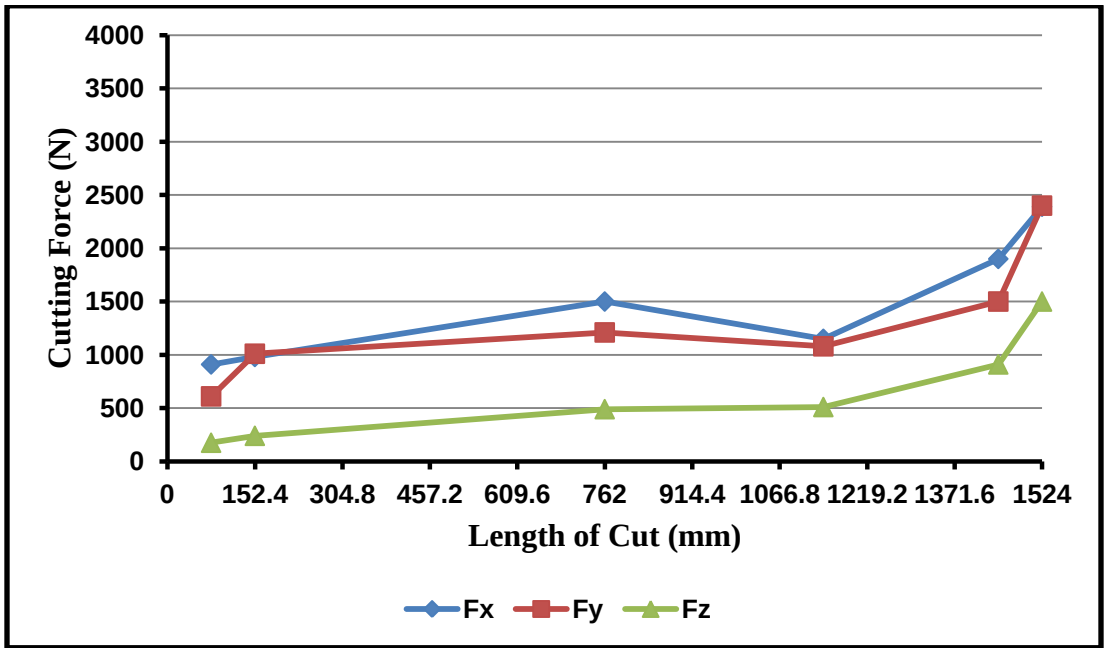

Figure 10.Plot of maximum cutting force components for MQL+LN_2, 250 rpm and 3 ipm

The plot shows that F_x to has the steepest increase from 76.2 mm to 762 mm length of cut, with F_y and F_z having a more gradual increase. Again, at a low machining speed of 250 rpm F_X was consistently greater than F_y with F_z being the least. This is because tool wear is moderate while machining at low speed, as compared with the severe tool wear obtainable during machining at high speed. For the entire 1524 mm length of cut, the wear induced in the cutting flutes was not enough to cause a drastic increase in F_y & F_z. Also, sparks were minimal during this machining condition and were only evident from a machining length of 1143 mm, which corresponds to the point where some chipping on the edge of the flutes was observed. The low spindle speed of 250 rpm (10 m/min) was very efficient in machining, and did not generate too much heat, which would have caused massive wear of the tool throughout most of the machining lengths.

Tool was still in a good condition with only slight chipping observed on the edges, while its color was still intact. The chips, however, was shinny for the most part but became a little burnt from 1447.8 mm to 1524 mm lengths of cut. For this machining condition, lots of vibration and noise were generated. This could be because the speed of 250 rpm was too slow for a fast feed rate of 3 ipm (76.2 mm/min), and so forced the machine tool to make a lot of noise as it laboriously tried to machine the slot. This severe vibration and noise were responsible for the seemingly high signals captured by the dynamometer. Therefore the high value of the signals captured for this experimental run, had more to do with vibration and noise than on the effects of tool wear. Lastly, the combined (MQL+ LN_2) was very efficient in removing the enormous amount of heat generated in the cutting zone. It combines the cooling quality of LN_2 with the excellent lubricating qualities of MQL in one piece. The maximum cutting force components Fx, Fy, Fz and Fr varies from 910, 610, 175, and 1109.4 N for the first pass to 2390, 2400, 1500, and 3704.3 N respectively for the 20^{th} pass.

4.4.2. Maximum Cutting Force Components Variation for MQL+LN_2 cooling Medium Spindle Speed (500 rpm) And Medium Feed Rate (2 ipm)

Figure 11 shows the plot of maximum cutting force components (F_x, F_y, and F_z) for combined (MQL+LN_2) cooling at medium speed of 500 rpm, and medium feed rate of 2 ipm.

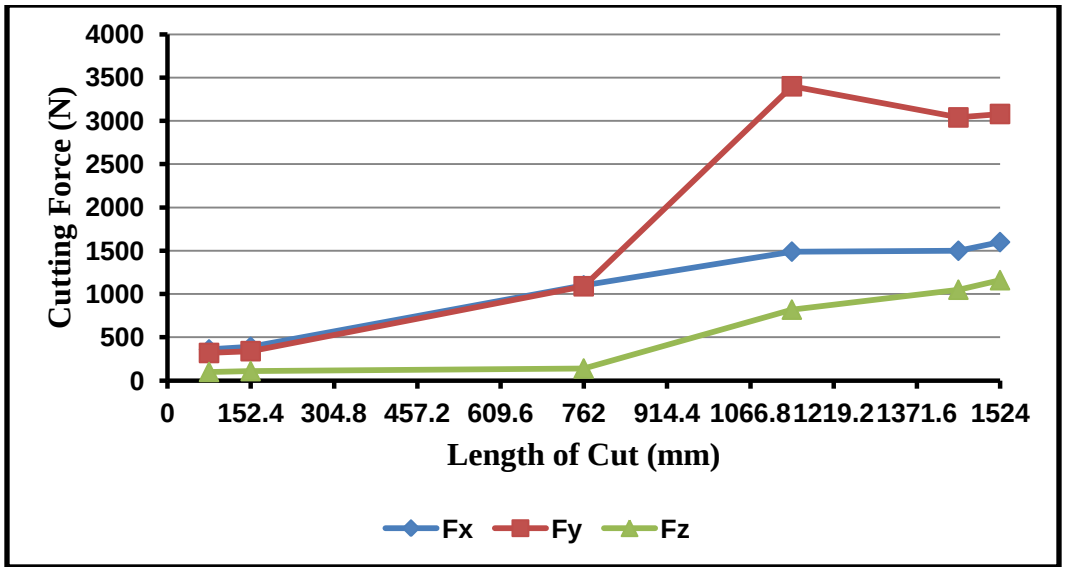

Figure 11. Plot of maximum cutting force components for MQL+LN_2, 500 rpm and 2 ipm

The plot shows that between 76.2 mm and 762 mm length of cut, the slope of F_y and F_x rose sharply, while that of F_z was fairly constant. Furthermore, F_x was slightly higher than F_y at the initial lengths of machining, with F_z being the least. Beyond 762 mm length of cut, F_y surpassed F_x and became the dominant cutting force component. In addition, F_Z rose steeply and tried to catch up with F_x. This is because there was massive increase in tool wear beyond the machining length of 762 mm, which led to a drastic increase in F_y and F_z. This again lends credence to previous observations made, which showed the effect of tool wear on F_y and F_z. As tool wear increases, F_Y tends to overtake F_x with F_z also rising. The increase in tool wear was as a result of the increased temperature at the cutting zone, which led to an increase in the chipping of the edge of the flutes. Sparks began to be visible from 762 mm length of cut, and increased towards 1524 mm length of cut. The enormous amount of heat generated at the cutting zone led to the chips being burnt in black coloration leading up to 1143 mm length of cut and beyond. The adverse effect of the increased speed to 500 rpm was evident on the tool life,

compared to when a low speed of 250 rpm was used. This was evident in the increased chipping of the cutting edge when machining with a speed of 500 rpm as compared to a speed of 250 rpm. From the plot, it is seen that the maximum cutting force for F_y was at 1143 mm length of cut. This maximum cutting force dropped subsequently as the tool progressed towards 1447.8 mm length of cut. The reason for this sudden increase and reduction may be due to the fact that during slot end milling of hard-to-cut Inconel 718 alloys, a lot of rough edges, protruding strands of work-piece material, and burrs are sometimes left behind at the corners and edges of the slots. When the tool meets any of these rough edges, burrs or protruding material strands left in a previous pass, it has to exert greater amount of force to remove it, which could lead to a very large increase in cutting force for that pass. This is because that extra rough edge at the corner of a slot presents increased hardness for the tool to machine, and this is what is evident in the increased cutting force. After the rough edge is removed, the cutting force may drop in subsequent passes if there are no more workpiece material protrusions or rough edges produced during those passes. The maximum cutting force components Fx, Fy, Fz and Fr varied from 360, 319, 100, and 491.3 N for the first pass to 1600, 3080, 1160, and 3659.5 N

4.4.3. Maximum Cutting Force Components Variation for combined MQL+LN_2 cooling at High Spindle Speed (750 rpm) and Low Feed Rate (1 ipm)

Figure 12 shows the plot of the maximum cutting force components for combined (MQL+LN_2) cooling at high spindle speed (750 rpm) and low feedrate 1 ipm (25.4 mm/min).

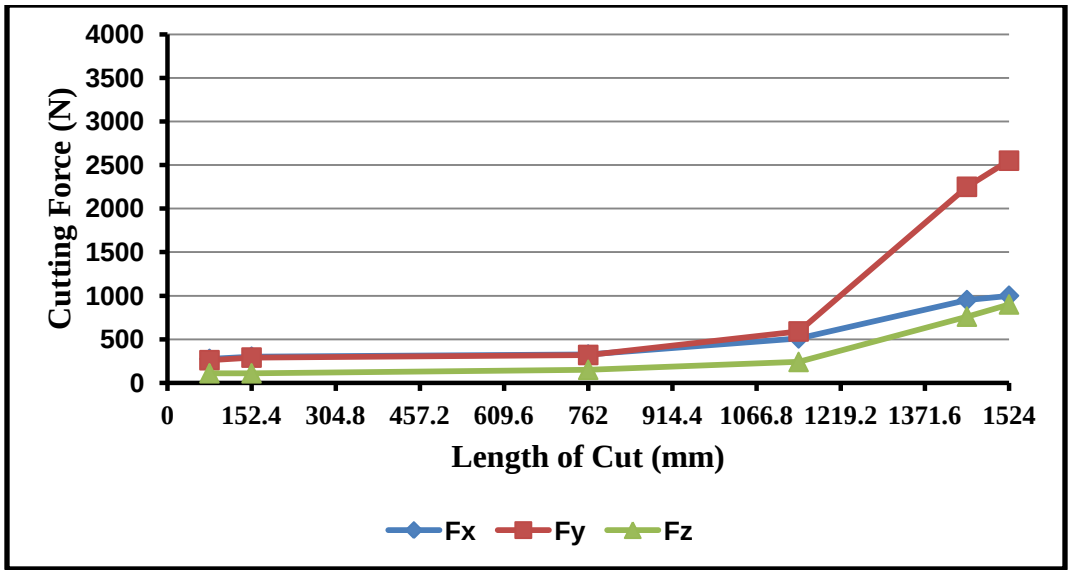

Figure 12. Plot of maximum cutting force components for MQL+LN_2, 750 rpm and 1 ipm

The plot shows that between 76.2 mm and 762 mm length of cut, the slope of F_x, F_y, and F_z were fairly constant. This means that the effects of tool wear on cutting force was moderate between these machining lengths. In addition, F_x was slightly higher than F_y and also higher than F_z, which is consistent with previous observations made during initial stages of machining. Also, within the same machining length, there were no visible sparks as the temperature generated was minimal, and the tool was still in very good condition, as there was little or no tool wear. However, beyond 762 mm and up to 1143 mm length of cut, the effects of tool wear began to take its toll on the cutting tool, which was evident in the gradual increase in the slope of F_x, F_y, and F_z. This period was marked by the presence of little sparks and the tool was slightly worn with little chipping observed along the cutting edges. Furthermore, F_y surpassed F_x to be the most dominant cutting force component, but the chips were still clear. With more machining time beyond 1219.2 mm length of cut, the three cutting force components had a sharp increase in slope with F_y increasing the steepest. At this point, there were visible signs of tool

wear on the cutting flutes, with the tool being burnt in brown coloration and the chips being burnt in black coloration. This was as a result of an increase in coefficient of friction which came about as a result of increased tool wear, which in turn led to increased temperature in the cutting zone. At 1524 mm length of cut, F_z came close and almost equaled F_x. This period most likely corresponds to a stage where severe wear was about to setting in. If machining had been sustained beyond a length of 1524 mm, it is likely Fz would have caught up and overtaken F_x. Furthermore, with more machining time and severe wear induced, F_z may tend to overtake F_y to be the most dominant force component. This has been found true with previous observations when machining with extreme parameters. In this case, the effect of machining with a high speed of 750 rpm was tempered by machining with a low feed of 1 ipm. This is why this machining condition was efficient. The combined (MQL+LN_2) cooling strategy was efficient in removing the heat generated from machining with a speed of 750 rpm and a feed of 1 ipm. This machining condition is good and highly recommended. The maximum cutting force components F_x, F_y, F_z, and F_r varied from 275, 260, 110, and 394.1 N for the first pass to 1000, 2550, 900, and 2883.1 N for the 20^{th} pass respectively.

4.5. EFFECTS OF MACHINING PARAMETERS AND COOLING STRATEGIES ON CUTTING FORCE COMPONENTS

Maximum cutting force values obtained at 76.2 mm (pass #1) and 152.4 mm (pass #2) lengths of cut were used as first and second replicates in conducting Analysis of Variance (ANOVA) in order to investigate the effects of machining parameters and cooling strategies on cutting force components (F_x, F_y, and F_z). Also, a Pareto chart was used to see the order of significance of each effect, while plots of marginal means and surface desirability were used to determine the values of the factors that gives the lowest

cutting force components, as well as to show a 3D plot of the desirability of the factors with respect to cutting force components. Tables 7 and 8 show the maximum cutting force values for all three cutting force components and resultant force for 76.2 mm (pass 1) and 152.4 mm (pass 2) lengths of cut respectively for all experimental runs.

Table 7. Maximum Cutting Force components for Pass 1 (76.2 mm)

		3 factors at 3 levels			Max. Cutting Forces			
Expt. Run	Treat. Comb.	Cooling Method	Speed rpm	Feed (ipm) mm/min	F_x (N)	F_y (N)	F_z (N)	F_r (N)
1	(0,0,0)	MQL	250	(1) 25.4	390	325	90	515.6
2	(0,1,2)	MQL	500	(3) 76.2	540	410	40	679.2
3	(1,0,1)	LN_2	250	(2) 50.8	400	350	175	559.6
4	(2,0,2)	MQL+LN_2	250	(3) 76.2	910	610	175	1109.4
5	(0,2,1)	MQL	750	(2) 50.8	225	200	100	317.2
6	(1,1,0)	LN_2	500	(1) 25.4	300	240	160	416.2
7	(1,2,2)	LN_2	750	(3) 76.2	300	200	100	374.2
8	(2,1,1)	MQL+LN_2	500	(2) 50.8	360	319	100	491.3
9	(2,2,0)	MQL+LN_2	750	(1) 25.4	275	260	110	394.1

Table 8. Maximum Cutting force components for pass 2 (152.4 mm)

		3 factors at 3 levels			Max. Cutting Forces			
Expt. Runs	Treat. Comb.	Cooling Method	Speed (rpm)	Feed (ipm) mm/min	F_x (N)	F_y (N)	F_z (N)	F_r (N)
1	(0,0,0)	MQL	250	(1) 25.4	410	400	110	583.3
2	(0,1,2)	MQL	500	(3) 76.2	460	400	90	616.2
3	(1,0,1)	LN_2	250	(2) 50.8	750	450	175	892
4	(2,0,2)	MQL+LN_2	250	(3) 76.2	980	1010	240	1427.6
5	(0,2,1)	MQL	750	(2) 50.8	330	290	100	450.6
6	(1,1,0)	LN_2	500	(1) 25.4	490	450	160	684.3
7	(1,2,2)	LN_2	750	(3) 76.2	350	275	90	454.1
8	(2,1,1)	MQL+LN_2	500	(2) 50.8	390	340	110	529
9	(2,2,0)	MQL+LN_2	750	(1) 25.4	300	290	110	431.5

4.5.1. Analysis of Variance (Anova)

Cutting force components data from the two tables above were entered into statistica 7, and used in performing ANOVA. A test for significance of all effects (main and interaction) was conducted using the p-values derived from ANOVA. For this experiment, the p-values of all effects were compared at significance level of 0.05. Tables 9, 10, and 11 present the results of ANOVA for cutting force component F_x, F_y and F_z.

Table 9. ANOVA for Cutting force F_x

Factor	ANOVA; Var. :F_x; R-sqr = 0.88189; Adj: 0.7769 3 3-Level factors, 1 block, 18 runs; MS Residual = 10297.22 DV: F_x				
	SS	df	MS	F	p
(1)cooling L+Q	65858.3	2	32929.2	3.19787	0.089287
(2)speed L+Q	279658.3	2	139829.2	13.57931	0.001915
(3)feed L+Q	100054.8	2	50027.4	4.85834	0.037073
1*2	89268.8	1	89268.8	8.66921	0.016371
1*3	22968.7	1	22968.7	2.23058	0.169508
Error	92675.0	9	10297.2		
Total SS	784650.0	17			

Table 10 ANOVA for cutting force component F_y

Factor	ANOVA; Var. :F_y; R-sqr = 0.80312; Adj: 0.62812 3 3-Level factors, 1 block, 18 runs; MS Residual = 13049.5 DV: F_Y				
	SS	df	MS	F	p
(1)cooling L+Q	77584.0	2	38792.0	2.972681	0.102050
(2)speed L+Q	157841.4	2	78920.69	6.047794	0.021639
(3)feed L+Q	87087.1	2	43543.55	3.336798	0.082382
1*2	73790.1	1	73790.08	5.654629	0.041367
1*3	7550.1	1	7550.08	0.578573	0.466332
Error	117445.5	9	13049.50		
Total SS	596546.5	17			

Table 11. ANOVA for cutting force component F_z

Factor	ANOVA; Var. :F_z; R-sqr = 0.90224; Adj: 0.81533 3 3-Level factors, 1 block, 18 runs; MS Residual = 406.9444 DV: F_z				
	SS	df	MS	F	p
(1)cooling L+Q	11575.00	2	5787.500	14.22184	0.001636
(2)speed L+Q	9013.10	2	4506.548	11.07411	0.003747
(3)feed L+Q	5159.52	2	2579.762	6.33935	0.019140
1*2	9352.08	1	9352.083	22.98123	0.000982
1*3	833.33	1	833.333	2.04778	0.186220
Error	3662.50	9	406.9444		
Total SS	37462.50	17			

Table 9 shows the combined linear and quadratic main effects of each of the factors, together with their two-factor interactions. From the results, only the main effects of spindle speed and feed have significant effects on F_x because their p-values are less than the significance level of 0.05. The main effect of cooling does not significantly affect F_x because its p-value is slightly higher than the significance level of 0.05. Furthermore, the two-factor interaction of cooling and speed has a significant effect on F_x, while the 2-factor interaction of cooling and feed does not significantly affect F_x. Additionally, Table 10 shows that only the main effect of speed significantly affects F_y. The main effects of cooling and feed do not have significant effects on F_y. Furthermore, the 2-factor interaction of cooling and speed significantly affects F_y, while the 2-factor

interaction of cooling and feed does affect F_y significantly. Lastly, figure Table 11 shows that the main effect of cooling, speed and feed all significantly affect F_z. Furthermore, the 2-factor interaction of cooling and speed also significantly affects F_z, while the 2-factor interaction of cooling and feed has no significance on F_z.

4.5.2. Pareto Chart of Effects on Cutting Force Components

A Pareto chart ranks each of the effects in order of their significance by using bars. Each bar represents an effect (main or interaction). Figure 13a, 13b and 13c presents the Pareto chart of effects on F_x, F_y, and F_z.

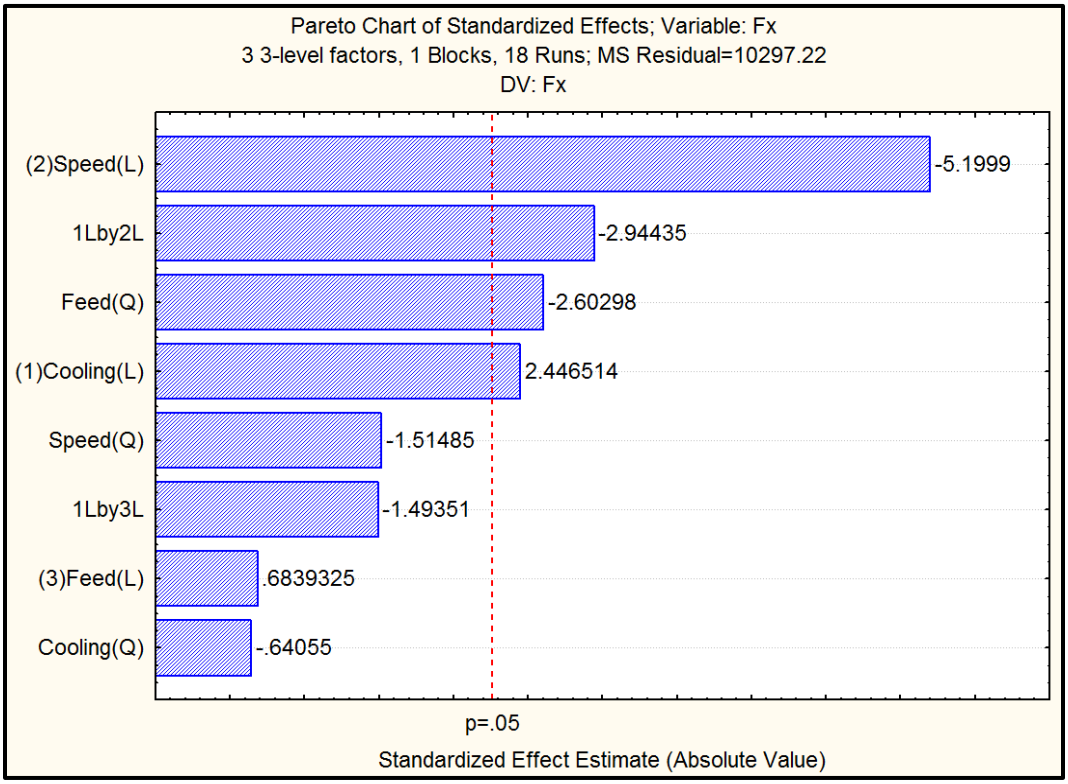

a. Cutting force component F_x

Figure 13. Pareto chart of effects on cutting force components.

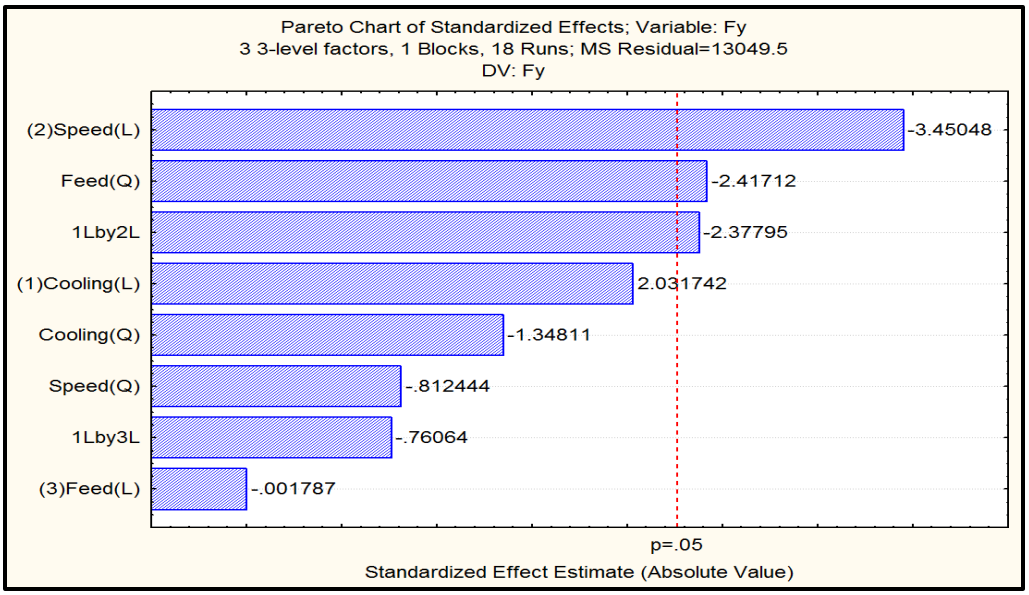

b. Cutting force component F_y

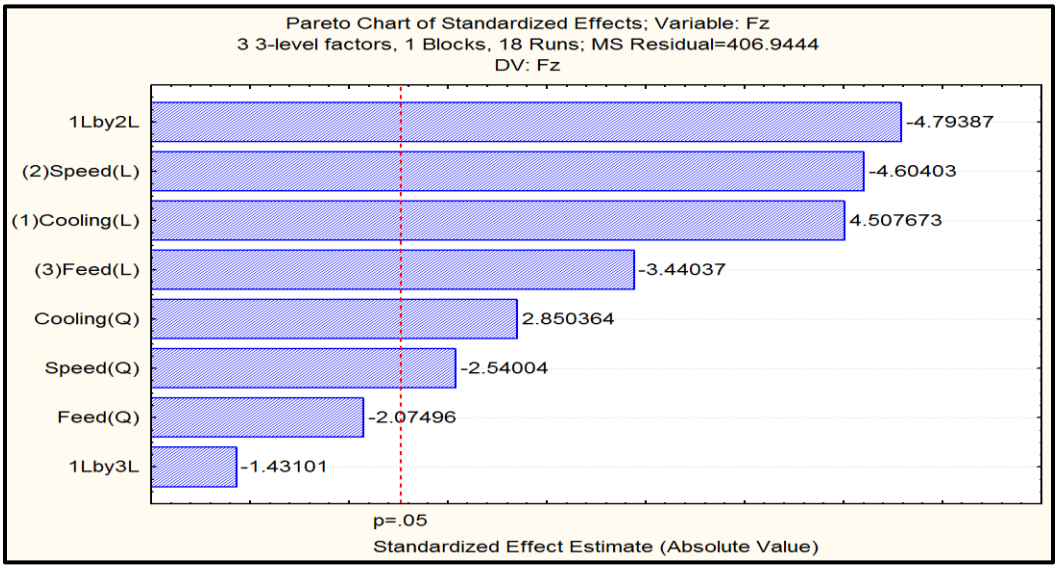

c. Cutting force component F_z

Figure 13. Pareto chart of effects on cutting force components (cont.)

The pareto chart of effects on F_x shows that linear effect of cutting speed has the most significant effect on F_x, followed by the 2-factor interaction of cooling and spindle speed, the quadratic main effect of feed and linear main effect of cooling are the 3rd and 4th most significant effects respectively. Similarly, that of F_y shows linear main effect of spindle speed to be the most significant effect, followed by the quadratic main effect of

feed, and the least being the 2-factor interaction of cooling and speed. Lastly, the 3rd plot in figure 13 shows that the most significant effect on F_z is the linear 2-factor interaction of cooling and speed, followed by the linear main effect of spindle speed. The linear main effect of cooling, linear main effect of feed, and the quadratic main effects of cooling and speed are the 3rd, 4th, 5th, and 6th most significant effects respectively.

4.5.3. Marginal Means Plot of Main Effects on Cutting Force Components

Figure 14 presents the marginal means plot for F_x, F_y, and F_z. The marginal means plot shows the profile for predicted values and desirability for the different factors and the response variable.

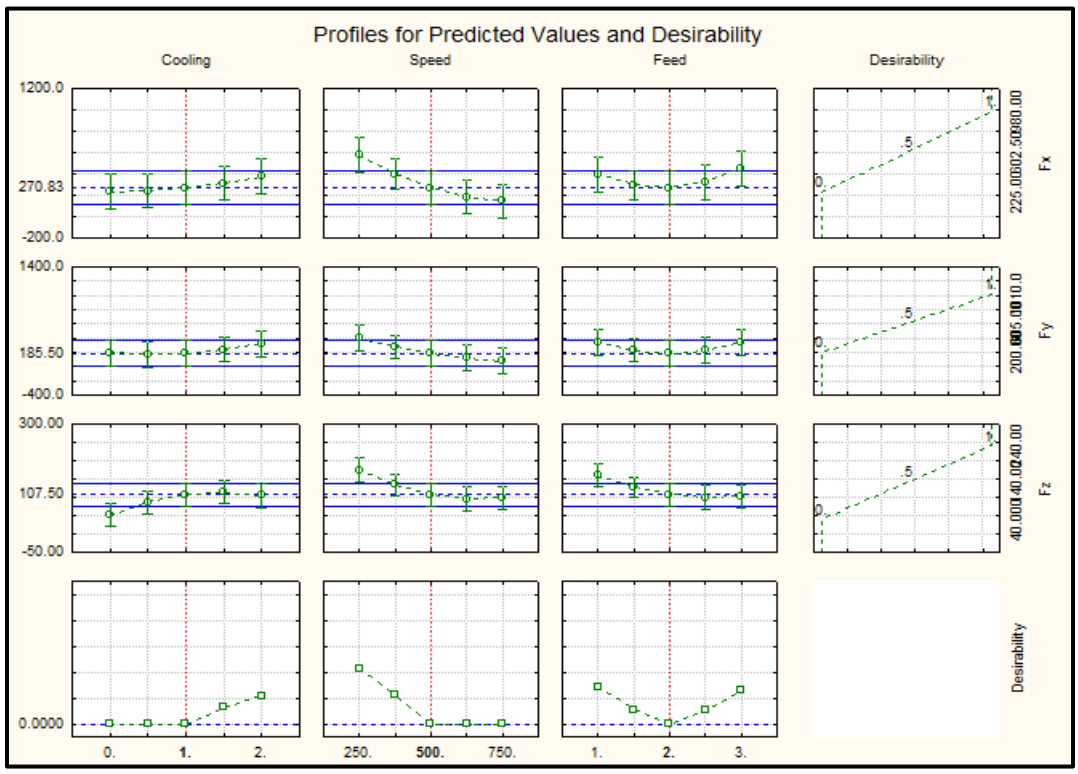

Figure 14.Marginal means plot of main effects on cutting force components

4.5.4. Effects of Cooling Strategies on Cutting Force Component F_x

Figure 13a shows that the linear main effect of cooling has the least significant effect on cutting force component F_x. It also shows that increase in main effect of cooling had an increasing effect on F_x. However, it shows that the 2-factor interaction of speed and cooling had a more significant effect on F_x compared to the main effect of cooling. This means that the 2-factor interaction of cooling and speed can be investigated more compared to the main effect of cooling in order to reduce $F_{x.}$ Furthermore, Figure 14 shows the variation of cooling on $F_{x.}$ It shows that as the cooling strategy was changed from MQL to combined (MQL+LN_2), cutting force F_x increased. This means that MQL gave the lowest cutting force component F_x. This reduction in F_x can be attributed to the superior lubricating properties of mineral oil at the tool-chip/tool-workpiece interface, which leads to a reduction in coefficient of friction, and tool wear. LN_2 on the other hand hardens the workpiece due to its extremely low temperatures which leads to increased tool wear, and consequently a higher cutting force component, $F_{x.}$

4.5.5. Effects of Cooling Strategies on Cutting Force Component F_y

Figure 13b shows that no main effect of cooling affected F_y significantly, instead only the 2-factor linear interaction of cooling and speed has significant effect. This means that to reduce F_y in the slot end-milling of Inconel 718, only the interaction between cooling and speed must be investigated. Furthermore, the second plot of figure 14 shows that F_y increased, as the cooling was changed from MQL to MQL+LN_2. This means just like in the case of F_x, MQL gave the lowest F_y while MQL+LN_2 gave the highest F_y. The increased hardness arising from the use of very low temperatures of the LN2 constituent of MQL+LN_2 may be the reason for the increase in $F_{y.}$

4.5.6 Effects of Cooling Strategies on Cutting Force Component Fz

Figure 13c shows that the linear and quadratic main effects of cooling had an increasing effect on F_z. Also, just like F_x and F_y, the 2-factor interaction of cooling and speed had a very high significant effect on F_z. Furthermore, Figure 14 shows that as the cooling strategy was changed from MQL to combined (MQL+LN_2), F_z increased just like in the case of F_x and F_y. Therefore, MQL gave the lowest F_z, compared to combined (MQL+LN_2) and LN_2.

4.5.7. Effects of Spindle Speeds on Cutting Force Components (F_x, F_y, and F_z)

Figure 13 shows that speed has the most significant effect on cutting force components F_x and F_y, and the 2nd most significant effect on F_z, and has a decreasing effect on each of them. Figure 14 shows that increasing the spindle speed resulted in a reduction in F_x, F_y, and F_z. It shows that as progression was made from a low speed of 250 rpm (10 m/min) to a high speed of 750 rpm (30 m/min), the 3 cutting force components reduced drastically. This means that high-speed slot end-milling of Inconel 718 reduces all cutting force components. In each case, 750 rpm gave the lowest cutting force component, while 250 rpm gave the highest cutting force component. It can be deduced from figure 14 that high-speed slot end-milling of Inconel 718 reduced F_x, F_y, and F_z by 6, 3.8 and 1.8 times respectively. The decrease in cutting force components when machining with a high speed of 750 rpm can be attributed to the increased cutting temperature during high-speed machining, which leads to a softening of the workpiece material at the cutting zone, and an increase in the plastic deformation, thereby reducing the force required to machine it.

4.5.8. Effects of Feed Rates On Cutting Force Components (F_x, F_y, and F_z)

Figure 13a and 13b show that increasing the quadratic effect of feed had a decreasing effect on F_x and F_y, while increasing the linear effect of feed had a decreasing effect on F_z. Furthermore, Figure 14 shows that the medium feed rate of 2 ipm (50.8 mm/min) gave the lowest cutting force components F_x and F_y compared to high and low feed rates of 3 ipm (76.2 mm/min) and 1 ipm (25.4 mm/min) respectively. Also, medium and high feed rates of 2 ipm and 3 ipm performed equally better in reducing F_z compared to a low feed rate of 1 ipm. From the figure, it can be deduced that medium feed rate of 2 ipm reduced F_x by approximately 1.5 times, and reduced F_y by approximately 2 times compared to low and high feed rates of 1 ipm and 3 ipm respectively.

4.5.9. Machinability Improvement by Cutting Force Components Reduction

Figure 15 gives a 3D surface desirability and contour plot which can be used for machinability improvement during slot end-milling of Inconel 718 alloy by cutting force component reduction

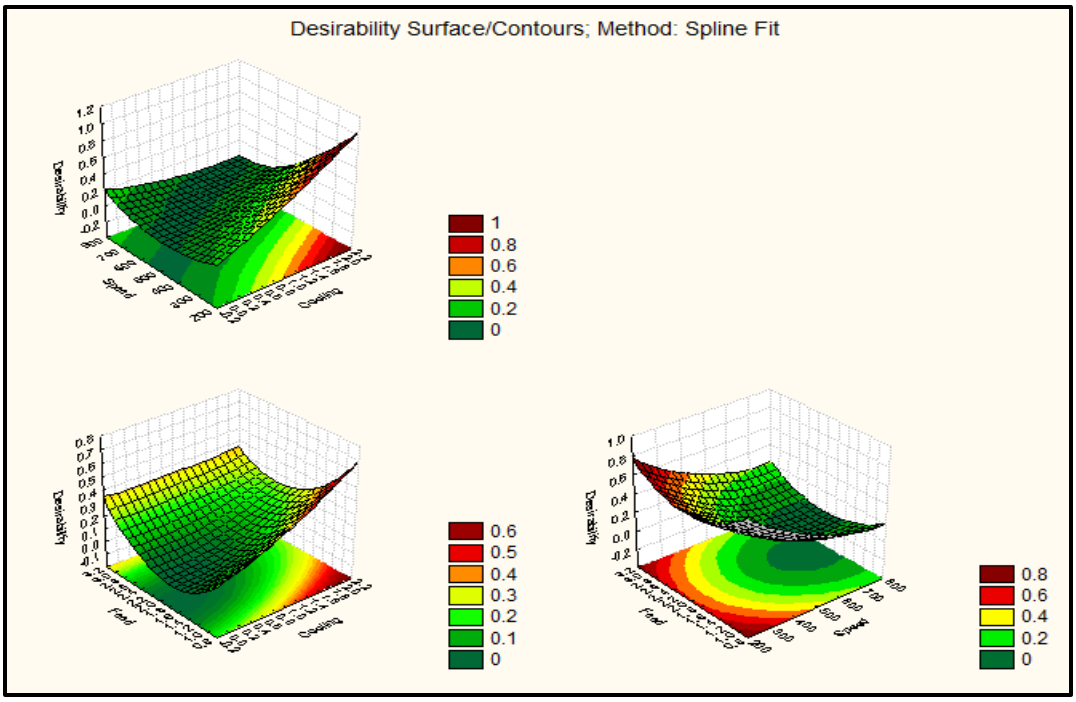

Figure 15. Surface Desirability/contour plot of Cutting Force Components

It can be seen from the first plot (top left) that high spindle speeds and low cooling method (MQL) gave the most desirable response as regards cutting force component reduction. From the 2nd plot (bottom left), low cooling strategy of (MQL) and medium feed rate of 2 ipm gave the best response in terms of reducing cutting force components. Lastly, the 3rd plot shows that high spindle speeds and medium feed rates gave the most desirable response on cutting force components. Therefore, from the analysis of cutting force components, high spindle speeds of 750 rpm together with a medium feed rate of 2 ipm and MQL cooling strategy gave the lowest cutting force components, and as such can be used to improve the machinability of Inconel 718 alloy.

4.6. EFFECTS OF MACHINING PARAMETERS AND COOLING STRATEGIES ON CUTTING TEMPERATURE

The effects of the factors on the cutting temperature were investigated and analyzed. Cutting temperature data was obtained by inserting a thermocouple at the

center of each slot for every machining pass. Temperature values obtained for each experimental run was entered into Statistica 7 software from Stat soft and analyzed. The effects of machining parameters and cooling strategies were analyzed for machining lengths 76.2 mm (Pass 1) and 152.4 mm (pass 2). ANOVA, Pareto chart, marginal means and surface desirability plots were used to analyze the effects of the factors on cutting temperatures. Table 12 shows the maximum temperature values for each experimental run for passes 1 and 2, while Table 13 shows the ANOVA results.

Table 12 Maximum Measured Temperature values for each experimental run

Expt. Runs	Treat. Combinations	3 factors at 3 levels			Cutting Temp. (˚C)	
		Cooling Method	Speed rpm	Feed ipm (mm/min)	Pass 1	Pass 2
1	(0,0,0)	MQL	250	1 (25.4)	20.6023	22.7388
2	(0,1,2)	MQL	500	3 (76.2)	18.349	19.9688
3	(1,0,1)	LN2	250	2 (50.8)	18.1923	18.4307
4	(2,0,2)	MQL+LN_2	250	3 (76.2)	16.3582	16.9835
5	(0,2,1)	MQL	750	2 (50.8)	18.1936	20.3689
6	(1,1,0)	LN_2	500	1 (25.4)	19.6223	24.211
7	(1,2,2)	LN_2	750	3 (76.2)	17.84	18.513
8	(2,1,1)	MQL+LN_2	500	2 (50.8)	16.5907	17.9634
9	(2,2,0)	MQL+LN_2	750	1 (76.2)	17.293	18.6582

4.6.1. Analysis Of Variance (ANOVA)

The result from ANOVA conducted is shown in table 13

Table 13 ANOVA for cutting temperature

Factor	ANOVA; Var. :Temperature; R-sqr = 0.99308; Adj: 0.98693 3 3-Level factors, 1 block, 18 runs; MS Residual = 82.28789 DV: Temperature				
	SS	df	MS	F	p
(1)cooling L+Q	26410.7	2	13205.36	160.4775	0.000000
(2)speed L+Q	2502.7	2	1251.33	15.2068	0.001299
(3)feed L+Q	28631.2	2	14315.6	173.9697	0.000000
1*2	14917.7	1	14917.69	181.2865	0.000000
1*3	14189.9	1	14189.86	172.4417	0.000000
Error	740.6	9	82.29		
Total SS	107033.2	17			

The ANOVA table shows that the main effects of cooling, speed and feed all significantly affect cutting temperature. Likewise, it shows that 2-factor interaction of cooling and speed, and cooling and feed significantly affect cutting temperature.

4.6.2. Pareto Chart of Effects on Cutting Temperature

Figure 16 gives the Pareto chart for all effects on cutting temperature

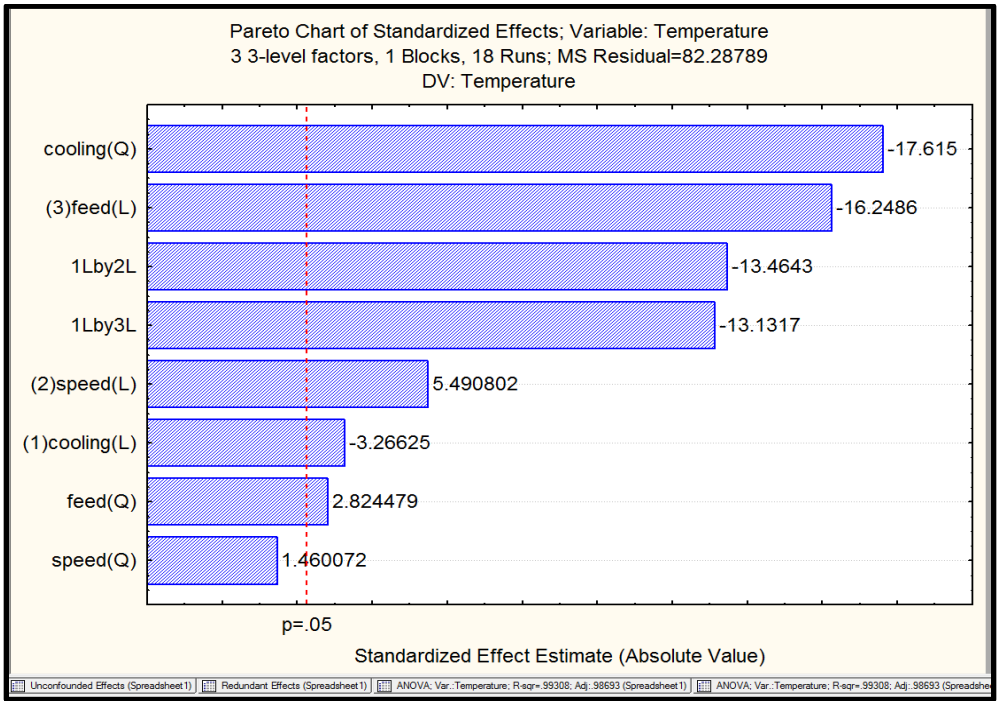

Figure 16. Pareto chart of effects on cutting temperature.

The Pareto chart plot shows that quadratic effect of cooling has the most significant effect on cutting temperature, followed by the linear effect of feed, and next by the 2-factor interaction of cooling and speed. The 2-factor interaction of cooling and feed, the linear effect of speed, the linear effect of cooling, and the quadratic effect of feed are the 4^{th}, 5^{th}, 6^{th}, and 7^{th} most significant effects respectively. Furthermore, the plot shows that as the quadratic effect of cooling, linear effect of feed, and linear effect of cooling increased, cutting temperature decreased. Likewise, as the 2-factor interactions of speed and cooling, and cooling and feed increased, cutting temperature decreased, while the increase in the quadratic effect of feed and the linear effect of speed both had increasing effects on cutting temperature.

4.6.3. Marginal Means Plot of Main Effects on Cutting Temperature

Figure 17 gives the marginal means plot of the main effects of the factors

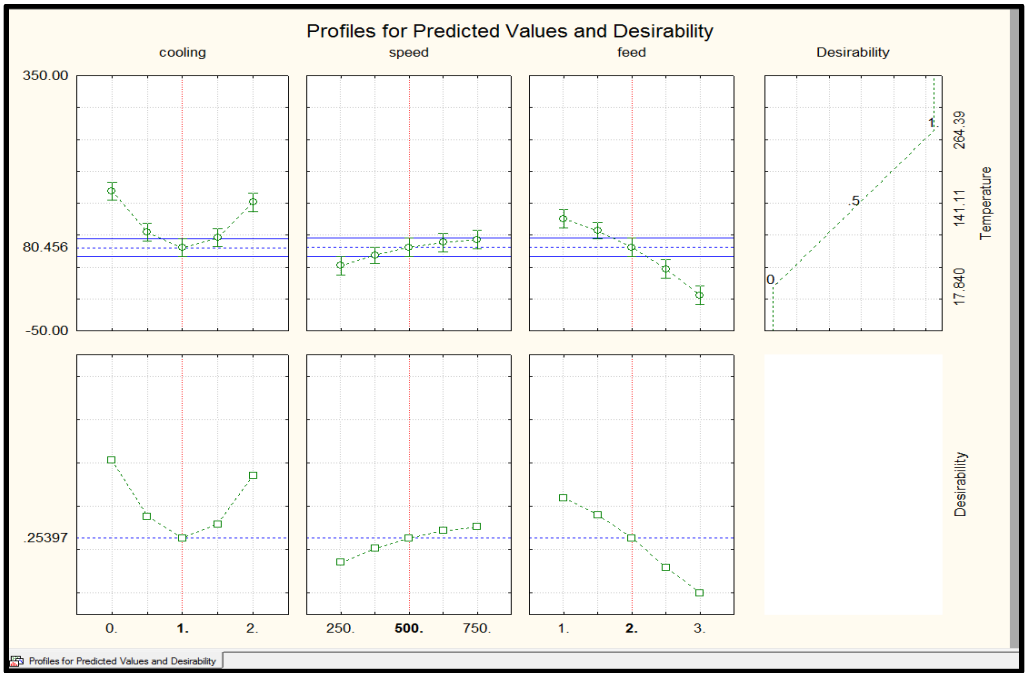

Figure 17. Marginal means plot of main effects on cutting temperature

4.6.4. Effects of Cooling Strategies on Cutting Temperature

The 1st plot in Figure 17 shows how the variation in cooling strategies affects cutting temperature. It shows that cryogenic liquid nitrogen gave the lowest cutting temperature, followed by MQL+LN_2 cooling strategy, and MQL gave the highest cutting temperature. The figure shows that as the cooling strategy was changed from MQL to LN_2, there was significant decrease in cutting temperature to a minimum value. Furthermore, with a change from LN_2 cooling strategy to MQL+LN_2, there was an increase in cutting temperature. The efficiency of LN_2 in reducing workpiece temperature can be attributed to its ability to remove the heat generated at the cutting zone during slot end-milling of Inconel 718. The extremely low temperatures of LN_2 impinging on the cutting zone makes it very efficient in cooling the tool-workpiece/tool-chip interface.

4.6.5. Effects of Spindle Speeds on Cutting Temperature

Marginal means plot shows that an increase in cutting speed from a low speed of 250 rpm to a high speed of 750 rpm increased cutting temperature. A low spindle speed of 250 rpm gave the lowest cutting temperature, while a high speed of 750 rpm gave the highest workpiece temperature. This means high-speed machining increases the workpiece temperature during slot end-milling Inconel 718. From Figure 17, it can be deduced that high-speed machining at 750 rpm (30 m/min) increased cutting temperature by approximately 2 times compared to low spindle speed of 250 rpm (10 m/min).

4.6.6. Effects of Feed Rates on Cutting Temperature

The 3rd plot of Figure 17 shows that the temperature at the slot reduced as feed rate changed from a low value of 1 ipm (25.4 mm/min) to a the high feed rate of 3 ipm (76.2 mm/min). Therefore, a high feed rate of 3 ipm gave the lowest workpiece temperature, while a low feed rate of 1 ipm gave the highest workpiece temperature. It can be inferred that a high feed rate reduced the temperature remarkably by 125 times compared to a low feed rate.

4.6.7. Machinability Improvement by Cutting Temperature Reduction

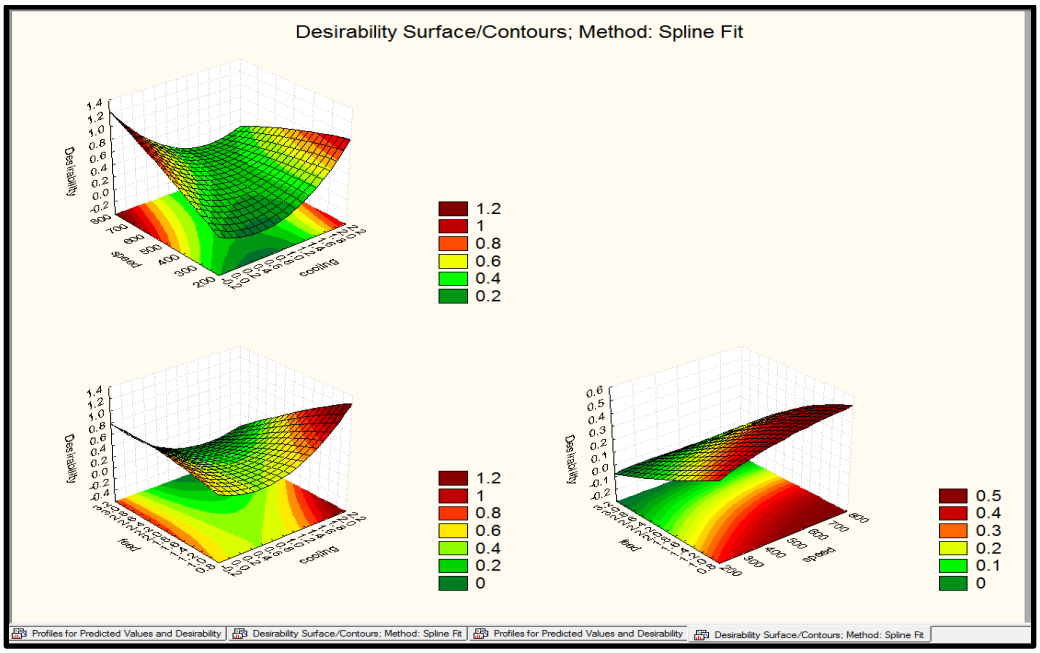

Figure 18.Desirability Surface/contour plots on cutting temperature

Figure 18 shows a desirability/contour plot on cutting temperature which can be used for machinability improvement during slot end-milling of Inconel 718. The 1st plot (top left) gives the relationship between speed and cooling, and shows that lower spindle speeds is the most desirable in reducing cutting temperature compared to medium and higher spindle speeds. Therefore, it can be concluded that a speed of 250 rpm is more desirable in reducing cutting temperature compared to medium and high spindle speeds of 500 and 750 rpm respectively. Also, the same plot shows that medium cooling strategy LN_2 was most desirable/efficient in reducing cutting temperature compared to MQL and MQL+LN_2. Furthermore, the 2nd plot (bottom left) shows the relationship between feed and cooling. Again, it is seen that LN_2 cooling strategy was most desirable in reducing cutting temperature compared to MQL and combined (MQL+LN_2) cooling strategies. In

addition, it once again proves that high feedrate (3 ipm) and medium feedrate (2 ipm) are more desirable/viable in reducing cutting temperature compared to a low feed rate of 1 ipm. Lastly, the 3rd plot (bottom right) gives a plot of the relationship between speed and feed. From the plot, a combination of lower spindle speeds and higher feed rates were the most desirable in reducing cutting temperature. Summarily, it can be concluded that the best factors that improve the machinability of Inconel 718 by cutting temperature reduction are: LN_2 cooling strategy, a low speed of 250 rpm, and high feed rate of 3 ipm.

4.7. EFFECTS OF MACHINING PARAMETERS AND COOLING STRATEGIES ON TOOL WEAR BY INDIRECT ANALYSIS

The effects of the factors on tool wear were also investigated and analyzed. Due to the breakdown of available tool maker's microscope used for direct measurement of tool wear, an indirect analysis of tool wear was performed. It involved analyzing maximum cutting force components data obtained for 1447.8 mm (pass 19) and 1524 mm (pass 20) lengths of cut. The idea is that in these machining lengths, the tool had undergone extreme wear, and since increase in tool wear often leads to an increase in cutting force components, an analysis of the cutting force component at these final lengths can give us a measure of the amount of wear the tool has undergone. In this research, an indirect analysis of tool wear was performed by conducting ANOVA on maximum cutting force components values obtained from the last 2 machining lengths. This is because tool wear is likely to be at a maximum in these final stages of machining, and so it is expected that there should be a commensurate increase in cutting force as wear progresses. Tables 14 and 15 present the maximum cutting force data obtained for

indirect measurement of tool wear in machining 1447.8 mm (pass 19) and 1524 mm (pass 20) lengths of cut.

Table 14. Maximum Cutting Force Components for each Expt. Run (pass 19)

		3 factors at 3 levels			Max. Cutting Forces			
Expt. Runs	Treat. Comb.	Cooling Method	Speed rpm	Feed (ipm) mm/min	F_x (N)	F_y (N)	F_z (N)	F_r (N)
1	(0,0,0)	MQL	250	(1) 25.4	710	1200	350	1437.6
2	(0,1,2)	MQL	500	(3) 76.2	2200	3940	2450	5134.8
3	(1,0,1)	LN_2	250	(2) 50.8	1800	1650	1100	2678.2
4	(2,0,2)	MQL+LN_2	250	(3) 76.2	1900	1500	910	2586.1
5	(0,2,1)	MQL	750	(2) 50.8	1890	3250	3900	5417.1
6	(1,1,0)	LN_2	500	(1) 25.4	1450	1750	850	2426.4
7	(1,2,2)	LN_2	750	(3) 76.2	NF	NF	NF	NF
8	(2,1,1)	MQL+LN_2	500	(2) 50.8	1500	3040	1050	3548.8
9	(2,2,0)	MQL+LN_2	750	(1) 25.4	950	2250	760	2557.9

Table 15. Maximum Cutting force components for each Expt. run (pass 20)

Expt. Runs	Treat. Comb.	3 factors at 3 levels			Max. Cutting Forces			
		Cooling Method	Speed (rpm)	Feed (ipm) mm/min	F_x (N)	F_y (N)	F_z (N)	F_r (N)
1	(0,0,0)	MQL	250	(1) 25.4	800	1400	350	1650
2	(0,1,2)	MQL	500	(3) 76.2	2000	4190	3000	5527.8
3	(1,0,1)	LN_2	250	(2) 50.8	2000	1700	1200	2886.2
4	(2,0,2)	MQL+LN_2	250	(3) 76.2	2390	2400	1500	3704.3
5	(0,2,1)	MQL	750	(2) 50.8	1910	3000	3750	5168.2
6	(1,1,0)	LN_2	500	(1) 25.4	1490	1700	1300	2607.7
7	(1,2,2)	LN_2	750	(3) 76.2	NF	NF	NF	NF
8	(2,1,1)	MQL+LN_2	500	(2) 50.8	1600	3080	1160	3659.5
9	(2,2,0)	MQL+LN_2	750	(1) 25.4	1000	2550	900	2883.1

4.7.1. Anova

Tables 16, 17 and 18 shows the ANOVA on cutting force components F_x, F_y, F_z for indirect tool wear analysis.

Table 16. ANOVA for cutting force component F_x (Indirect tool wear)

Factor	ANOVA; Var. :F_x; R-sqr = 0.95576; Adj: 0.91706 3 3-Level factors, 1 block, 16 runs; MS Residual = 21418.75 DV: F_x				
	SS	df	MS	F	p
(1)cooling L+Q	338076	2	169038.1	7.89206	0.012800
(2)speed L+Q	99319	2	49659.5	2.31851	0.160614
(3)feed L+Q	840221	2	420110.4	19.61414	0.000823
1*2	97200	1	97200.0	4.53808	0.065765
Error	171350	8	21418.7		
Total SS	3873494	15			

Table 17. ANOVA for cutting force component F_y (Indirect tool wear)

Factor	ANOVA; Var. :F_y; R-sqr = 0.9581; Adj: 0.92144 3 3-Level factors, 1 block, 16 runs; MS Residual = 66975 DV: F_y				
	SS	df	MS	F	p
(1)cooling L+Q	501733	2	250867	3.74568	0.071122
(2)speed L+Q	6248410	2	3124205	46.64733	0.000039
(3)feed L+Q	2999142	2	1499571	22.39001	0.000528
1*2	598533	1	598533	8.93667	0.017349
Error	535800	8	66975		
Total SS	12787700	15			

Table 18. ANOVA for cutting force component F_z (Indirect tool wear)

Factor	ANOVA; Var. :F_z; R-sqr = 0.97572; Adj: 0.95447 3 3-Level factors, 1 block, 16 runs; MS Residual = 57331.25 DV: F_z				
	SS	df	MS	F	p
(1)cooling L+Q	4751967	2	2375983	41.44308	0.000060
(2)speed L+Q	4815238	2	2407619	41.99488	0.000057
(3)feed L+Q	1181771	2	590885	10.30652	0.006111
1*2	653333	1	653333	11.39576	0.009702
Error	458650	8	57331		
Total SS	18888744	15			

Table 16 shows that the main effect of cooling and feedrate significantly affected F_x, while the main effect of speed had no effect on F_x. Furthermore, the 2-factor interaction of cooling and speed did not significantly affect F_x. This result is different from the analysis performed for F_x in the initial machining passes when tool wear was only moderate, in which speed, feed and the interaction between cooling and speed were significant. This means that as extreme tool wear sets in, only cooling and feed become important on F_x. The effects of speed, feed and the interaction between speed and cooling become less important or significant on F_x during extreme tool wear. Furthermore, Table 17 shows that the main effect of speed and feed significantly affect F_y, while the main effect of cooling does not significantly affect F_y. Furthermore, the interaction of cooling and feed also significantly affects F_y. This contrasts with results obtained when the tool was moderately worn, in which only the main effect of speed and the interaction between cooling and speed significantly affected F_y. This means that during slot end-milling Inconel 718, extreme tool wear brings with it an additional significant effect of feed. The combined linear and quadratic effect of cooling had no effect on F_y irrespective of the condition of the tool. Lastly from table 18, it can be seen that all the effects of the factors, both main and interaction significantly affect F_z, by virtue of their p-values being less than the significance level of 0.05. This result is similar to that obtained when the tool's cutting edges were sharp, in which all effects were significant.

4.7.2. Pareto Chart of Effects on Cutting Force Components (Indirect Tool Wear Analysis)

Figure 19 presents the Pareto chart of effects for cutting force components F_x, F_y, and F_z.

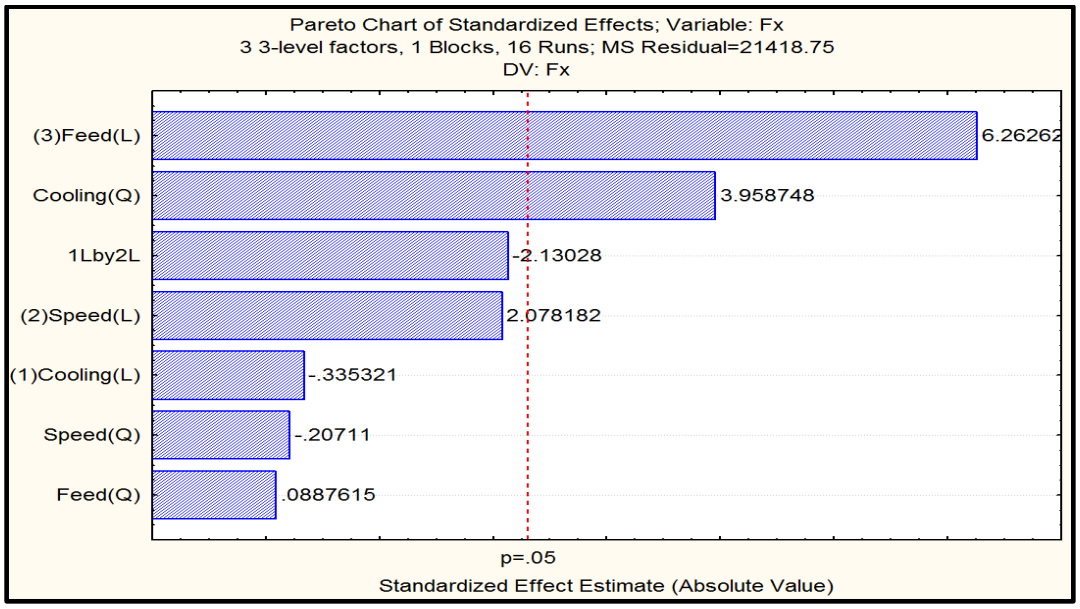

a. Cutting force component F_x (indirect tool wear analysis)

Figure 19. Pareto chart of effects on cutting force components (indirect tool wear analysis)

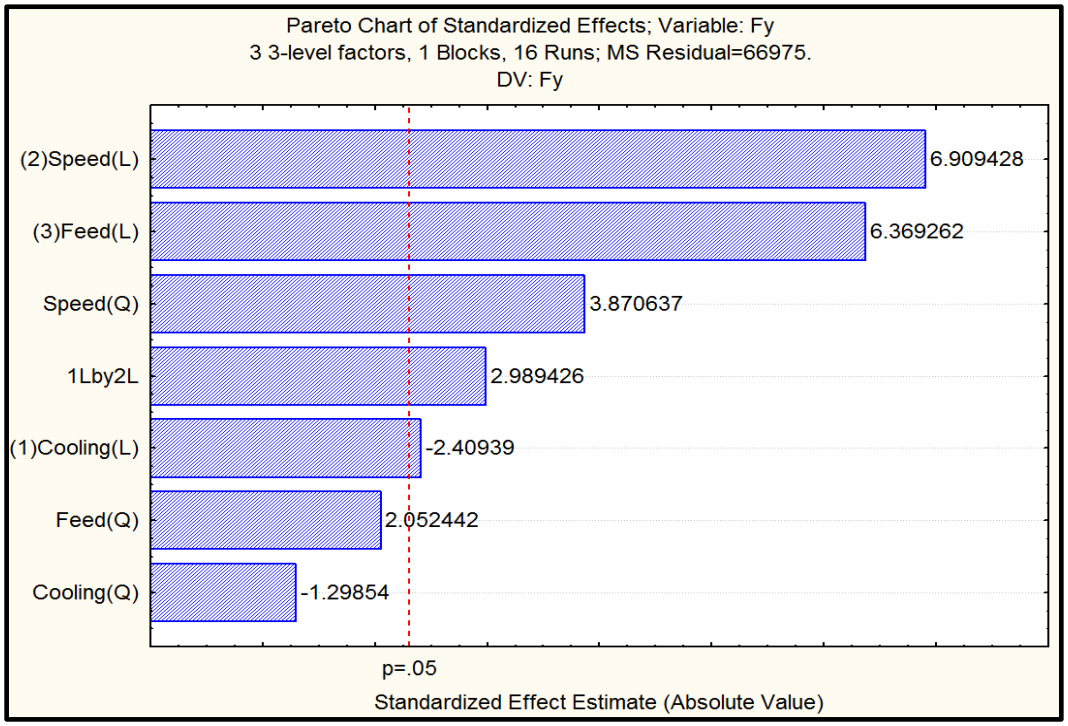

b. Cutting force component F_x (Indirect tool wear analysis)

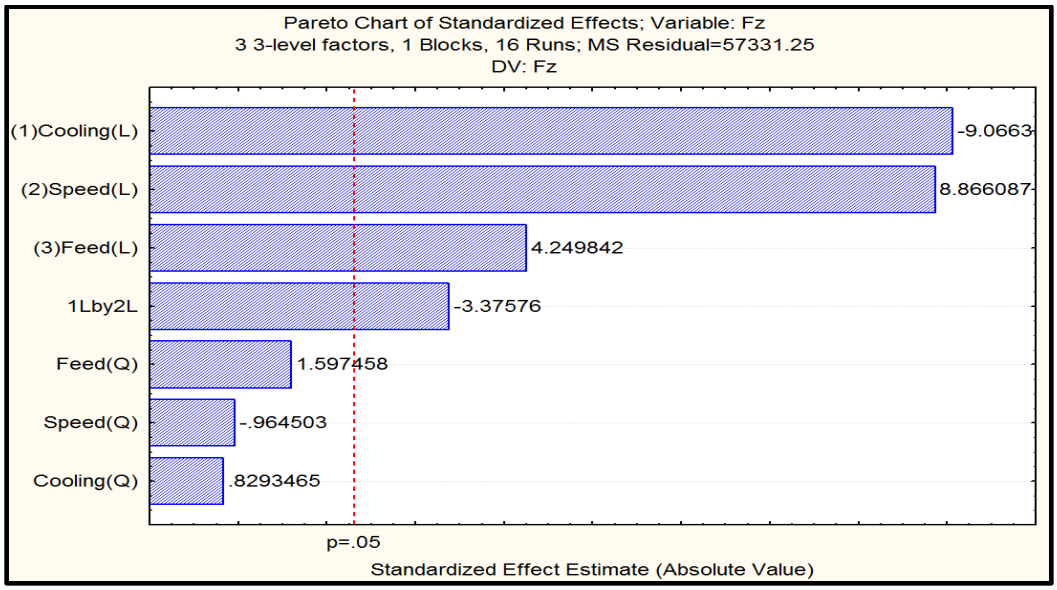

c. Cutting force component F_Z (Indirect tool wear analysis)

Figure 19. Pareto chart of effects on cutting force components (indirect tool wear analysis) (cont.)

The Pareto chart agrees with the ANOVA results in that only feed and cooling significantly affect F_x. However, in this case of extreme tool wear an increase in feed led to an increase in F_x. This is in stark contrast with results obtained when the tool was sharp, where an increase in feed actually decreased F_x. Furthermore, the plot shows that in extreme wear, the quadratic effect of cooling has the 2nd most significant effect and its increase leads to an increase in F_x. Figure 19b shows the linear effect of speed has the most significant effect on F_y, while linear main effect of feed, quadratic effect of speed, 2-factor interaction of speed and cooling, and linear main effect of cooling are the 2nd, 3rd, 4th, and 5th significant effects respectively. However, unlike the results obtained when the tool flutes were moderately worn, an increase in linear main effect of speed had an increasing effect on F_y. Furthermore, the plot also shows that when the 2-factor interaction of cooling and speed increased, F_y increased as a result of extreme tool wear. This is different from results obtained when the tool's cutting edges were still sharp in

which increasing a 2-factor interaction of cooling and speed had a decreasing effect on F_y. Also, the plot shows that an increase in linear effect of feed increased F_y, while increase in linear effect of cooling decreases F_y. Lastly, figure 19c shows that the linear main effect of cooling is the most significant effect followed by the linear main effect of speed. The linear main effect of feed and the 2-factor interaction of cooling and speed are the 3rd and 4th most significant effects on F_z respectively. The plot also shows that as the linear effect of speed and feed increased, F_z increased due to severe tool wear. This contrasts with results obtained when the tool flutes were sharp, in which increase in speed and feed actually reduce F_z. This once again shows that machining parameters reduce F_z during moderate tool wear, but increases it when there has been extreme wear of the cutter flutes. Furthermore, the plot shows that as the 2-factor interaction of cooling and speed increased, F_z increase which was the same result obtained when the tool was still sharp. Another contrast of the results is that when the tool is sharp, a move towards the higher cooling methods of LN_2 and combined (MQL+ LN_2) led to an increase in F_z. However with a severely worn tool, a move towards the higher cooling methods reduced Fz.

4.7.3. Effects of Cooling Strategies and Machining Parameters on Cutting Force Component F_x (Indirect Tool Wear Analysis)

Figure 20 presents marginal means plot of how the main effects of the factors affect cutting force components during extreme tool wear. It shows that MQL and combined MQL+LN_2 gave the lowest F_x during severe tool wear. LN_2 produced the highest cutting force F_x. This is similar to the analysis obtained when the tool flutes were only moderately worn in which MQL gave the lowest F_x. The efficiency of MQL in

reducing F_x can be attributed to the its ability to lubricate the cutting zone thereby reducing coefficient of friction, tool wear, and consequently cutting force. Similarly, MQL+LN_2 has a dual advantage of cooling and lubrication, which reduces cutting temperature and friction, thereby reducing F_x. Furthermore the plot also shows that during extreme tool wear, F_x increased when a change was made from a low speed of 250 rpm (10 m/min) to a high speed of 750 rpm (30 m/min). This means that during extreme tool wear, high-speed machining is not recommended because it drastically increases F_x. This once again contrasts with results obtained while using a sharp tool, in which high-speed machining gave the lowest cutting force F_x. Therefore, it can be concluded that when the tool is moderately worn, machining at high speed reduces F_x but when the tool has undergone extreme wear, machining in high speed increases F_x. Lastly, the plot shows that the lowest feed rate of 1 ipm gave the lowest F_x compared to medium and high feed rates of 2 ipm (50.8 mm/min) and 3 ipm (76.2 mm/min) respectively. From results obtained when tool was sharp, machining with a feed rate of 2 ipm (50.8 mm/min) gave the lowest F_x. Summarily, from previous analysis when tool flutes are sharp, a high speed of 750 rpm (30 m/min), medium feed of 2 ipm (50.8 mm/min), and MQL cooling strategy gave the lowest F_x. However, with severe tool wear, it is best to machine at a low speed of 250 rpm (10 m/min) and low feed of 1 ipm (25.4 mm/min) in order to get the lowest F_x.

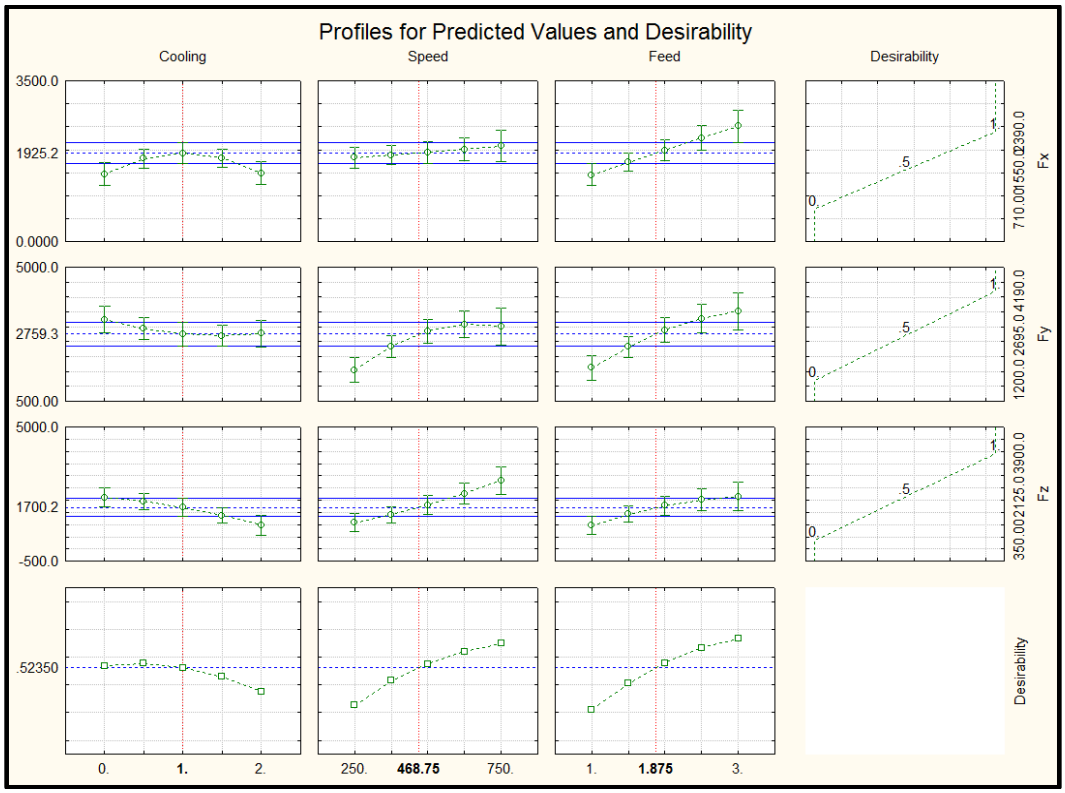

Figure 20.Marginal means plot of main effects on cutting force components (Indirect tool wear)

4.7.4. Effects of Cooling Strategies and Machining Parameters on Cutting Force Component F_y (Indirect Tool Wear Analysis)

The marginal means plot shows that as the cooling strategy was changed from MQL through LN_2 to combined (MQL+LN_2), F_y decreased. It shows that the combination of MQL+LN_2 cooling strategy gave the lowest F_y. Furthermore, the plot shows as the speed was increased from a low value of 250 rpm to a high value of 750 rpm, F_y increased. This result agrees with what was obtained for F_x and shows that a move to high-speed machining when the tool's cutting edges are extremely worn increases F_y drastically. Results obtained for F_y when cutting edges were sharp appear to show the opposite. This means that high-speed machining is favorable for sharp tools, but unfavorable for severely worn tools. In this case, a speed of 250 rpm gave the lowest F_y. Lastly the plot shows increase in the feed rate from a low value of 1 ipm through a

medium value of 2 ipm to a high value of 3 ipm, led to an increase in F_y. Once again, this agrees with results obtained for F_x which showed that low feed rate of 1 ipm gives the lowest F_y. In all, it can be concluded that when the tool is sharp high spindle speed and medium feed rate give the lowest F_y, while low feed rate and low spindle speed gave the lowest F_y during extreme wear of the tool.

4.7.5. Effects of Cooling Strategies and Machining Parameters on Cutting Force Component F_z (Indirect Tool Wear Analysis)

The marginal means plot shows that as the cooling strategy was changed from MQL to combined (MQL+LN_2), cutting force F_z decreased. Therefore, combined (MQL+LN_2) gave the lowest cutting force F_z compared to the other 2 cooling strategies. Furthermore, the plot shows that as the speed was increased from a low speed of 250 rpm to a high speed of 750 rpm, cutting force F_z increased, which resulted from an increase in tool wear. This once again agrees with previous analysis made on F_x and F_y during severe tool wear. It however, contradicts the result obtained for F_z when the tool was sharp, in which high-speed machining gave the lowest F_z. Therefore, it can once again be confirmed that high-speed machining favors the reduction of cutting force F_z when the cutting edges are not severely worn. When they attain severe wear, it is more advantageous to use a low speed of 250 rpm if the aim is to reduce F_z. Lastly, the plot of feed rate shows that an increase in feed had increasing effect on F_z as a result of severe tool wear. It shows that the lowest feed value of 1 ipm (25.4 mm/min) gave the lowest F_z compared to medium and high feed rates of 2 ipm (50.8 mm/min) and 3 ipm (76.2mm/min).

4.7.6. MACHINABILITY IMPROVEMENT BY TOOL WEAR REDUCTION

Figure 21 shows a 3D surface desirability and contour plot for tool wear improvement during slot end-milling Inconel 718.

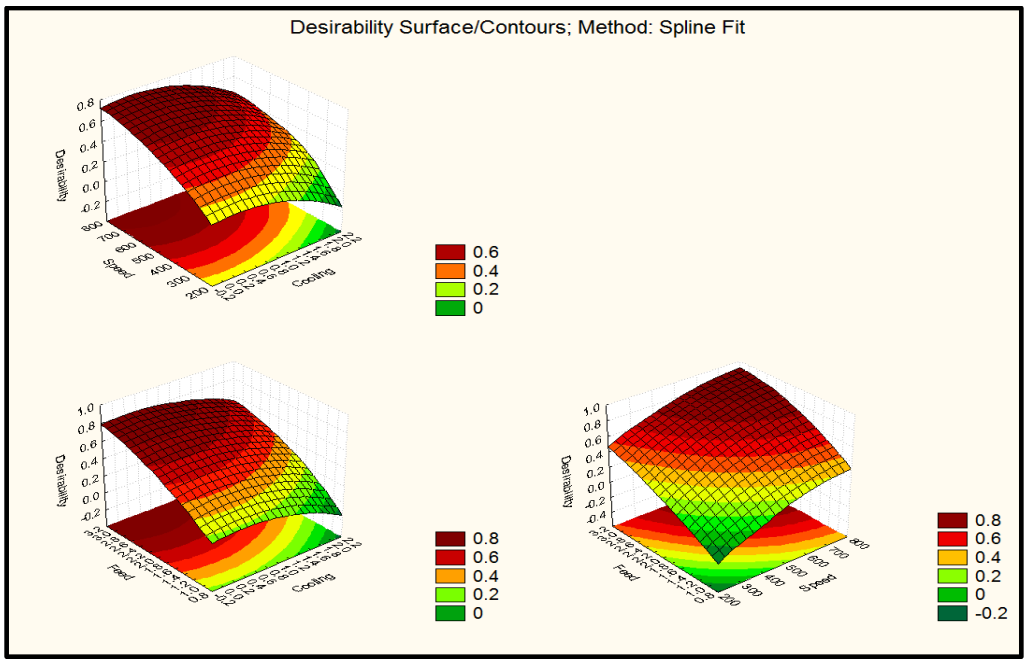

Figure 21. Surface Desirability/contour plot of Cutting Force Components

From the 1st plot (top left) of Figure 21 showing cooling and speed, a combination of high cooling strategy combined (MQL+LN_2) and low spindle speed gave the most desirable response in terms of reducing cutting force components and may most likely reduce tool wear. Furthermore, the 2nd plot shows that low feed rates and high cooling method gave the most desirable response on cutting force components and tool wear. Lastly, the 3rd plot gives the relationship between speed and feed and shows that low spindle speeds and low feed rates give the most desirable response in terms of reducing cutting force components. Therefore, to improve the machinability of Inconel 718 alloy with reference to tool wear reduction, it is recommended to use a low speed of 250 rpm and a low feed rate of 1 ipm (25.4 mm/min), and combined (MQL+LN_2) cooling strategy as optimum cooling strategy and machining parameters.

In summary, from the statistical results/analysis obtained above, a high spindle speed of 750 rpm (30 m/min) and medium feed rate of 2 ipm (25.4 mm/min) gave the lowest cutting force components, while a low spindle speed of 250 rpm (10 m/min) and 1 ipm gave the lowest tool wear. Therefore, to derive a combined advantage of the lowest cutting force and tool wear, a high spindle speed of 750 rpm (30 m/min) low feed rate of 1 ipm (25.4 mm/min) were chosen as the optimum machining parameters that gives the lowest cutting force components and tool wear. These recommended optimum machining parameters were used in performing a comparative evaluation of the 3 cooling strategies.

4.8. COMPARATIVE INVESTIGATION OF THE 3 COOLING STRATEGIES USING OPTIMUM FEED RATE AND SPINDLE SPEED

A comparative performance evaluation of the 3 cooling strategies MQL, LN_2, and combined (MQL+LN_2) was investigated using the recommended optimum machining parameters (high speed 750 rpm and low feed 1 ipm) obtained from the statistical analysis. Maximum cutting force component were compared among the 3 cooling strategies to evaluate the performance during slot end-milling of Inconel 718. Table 19 presents values of maximum cutting force components obtained for varying lengths of cut (number of passes) and cooling strategy.

Table 19. Cutting force component data for comparative evaluation

Length of cut (mm)	MQL				LN_2				MQL+LN_2			
	F_x (N)	F_y (N)	F_z (N)	F_r (N)	F_x (N)	F_y (N)	F_z (N)	F_r (N)	F_x (N)	F_y (N)	F_z (N)	F_r (N)
76.2	350	325	150	501	325	290	100	447	275	260	110	394
152.4	NA	NA	NA	NA	NA	NA	NA	NA	300	290	110	432
381	350	360	150	524	1090	2200	1300	2778	NA	NA	NA	NA
762	360	370	210	557	1400	2200	1900	3227	325	320	150	480
1143	360	390	225	577	1450	2050	2350	3439	510	590	240	816
1448	NA	NA	NA	NA	NF	NF	NF	NF	950	2250	760	2558
1524	525	510	200	759	NF	NF	NF	NF	1000	2550	900	2883

Table 19 shows the acquired maximum cutting force component values for 76.2, 152.4, 381, 762, 1143, 1447.8 and 1524 mm lengths of cut for the 3 cooling techniques. The cells in the table marked as N/A denotes “Not Applicable” and this means that cutting force data were not acquired for that particular machining length. Furthermore, the cells marked as N/F denotes “Not Feasible” (tool broke) and this was used to represent the machining lengths which could not be attained due to plastic deformation of cutting flutes while machining using that particular cooling strategy. The comparative plots of the maximum cutting force components for each cooling strategy are shown in Figures 22, 23 and 24.

4.8.1. COMPARATIVE INVESTIGATION OF CUTTING FORCE COMPONENT F_x

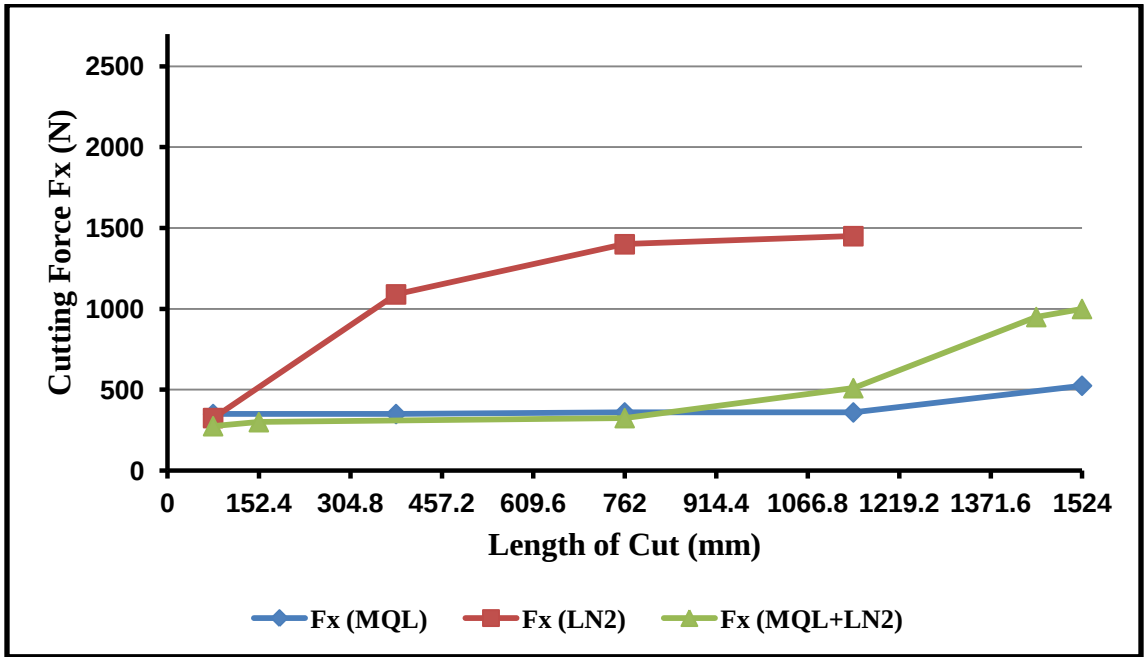

Figure 22 Comparative investigation for cutting force component F_x among the 3 cooling strategies

Figure 22 shows the comparative plot of the cutting force component F_x for the 3 cooling strategies investigated at optimum spindle speed and feed rate of 750 rpm and 1 ipm (25.4 mm/min) respectively. It can be seen that at 76.2 mm length of cut, combined (MQL+LN_2) produced the least cutting force followed by LN_2, while MQL produced the highest cutting force. MQL+LN_2 reduced F_x by 21.4 % and 15.4 % compared to MQL and LN_2 respectively, while LN_2 reduced F_x by 7.14 % compared to MQL. However, as the machining length increased further, LN_2 caused a sharp increase in the slope of F_x, compared with MQL and combined (MQL+LN_2) which both had a more gradual increase in the slope. Throughout the machining lengths leading up to 762 mm, MQL+LN_2 produced the least cutting force component F_x, followed by MQL. LN_2 generated such sharp rise in F_x because the use of cryogenic machining causes extreme hardening of the workpiece with sustained machining time. Conversely, combined (MQL+LN_2) generated

in the least F_x because of the dual advantages provided by the individual cooling property of LN_2 and the lubricating property of MQL. At this length of cut, LN_2 cooling increased F_x by 74.28% and 77% compared to MQL and MQL+LN_2 cooling respectively, while MQL+LN_2 reduced F_x by only 9.7% compared to MQL. However, beyond the machining length of 762 mm, F_x under combined (MQL+LN_2) cooling began to increase slightly until it surpassed F_x under MQL. This can be attributed to the work-hardening effect due to the extremely low temperature (at -15˚C) of the LN_2 constituent of the combined MQL+LN_2 with increased machining time. This means that combined (MQL+LN_2) gives the lowest F_x compared to MQL during initial lengths of cut, however, with an increase in machining time, the LN_2 constituent of the combination begins to harden the workpiece thereby making MQL more favorable for a sustained machining operation.

The use of LN_2 cooling method only is not advisable beyond 762 mm length of cut using uncoated carbide tool. This is because beyond this length of cut, there was a massive increase in tool wear due to a very high increase in workpiece hardness and temperature at the cutting zone. There was high increase in temperature because the tool flutes had to machine against an increasingly hardening workpiece from the LN_2 cooling strategy, which led to greater tool wear, and consequently a corresponding rise in temperature. When the tool got to 1143 mm length of cut (15^{th} pass), the cutting flutes had almost undergone complete plastic deformation and were beginning to rub on the ribs of the slot instead of cutting. As a result, chips were no longer produced, only large peels of burnt workpiece material. As a result, machining was discontinued because all the cutting flutes were completely burnt out. However, MQL and combined (MQL+LN_2) cooling strategies each got to the final length of cut of 1524 mm (20 passes). At final

length of cut of 1524 mm, MQL gave the best performance by reducing F_x by 47.5 % compared to combined (MQL+LN_2).

4.8.2. Comparative Investigation of Cutting Force Component F_y

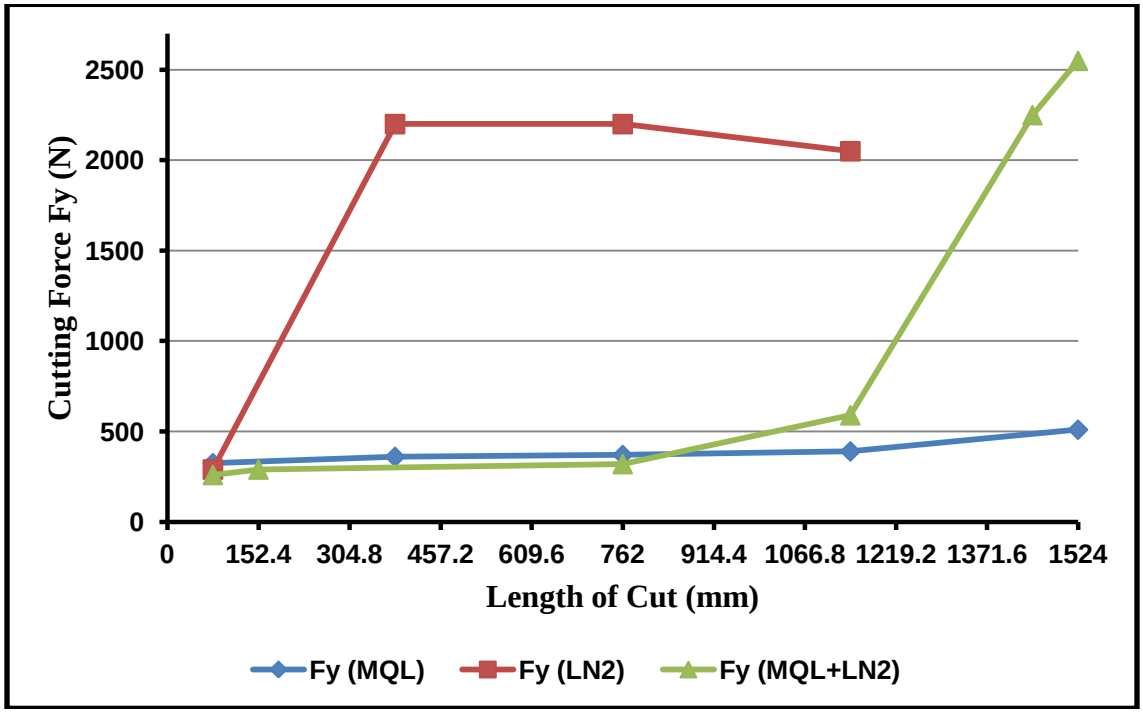

Figure 23. Comparative investigation for cutting force component F_y among the 3 cooling strategies

Figure 23 shows the comparative plot of the cutting force component F_y for all 3 cooling strategies. Once again as was observed in the case of F_x, combined (MQL+LN_2) generated the least cutting force, followed by LN_2 with the highest being MQL at the 1st machining length of 76.2 mm. The results show that combined (MQL+LN_2) reduced F_y by 10.3% and 20% compared to LN_2 and MQL respectively. However, with increase in length of cut beyond 76.2 mm, there was a steep rise in the slope of the cutting force for LN_2. Conversely the slopes of MQL and combined (MQL+LN_2) were more or less steady with MQL+LN_2 still generating the least cutting force F_y up to 762 mm length of cut. At this length of cut, LN_2 increased cutting force by 83.2 % and 85.4% compared to MQL and MQL+LN_2 respectively, while MQL+LN_2 reduced F_y by 13.5% compared to MQL.

The was due to the increased hardness of the workpiece as a result of the effects of cryogenic temperatures at -15 ˚C together with a lack of lubrication at the cutting zone. As a result, there was an increase in the coefficient of friction which led to massive tool wear, which also led to a high degradation of the surface integrity of the machined slot. As a result of severe tool wear, the tool was no longer cutting but rubbing on the ribs of the slot, and this led to an increase in the cutting temperature and cutting forces, which resulted in the slot being burnt in brownish black coloration. Similarly as in the case of F_x, MQL+LN_2 began to cause a slight increase in cutting force F_y beyond machining lengths of 762 mm. This made MQL the best in performance, with regard to cutting force components reduction beyond machining length of 762 mm. The reason for this can once again be attributed to the fact that the extremely low temperature of the LN_2 constituent of the combination began to take its toll on the hardness of the workpiece material with an increase in machining time and beyond the machining length of 762 mm. Machining did not go beyond a length of 1143 mm for LN_2 cooling strategy because all the cutting flutes had under gone complete plastic deformation at that point, making it impossible to machine further. However, MQL+LN_2 performed worse than MQL beyond cutting length of 762 mm up to final machining length of 1524 mm. MQL reduced F_y by 80% compared to combined (MQL+LN_2) at final machining length.

4.8.3. COMPARATIVE INVESTIGATION OF CUTTING FORCE COMPONENT F_z

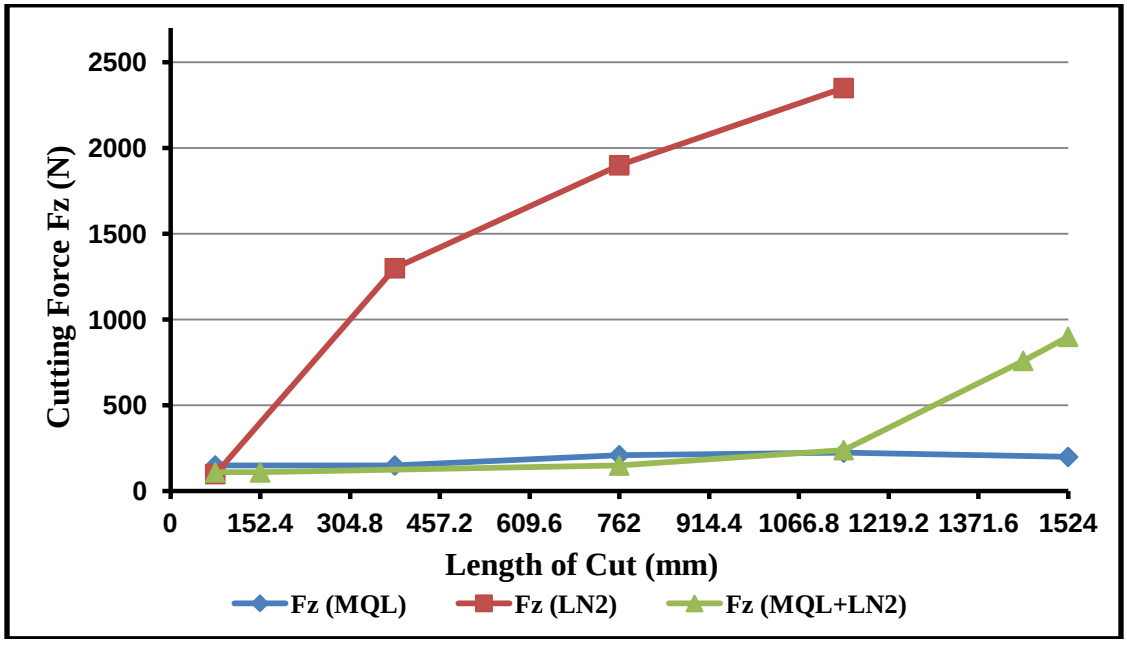

Figure 24. Comparative investigation for cutting force component F_Z among the 3 cooling strategies

The plot for F_z is also similar to that of F_x and F_y. In this case, LN_2 also caused a sharp rise in the slope of F_z relative to MQL and combined (MQL+LN_2). The least cutting force component was achieved when using combined (MQL+LN_2) followed by MQL for much of the machining lengths. However, as was the case with F_x and F_y, the cutting force slope under combined (MQL+LN_2) tended to catch up with that of MQL and surpassed it leading up to 1524 mm length of cut. This once again shows that during initial lengths of cut, combined (MQL+LN_2) cooling strategy gives the lowest cutting force compared to MQL cooling strategy. However, with more machining time, the cutting force F_z of MQL+LN_2 caught up and overtook the cutting force of MQL. Similarly, just like the plot of F_x and F_y, the plot shows the cutting force F_z of LN_2 cooling to be consistently higher than under the other 2 cooling strategies. The results show that during 76.2 mm length of cut, LN_2 cooling reduced F_z by 33.3% and 9%

compared to MQL and MQL+LN_2 respectively. At machining length of 762 mm (pass 10), LN_2 increased F_z by 83% and 92% compared to MQL and combined (MQL+LN_2), while MQL+LN_2 reduced F_z by 13.5%. Lastly, at 1524 mm length of cut, combined (MQL+LN_2) increased F_z by 77.7% compared to MQL.

Figure 25 gives a plot of bar charts for passes 1 (76.2 mm) and 10 (762 mm) for each cutting force component, F_x, F_y, F_z and resultant force F_r and cooling strategy.

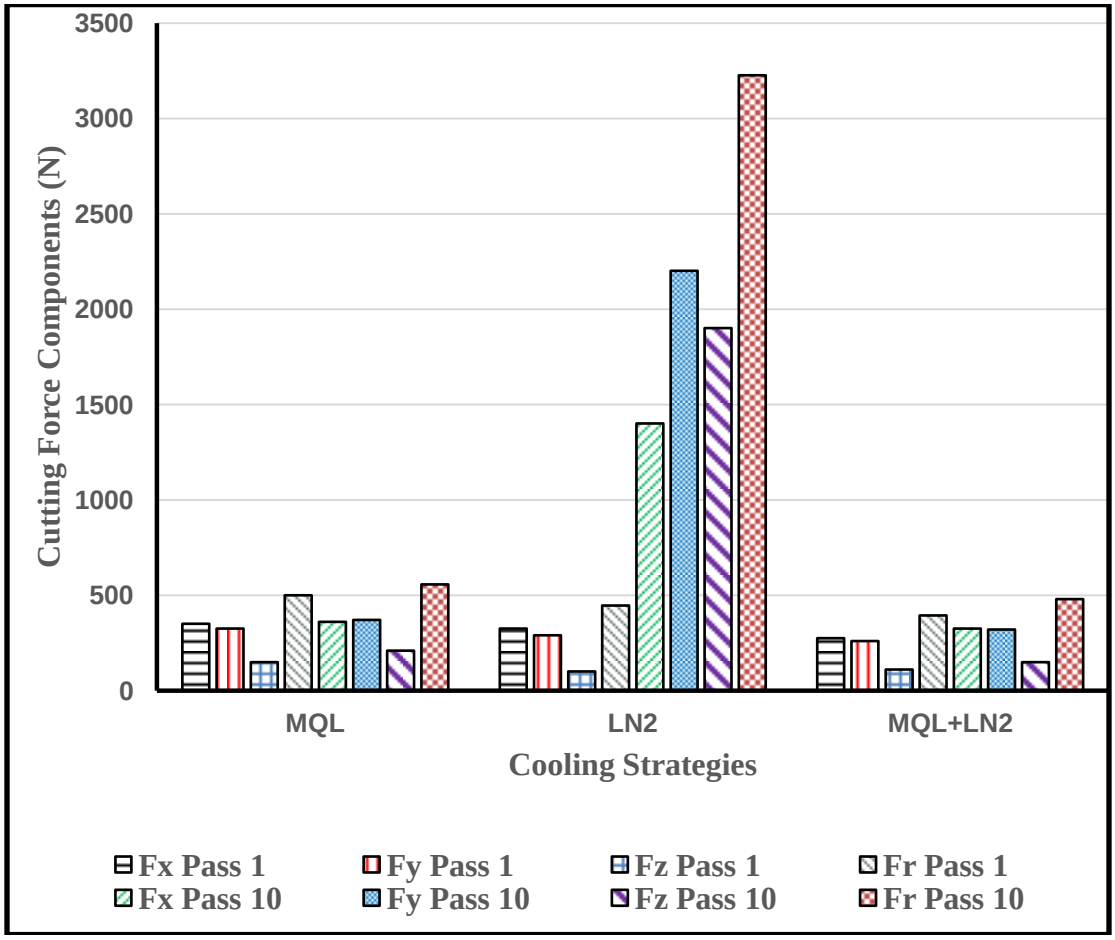

Figure 25. Cutting force component plots for passes 1, and 10 for the 3 cooling strategies

The figure further lends credence to the results previously obtained. It again shows that combined (MQL+LN_2) produced the lowest cutting force components and resultant force for passes 1, followed by LN_2 with the highest being MQL. For pass 1,

combined (MQL+LN_2) reduced resultant force by 11.81% and 21% compared with LN_2 and MQL respectively. Half-way at the 10^{th} pass, combined (MQL+LN_2) still produced the lowest cutting force component and resultant force, and reduced the resultant force by 13.8% and 85% compared with MQL and LN_2 respectively. Therefore, at pass 10, combined (MQL+LN_2) produced the least resultant force, followed closely by MQL while LN_2 produced a drastic rise in resultant force.

Beyond pass 10 however, and before the 20^{th} pass (1524 mm), the tool used for LN_2 cooling had attained complete plastic deformation and machining was discontinued. However, MQL and combined (MQL+LN_2) were able to reach the 20^{th} pass. At the 20^{th} pass, MQL performed much better than combined (MQL+LN_2) and reduced resultant force by 73.6% compared to combined (MQL+LN_2), while LN_2 suffered complete plastic deformation and could not get up to the 20^{th} pass. From the results, it can be deduced that MQL and combined (MQL+LN_2) cooling strategy can lead to a 25 % improvement in tool life compared to LN_2 cooling. Figure 26 gives a comparative evaluation for MQL and combined (MQL+LN_2) cooling strategies only for the 1^{st} and 20^{th} pass.

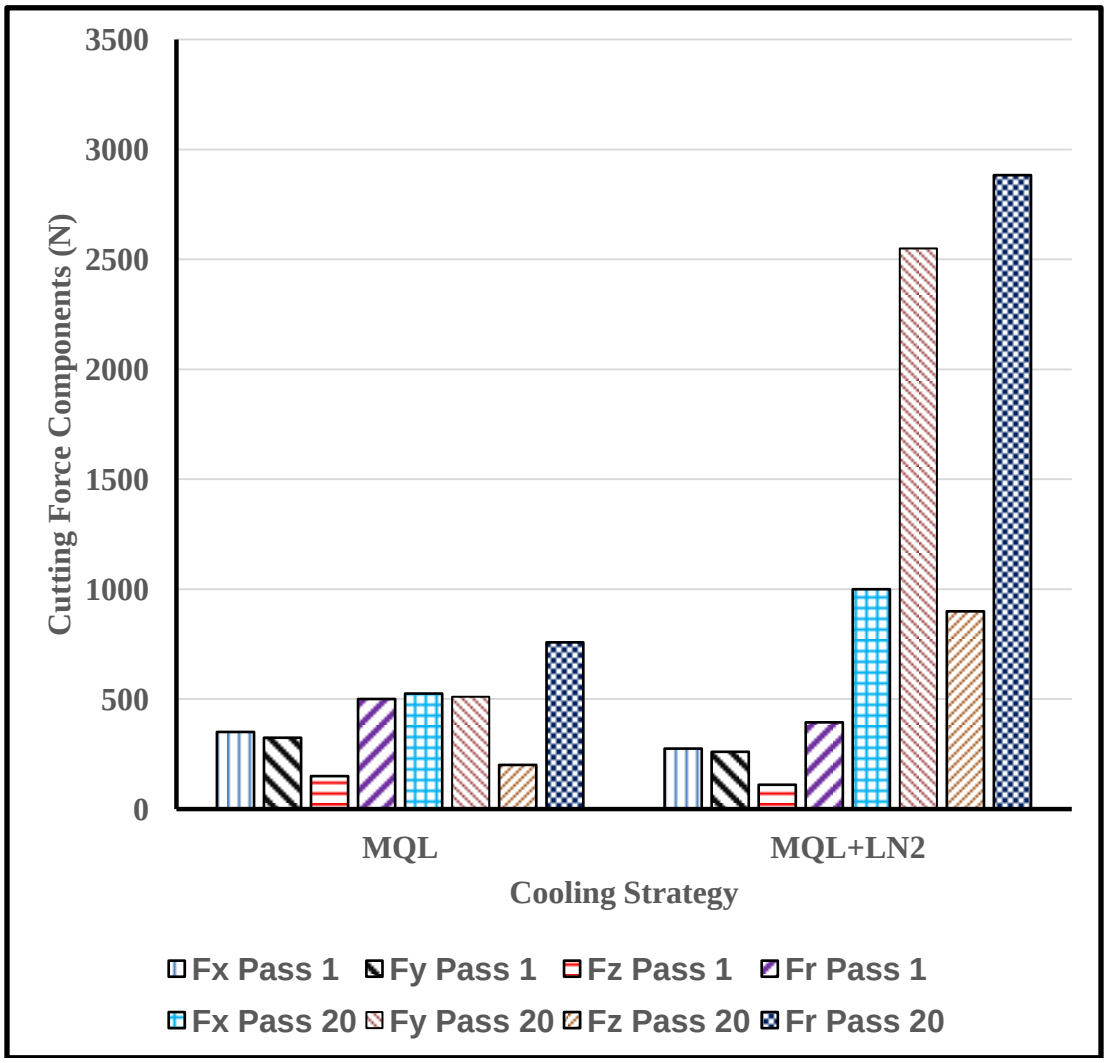

Figure 26. Cutting force component plots for passes 1 and 20 for MQL and MQL+LN_2 cooling strategies

5. CONCLUSIONS

This research investigated the effects of machining parameters (speeds and feeds) and cooling strategies (MQL, LN_2, and combined (MQL+LN_2)) on cutting force components, tool wear, and cutting temperature during bullnosed slot end-milling of Inconel 718 alloy. From the results obtained, the following conclusions were made:

1. The cutting force component F_y (feed force) is the most sensitive to tool wear, followed by the axial cutting force component (F_z), and are recommended for indirect monitoring of tool wear.

2. Cutting speed, interaction of cooling strategy and cutting speed are the significant factors affecting F_y, while cooling strategy, cutting speed, feed rate, and the interaction of cooling strategy and cutting speed are the significant factors affecting F_z.

3. High cutting speed and medium feed rate decrease cutting force components for sharp cutting flutes and moderate tool wear.

4. Cutting speed, feed rate and the interaction of cooling strategy and spindle speed are the significant factors affecting feed force, while cooling strategy, spindle speed, feed rate and interaction of cooling strategy and speed are the significant factors affecting F_z for intermediate or severe tool wear.

5. MQL+LN_2 and MQL cooling at high spindle speed of 750 rpm and a medium feed rate of 2 ipm are the optimum cooling strategy and machining parameters that gave the lowest cutting force components F_x, F_y, and F_z in slot end-milling Inconel 718 and are recommended for improving machinability of Inconel 718 with reference to cutting force components reduction.

6. MQL+LN_2 cooling at low spindle speed (250 rpm) and low feed rate (1 ipm) are the optimum cooling strategy and machining parameters that gave the lowest tool wear, and are recommended for improving the machinability of Inconel 718 with reference to tool wear.

7. Cutting force component F_x was found to be consistently higher than cutting force components F_y and F_z for initial machining lengths, however, F_y always surpassed F_x to become the dominant cutting force component during severe tool wear.

8. Cutting force component F_z rises above F_y and Fx to become the dominant cutting force component during extreme tool wear and just before complete plastic deformation.

9. LN_2 cooling strategy at -15 ˚C gave the lowest workpiece temperature but the highest cutting force components compared to MQL and MQL+LN_2.

10. Low spindle speed of 250 rpm and high feed rate of 3 ipm gave the lowest workpiece cutting temperature.

11. High spindle speed of 750 rpm, and low feed rate of 1 ipm are recommended as optimum machining parameters, taking advantage of the low cutting force components (due to high speed) and low tool wear (due to low feed) for Inconel 718.

12. A comparative evaluation of the three cooling strategies at the recommended optimum machining parameters of 750 rpm and 1 ipm shows that MQL generates the lowest cutting force components, followed by combined MQL+LN_2 with the least being LN_2.

13. Comparative evaluation of cooling strategies shows that MQL and combined MQL+LN_2 cooling strategies increase tool life by 25% compared to LN2 cooling strategies.

ACKNOWLEDGEMENTS

The financial support from the National Science Foundation (NSF) under grant No. CMMI800871 and the Intelligent Systems Center (ISC) of the Missouri University of Science and technology are gratefully acknowledged. The financial assistance provided in the form of graduate teaching assistantship by the Department of Mechanical and Aerospace Engineering at Missouri University of Science and Technology is also gratefully acknowledged.

REFERENCES

(1) D. Dudzinski, A. Devillez, A. Moufki, D. Larrouquere, V. Zerrouki, J. Vigneau, "A Review of Developments towards dry and high speed machining of Inconel 718 alloy", International Journal of Machine Tools and Manufacture, 44, (2012) 439-456.

(2) E. O. Ezugwu and Z. M. Wang, "A review of Titanium alloys and their machinability", Journal of Materials processing technology, (1997) 262-274.

(3) A. Chukwujekwu Okafor and B. Oguejiofor, "Investigating the effects of cutting parameters on temperature in high speed end-milling of thin-walled titanium structure", Proceedings of the 10^{th} CIRP international workshop on modeling of machining operations, Regio-Calabria, (2007) 381-388.

(4) E. Abele and B. Frohlich, "High speed milling of titanium alloys", Journal of advances in production engineering and management, 3, (2008) 131-140.

(5) H. Safari, S. Sharif, S. Izman, H. Jafari, D. Kurniawan, "Cutting force and surface roughness characterization in cryogenic high speed end-milling of Ti-6Al-4V", Materials and Manufacturing Processes, (2014) 350-356.

(6) J. H. Balaji, V. Krishnaraj, S. Yogeswaraj, "Investigation on high speed turning of titanium alloys", International Conference on Design and Manufacturing, 64, (2013) 926-935.

(7) Y. S. Liao, H. M. Lin, J. H. Wang, "Behaviors of end milling Inconel 718 super alloy by cemented carbide tools", Journal of materials processing technology, 201, (2008) 460-465.

(8) E.O. Ezugwu and J. Bonney, “Effects of high pressure supply when machining nickel base, Inconel 718 alloy with coated carbide”, Journal of Materials processing technology, 53-154, (2004) 1045-1050.

(9) Y. Su, N. He, L. Li, X. L. Li, “An experimental investigation of the effects of cooling/lubrication conditions on tool wear in high-speed end-milling of Ti-6Al-4V”, Wear 261, (2006) 760-766.

(10) Ahsan Ali Khan and Mirghani Ahmed, “Improving tool life using cryogenic cooling”, Journal of Materials processing technology, 196, (2008) 149-154.

(11) K. Yusuf, “Evaluation of machining performance in cryogenic machining of Inconel 718 and comparison with dry and MQL machining”, International Journal for Advanced Manufacturing Technology, (2014) 919-933.

(12) Shane Y. Hong, Irel Markus, Wool-cheol Jeong, “New cooling approach and tool life improvement in cryogenic machining of titanium alloy Ti-6Al-4V”, International Journal of Machine Tools and Manufacture, (2001) 2245-2260.

(13) K. E. Ying-lin, L. Gang, Z. Ming, D. Hui-Yue, “Use of Nitrogen gas in High-Speed Milling of Ti-6Al-4V”, Transactions of non-ferrous Metals Society of China, (2009), 530-534.

(14) F. Pusavec and J. Kopac, “Sustainability assessment of: Cryogenic machining of inconel 718”, Journal of mechanical engineers, (2011) 637-647.

(15) Z. Zhao and S. Y. Hong, “Cooling strategies for cryogenic machining from a material view-point”, Journal of Materials Engineering and Performance, Volume 1(5), (1992) 669-678.

(16) Shane Y. Hong, Y. Ding, Wool –cheol Jeong, “Friction and cutting forces in cryogenic machining of Ti-6Al-4V”, International Journal of Machine Tools and Manufacture, (2001) 2271 - 2285.

(17) W. Zhao, N. He, L. Li, “High Speed milling of Ti-6Al-4V Alloy with Minimum Quantity Lubrication”, Key Eng Materials Trans tech publications Switzerland, 329, (2007) 663-668.

(18) E. O. Ezugwu, “High speed machining of aero-engine alloys”, Journal of the Brazilian society of mech. Sci. & Eng, Vol. 16, No 1, (2004).

(19) S. Zhang, J. F. Li, Y. W. Wang, “Tool life and cutting forces in end-milling of Inconel 718 under dry and minimum quantity cooling lubrication”, Journal of cleaner production, 32, (2012) 81-87.

(20) S. Thamizhmanii, Rosli, S. Hasan, “A study of minimum quantity lubrication on Inconel 718”, Archives of materials science and technology, 39, (2009) 38-44.

(21) Y. S. Liao, H. M. Lin, Y. C. Chen, “Feasibility study of the minimum quantity lubrication in high speed end-milling of NAK80 hardened steel with coated carbide tool”, International Journal of machine tools and manufacture, (2007) 1667-1676.

(22) N. Boubekri and V. Shaikh, “Machining using Minimum Quantity Lubrication: A technology for sustainability”, International Journal of Applied Science and technology, volume 2, No1, (2012).

(23) S. M. Yuan, L. T. Yan, W. D. Liu, Q. Liu, “Effects of cooling air temperature on the cryogenic machining of Ti-6Al-4V Alloy”, Journal of Materials Processing Technology, 211, (2011) 356-362.

(24) A. Chukwujekwu Okafor, S. Aramalla, “Modeling of cutting forces in high speed end-milling of titanium alloys using finite element analysis mechanistic model”, Proceedings of the 9th CIRP international workshop on modeling of machining operations, Ljubljana Slovenia 219-226.

II. COMPARATIVE EVALUATION OF COOLING STRATEGIES AND THE EFFECTS OF MACHINING PARAMETERS ON SURFACE ROUGHNESS AND RESIDUAL STRESSES IN HIGH-SPEED END-MILLING OF INCONEL 718

A. Chukwujekwu Okafor*, Chukwujekwu Nnadi
Computer Numerical Control and Virtual Manufacturing Laboratory
Department of Mechanical and Aerospace Engineering
Missouri University of Science and Technology
327 Toomey Hall, Rolla, MO-65409-0050, USA
Email:okafor@mst.edu
*Corresponding Author: Tel: 1-(573) 341-4695, Fax: 1-(573) 341-6899

ABSTRACT

Surface roughness and residual stresses induced on machined parts are two very important surface integrity parameters used in evaluating machined parts overall quality and performance. Surface roughness affects surface friction, wear resistance, ability to distribute and hold lubricants. Residual stresses induced during machining are very critical due to safety and sustainability concerns. This paper presents the results of experimental investigations of the effects of machining parameters (spindle speed and feedrate) and cooling strategies (Minimum Quantity Lubrication (MQL), cryogenic Liquid Nitrogen (LN_2) and a combined (MQL+LN_2) on surface roughness and residual stresses in slot end-milling of Inconel 718 using bull-nose helical carbide end-mill and design of experiments (DOE). A one-third fractional factorial design of experiment having 3 factors at 3 levels was used to analyze these effects, and determine optimum machining parameters. Also a comparative performance evaluation of the three cooling strategies was conducted at the identified optimum machining parameters with reference to induced surface roughness and residual stresses. All the slot milling experiments were conducted on a Cincinnati Milacron Sabre 750 Vertical Machining Center equipped with

acramatic 2100 controller, using a 4-flute, 0.5 inch (12.7 mm/min) diameter, uncoated solid carbide bull-nosed helical end-mill with 0.03 inch (0.762 mm) corner radius. Surface roughness was measured on the slot left rib in a direction perpendicular to the feed direction and on the slot web parallel to the feed direction using a profilometer, while residual stress was measured using x-ray diffraction method on the slot left rib and on the web. Results obtained from analysis of variance show that low spindle speed (250 rpm) (10 m/min), low feed rate (1 ipm), MQL, and combined (MQL+ LN_2) cooling strategies generated the lowest surface roughness on the left rib and on the web. MQL and (MQL+LN_2) cooling strategies improved surface roughness on the left rib by 71.68% and 64.7% respectively compared to LN_2 cooling strategy which produced highly degraded surface finish. Similarly MQL cooling improved surface finish by 20% compared to combined (MQL+LN_2). From the comparative evaluation of the three cooling strategies at high spindle speed, (750 rpm) (30 m/min) and low federate (1 ipm) (25.4 mm/min), MQL gave the best performance by generating high compressive residual stress (-49Ksi) on the surface and sub-surface, while LN_2 and combined (MQL+LN_2) generated tensile residual stresses (58 Ksi and 45 Ksi respectively) on the rib surface and sub-surface of Inconel 718. The results show that MQL cooling strategy will likely increase fatigue life of Inconel 718 parts the most compared to combined (MQL+LN_2) and LN_2 cooling because of the induced compressive stresses. LN_2 cooling strategy induces the highest tensile residual stresses.

Key words: High-Speed Slot End-milling, Inconel-718, Cryogenic Machining, Minimum Quantity Lubrication, Surface roughness, Residual stresses.

1. INTRODUCTION

Inconel 718 is widely used in the aerospace, petroleum, nuclear, automotive, and medical industries due to its very high strength, high corrosion, and high temperature resistance, its ability to retain most of their strength after being exposed for a long time to extremely high temperatures. Common applications of this alloy are in the hot sections of mission of critical components in jet engines and gas turbine engines, which include: gas turbine blades, space craft, nuclear reactors, pumps, pressure vessels, and heat exchanger tubing etc. It is mainly used in harsh environments that are subject to excessive corrosion, high temperatures and pressures. Inconel 718 and a host of other alloys like Ti-6Al-4V, and Hastelloy are mostly desired in such harsh conditions because of their excellent combination of peculiar properties like: high capacity to resist fracture, high resistance to corrosion, and high strength-to-weight ratio etc. However, they are characterized as "difficult-to-cut" because of the inherent problems they pose during machining. Some of these problems include: low thermal conductivity, work hardening tendencies, high chemical affinity with cutting tools, ability to form built up edges (BUE) and formation of burrs. Inconel 718 alloy has a uniquely low thermal conductivity and as such the enormous amount of heat generated during its machining does not get removed as fast as it is generated. In other words, much of the heat generated during machining remains in the cutting zone, and is mostly concentrated on the cutting flutes of the tool. The extreme heat generated adversely affects the tool by causing severe tool wear. Inconel 718 alloy also displays a high chemical reactivity with cutting tool materials, because the high temperatures generated during machining causes some particles from the work-piece material to be welded on the cutting edges of the flutes. Most difficult-to-cut metals pose

problems during machining which may affect the part's surface integrity. Surface roughness and residual stresses induced on machined parts are two very important surface integrity parameters used in evaluating machined parts overall quality and performance. Surface roughness effects surface friction, wear resistance, ability to distribute and hold lubricants, and coatings. Residual stresses affect component fatigue life, corrosion resistance, part distortion, crack initiation and propagation. The performance of machined components can be enhanced or impaired by residual stresses. Tensile residual stresses on machine part surface will induce crack initiation and propagation; reduce fatigue life; while compressive residual stresses will extend fatigue life. Because of these, a good understanding of residual stresses induced by machining is essential in understanding machining general part quality. Therefore, there's the need for a perfectly finished part with highly compressive residual stresses which could be achieved by the selection of appropriate machining parameters and cooling strategies

Due to the enormous amount of heat generated, tool wear is accelerated because of the increased coefficient of friction. Excessive heat causes the edge of the tool to become dull, which invariably leads to detrimental effects on the surface integrity of the part. Therefore, it is pertinent to employ methods that will reduce the enormous amount of heat generated, reduce coefficient of friction, thereby reducing tool wear and consequently improving surface finish and reducing residual stresses. To this end, it is necessary to use an efficient cooling and lubrication strategy. The contemporary method of cooling and lubrication employed by most industries is the emulsion-based lubricant. The use of this type of lubricant has come under intense pressure from environmental regulators like the Environmental Protection Agency (EPA) due to its adverse effects on

the environment when disposed. Furthermore, various manufacturing industries are looking for ways to cut overhead costs, and as such are looking to eliminate the costs of disposing this water-based coolant after it is used. To this end, there has been a recent surge of interest by many researchers and companies on cooling strategies that are more effective to replace the use of water-based coolants, and at the same time limiting their environmental effects and cut costs. One of such cooling strategy that has been investigated by a few researchers is the use of a cryogenic fluid in machining. It involves the use of liquid nitrogen at sub-zero temperatures as the cryogenic fluid. Liquid nitrogen is appropriate because it is a safe, non-combustible and an inert gas. Cryogenic machining involves applying liquid nitrogen at sub-zero temperatures to the cutting zone, at the tool-chip/tool-work-piece interfaces. Cryogenic machining when impinged directly on the cutting zone helps to reduce the enormous amount of heat generated, which prolongs the life of the tool, improves surface roughness, and reduces residual stresses. Ying-Lin et al. (2009) investigated the use of nitrogen gas in high-speed milling of titanium alloy Ti-6AL-4V. The authors also compared the results obtained from cryogenic machining to dry machining. They reported that the use of liquid nitrogen as a cryogenic fluid helped in preventing the adhesion between the chips and the cutting edge, thereby improving the abrasion condition of the tool and also the integrity of the machined surface compared to dry machining. They attributed this improvement to be due to the fact that during dry machining, the chips produced absorbed a large amount of heat in the cutting zone and could not be removed immediately, which caused them to burn and adhere to the machined surface thereby degrading the surface integrity of the machined part. Shokrani et al. (2012) presented a study on the effects of using nitrogen

coolant on surface roughness of Inconel 718 in CNC milling using TiAlN coated carbide end-mills. They compared the effects of cryogenic and dry milling of Inconel 718 on surface roughness. They reported that the average arithmetic surface roughness while using cryogenic machining improved by more than 33%, while the ISO Rz value of the surface roughness improved by 40 % compared with when using dry machining without a noticeable increase in power consumption of the machine tool. Furthermore, there appears to be no general consensus among researchers on the effects of machining parameters (especially speeds) on surface roughness. Che-Haron (2001) investigated surface integrity at various cutting speeds of 100, 75, 60, & 45 m/min while turning titanium alloy. He reported that the surface roughness values tended to increase as the tool approached its tool life, and this was irrespective of the machining speed. Furthermore, he explained that at the initial stages of cutting, plastic flow of the microstructure was not detected due to moderate tool wear. However, towards the end of cutting, severe plastic flow of the microstructure was detected as a result of severe tool wear. This caused the formation of a white-layer of hardened material on top of the machined surface, which degraded the machined surface. However, Mhamdi et al. (2012) investigated surface integrity of titanium alloy during ball end-milling using a hemispherical tool, and reported that average surface roughness was affected by the speed, and increased as the speed increased. They explained that as the speed increased, the hemispherical tool produced a thin layer of plastically deformed surface beneath the machined surface which compromised the surface integrity. A rough surface in a machined part most times may contain inclusions and impurities, and this usually increases the residual stresses of a machined part. Residual stresses could be tensile or

compressive. In most aerospace applications, compressive stresses are more favorable than tensile stresses. This is because compressive stresses increase the fracture toughness of a structure compared to tensile stresses. A number of experimental works have been conducted on residual stresses while machining difficult-to-cut metals. Sun and Guo (2009) presented a comprehensive study on surface integrity during end-milling titanium alloy Ti-6Al-4V. They reported that during end-milling titanium alloy Ti-6Al-4V; compressive residual normal stress in feed direction was about 30 percent larger than in the cutting direction**.** Additionally, they stated that the magnitudes of the residual shear stresses were much smaller than those of the residual normal stresses; however, they pointed out that the compressive residual normal stress decreased with feed. Residual stress measurement is very important in manufacturing, and can be used to evaluate machining processes and to optimize machining parameters. Residual stress measurement can be used for effective quality control, as well as to extend the service life of a machined component used in engineering applications. Tensile residual stresses induced during machining are the primary cause of a reduction in the fatigue life of parts, while compressive stresses improve the fatigue life of a machined surface. Therefore, it will be more beneficial to avoid machining parameters and cooling condition that will induce tensile residual stresses. This is what Sasahara (2005) sought to do when he investigated the effects of residual stresses and surface hardness on fatigue life resulting from different cutting conditions during machining of 0.45% C steel. He discovered that the circumferential residual stresses induced by the turning process tended to become more compressive as the feed rate decreased and when a chamfered tool was used. Also, he stated that the axial residual stress stays around 0 when a 0.2 mm corner radius is used,

regardless of the feed rate and the type of tool edge used. Therefore, he concluded that it was possible to induce compressive stresses and thus, give a higher fatigue life to a machined part by applying cutting conditions like a low feed rate, a small corner radius, and a chamfered cutting edge tool. Due to the significant effects of residual stresses in a machined surface, it is necessary for it to be detected and quantified through measurement. The most common method used in the measurement of residual stresses is the X-ray diffraction method. Pinault et al. reported it to be the most common method used in situations where failure results from overloading, stress corrosion, fatigue, and inappropriate manufacturing processes. They further reported that it can be applied to the evaluation of corrective measures and the optimization of production parameters for extending the service life of components. From the results of the above reviewed published literature, it is obviously imperative to control and limit residual stress generation, especially tensile stress due to its adverse effects on the life of a machined part. In order to effectively control residual stress generation, it is necessary for it to first be predicted accurately and estimated. To this end, X. Jiang et al. (2012) conducted an experiment with an aim of trying to analyze and control residual stress generation during high-speed circular milling of 7050-T7451 alloy. They validated the results of their experiment in the feed and vertical feed direction with a finite element simulation. They stressed the difficulty in optimizing residual stresses. However, they emphasized the importance of studying its generation process and distribution so that good solution methodologies can be proposed. In their work, they explained the significance of the relationship between uncut chip thickness and residual stresses, and concluded that it is possible to optimize the residual stress distribution by controlling the uncut chip

thickness (feed rate and tool diameter) with high-speed milling. Similarly, Su et al. (2012) utilized cutting force and cutting temperature to predict surface and sub-surface residual stress profiles during slot and face milling titanium alloy Ti-6Al-4V. The authors also compared their predictions with published experimental data, and reported both to be in agreement. Additionally, they concluded that the measured sub-surface residual stress profiles were compressive for all the cases explored. The efficiency of the cooling strategy used is a factor that can help in improving surface integrity and limiting tensile residual stresses induced during machining. Umbrello et al. (2011) investigated the effects of cryogenic cooling on surface integrity in machining of hardened steel and reported that the use of cryogenic coolant in the machining of hardened steel significantly affected the surface integrity positively. They explained that cryogenic cooling conditions limited the formation of white-layered thickness and thus, offered better surface roughness. However, they stated that dry machining offered a better performance on residual stress profiles, and thus would contribute to an improved fatigue life compared to cryogenic machining even though it produced a thicker white layer which is detrimental to the product's performance. Furthermore, Aramcharoen and Chuan (2014) conducted an experimental investigation on the sustainability of cryogenic milling of Inconel 718. They reported that plastic deformation occurred near the machined surface during conventional coolant and dry machining, but not with cryogenic machining. Furthermore, they explained that the reduction in plastic deformation when machining with cryogenic cooling maybe as a result of the increased efficiency of LN2 being able to penetrate the cutting zone better. Lastly, they reported that surface defect such as uneven surface and tearing were not observed in the samples machined using cryogenic cooling.

Additionally, increase in surface roughness and residual stresses while machining difficult-to-cut alloys can also depend on the condition of the tool used. Ezugwu and Wang (1997) in their review of titanium alloys and their machinability reported that machining titanium alloy Ti-6Al-4V with a dull tool led to the formation of an overheated white layer, which may be harder or softer than the base material. This ultimately degraded the surface integrity of the machined part and increased residual stresses. Therefore, they recommended the use of sharp tools in the machining of these alloys. Also, a shift to high-speed machining may also enhance surface integrity by inducing compressive stresses in a machined part which is more favorable. Rao et al. (2011) conducted an experimental and numerical study on the face-milling of Ti-6Al-4V alloy using uncoated carbide cutters. They reported that speed had a somewhat negligible effect on residual stresses, however at higher cutting speeds, increasing the feed rate increased the compressive residual stresses on the machined surface. Minimum quantity lubrication is another cooling method that can improve the surface integrity of difficult-to-cut alloys. It is a mixture of mineral oil and compressed air that is sprayed on the cutting zone in the form of mists. It gives the advantage of reducing the cost of disposing conventional fluids, as well as also being non-contaminating. The minimal quantity of oil reduces the tool's friction and prevents the adherence of material on the cutting edges of the tool. Many published literature have found MQL to be very effective in improving the surface roughness of a machined part. Dudzinski et al (2012) presented a review of developments towards dry and high-speed machining of Inconel 718, where they reported MQL to be best in reducing surface roughness compared to wet and dry machining during turning of hardened steel AISI 4340. They further explained that this was because

MQL was most efficient at preserving tool life and reducing cutting force. Thamizhmanii et al (2009) conducted a study of the effects of minimum quantity lubrication on surface roughness while milling Inconel 718. They reported that using MQL cooling strategy offered better results than dry machining in terms of surface roughness. They stated that the total length of travel by super cobalt cutting tool in MQL condition was higher than that in dry cutting. According to the authors, machining using MQL with a high speed of 30 m/min improved surface roughness compared to machining with a medium and low speed of 20 m/min and 10 m/min respectively, and that MQL at a high speed of 30 m/min performed better than dry machining at the same speed. Surface roughness has a great influence on the functional properties of a product. Therefore, it is imperative to find ways to predict and control surface roughness. This would ensure the optimization of production parameters to improve production quality and efficiency. To this end, Zhang et al (2007) conducted a surface roughness optimization experiment during end-milling aluminum alloy using Taguchi Statistical design approach. The aim was to determine optimal face-milling parameters that would achieve the smallest roughness value for the aluminum part. They employed various control and noise factors. Spindle speed, feed rate and depth-of-cut were used as control factors, while operating chamber temperature and the usage of different tool inserts were used as noise factors. An orthogonal array was used and ANOVA was conducted to determine the significant factors affecting roughness, and the optimal cutting conditions that best minimizes surface roughness were determined. They reported the effects of spindle speed and feed rate on surface roughness to be larger than that for depth-of-cut for milling operation. In addition, they found one of the noise factors, tool wear have significant effect on surface roughness.

From the above review of published works, it is clear that not much work has been done in investigating the effects of machining parameters and cooling strategies on surface roughness and residual stresses during slot end-milling of Inconel 718. Also, only a few studies of the individual merits of minimum quantity lubrication and cryogenic cooling on surface roughness and residual stresses have been done. There has been no comprehensive study of the combined effects of machining parameters (speeds and feeds), and cooling strategies (cryogenic cooling and minimum quantity lubrication) on surface roughness and residual stresses during slot end-milling Inconel 718. Furthermore, the potential benefits of combining Minimum Quantity Lubrication (MQL) and Liquid Nitrogen (LN_2) have not been explored in previous works. This work investigates the effects of machining parameters and various cooling strategies on surface roughness and residual stresses during slot end-milling Inconel 718. The aim is to optimize the machining process with reference to surface roughness and residual stress reduction. Furthermore, the potential benefits in combining minimum quantity lubrication and liquid nitrogen will be investigated. A comparative evaluation of the new cooling approach combined (MQL+LN_2), MQL, and LN_2 was be conducted to ascertain its viability in reducing surface roughness and tensile residual stresses.

2. EXPERIMENTAL DESIGN

A three-factor and three-level experiment was chosen for this experiment. This makes the total treatment combinations or experimental runs for a full factorial design 3^3. In order to conduct Analysis of Variance (ANOVA) to find experimental error, there should be at least 1 replication of the experimental runs, which makes the total number of runs 54. This is obviously a lot of experimental runs to conduct in terms of the time and resources that will be employed. Therefore, it is unreasonable to conduct such large number of experimental runs. A fractional factorial design of experiment is useful in scaling down the number of experimental runs required for a full factorial design. It eliminates many higher order interactions that are not of interest. For this experiment, a one-third fractional factorial experimental design was chosen, which resulted in 9 experimental runs. Surface roughness measurement was made in 3 different locations, which makes it a total of 27 points to be used in conducting Analysis of Variance (ANOVA)

2.1. EXPERIMENTAL PARAMETERS AND LEVELS

The 3 factors selected for this experiment are: spindle speed, feed rate, and cooling strategy. As stated earlier, the aim of this experiment is to investigate the effects of the factors (cooling strategies and cutting parameters) on surface roughness and residual stress in slot end-milling Inconel 718. To find the optimum cutting parameters and cooling strategy that will give the lowest surface roughness and residual stress. Spindle speed at 3 levels of 250 (10 m/min), 500 (20 m/min) and 750 rpm (30 m/min)

were chosen, while feed rate at 3 levels of 1 (25.4), 2 (50.8), and 3 ipm (76.2) mm were chosen. Cooling strategies at 3 levels were also chosen namely: Minimum Quantity Lubrication (MQL), Liquid Nitrogen (LN_2) and combined Minimum Quantity Lubrication and Liquid Nitrogen ($MQL+LN_2$). The machining parameters above were chosen after consultations with some cutting tool manufacturers and vendors in order to determine the standard machining range used by most companie machining Inconel with uncoated carbide tool. The speed ranges were chosen to encompass low, medium, and high spindle speed. Other factors that were not being investigated were kept constant throughout the experiment, like the axial depth of cut at 0.05" (1.27 mm) and a radial depth of cut at 0.5" (12.7 mm). Table 1 shows the factors at their respective levels.

Table 1. Factors and levels

Factors			
Level	Cooling Methods	Speed rpm (m/min)	Feed ipm (mm/min)
0	MQL	250 (10)	1 (25.4)
1	LN_2	500 (20)	2 (50.8)
2	$MQL+LN_2$	750 (30)	3 (76.2)

2.2. SELECTION OF TREATMENT COMBINATIONS/METHOD OF STATISTICAL ANALYSIS

As mentioned earlier for a full factorial experiment, there will be a total of 27 experimental runs derived from 3 factors at 3 levels. This large experimental runs will consume a lot of time as well as resources, especially considering the replication also. Therefore, a one-third fractional factorial design was constructed in order to reduce the

total number of experimental runs to 9. To do this, higher order interactions were aliased with the mean. The aim is to construct 3 blocks with 9 experimental runs in each of them. After performing the analysis and applying modulo 3 arithmetic, the block that contained the principal fraction (0, 0, 0,) was chosen for this experiment. Table 2 shows the 9 treatment combinations that were generated and used. After performing end-milling experiments, surface roughness measurements were made at 3 different locations making it a total of 27 points to be used in conducting ANOVA to find experimental error.

Table 2. Table of treatment combinations

Experimental Runs	Treatment Combinations	3 factors at 3 levels		
		Cooling Method	Speed rpm (m/min)	Feed ipm (mm/min)
1	(0,0,0)	MQL	250 (10)	1 (25.4)
2	(0,1,2)	MQL	500 (20)	3 (76.2)
3	(1,0,1)	LN_2 (-15˚C)	250 (10)	2 (50.8)
4	(2,0,2)	MQL+LN_2	250 (10)	3 (76.2)
5	(0,2,1)	MQL	750 (30)	2 (50.8)
6	(1,1,0)	LN_2 (-15˚C)	500 (20)	1 (25.4)
7	(1,2,2)	LN_2 (-15˚C)	750 (30)	3 (76.2)
8	(2,1,1)	MQL+LN_2	500 (20)	2 (50.8)
9	(2,2,0)	MQL+LN_2	750 (30)	1 (25.4)

2.2.1. Analysis of Variance (ANOVA)

Analysis of Variance (ANOVA) is used to ascertain that the variation in the results of the dependent variable is due to the change from one factor to the other in each

of the levels and not just due to random chance. In other words, ANOVA provides the statistical test of whether or not the means of several groups are equal. In this experiment, results from ANOVA were used to test whether or not there was significant difference between the means of the factors. The ANOVA uses an F-test with a p-value to test for significance. The F- test uses an F ratio (variance ratio) which is the ratio of the mean square effect to the mean square error. The larger the F-ratio for a given factor, the more likely the test for significance is not due to random chance. Also, the p-value gives the probability of the test for significance of the effects on the dependent variable. The p-value is compared with a significance level ($\alpha = 0.05$), and if the p-value given in the ANOVA result is less than the significance level then the difference between means of that effect is said to be significantly different from zero.

2.2.2. Pareto Chart of Effects

A Pareto chart is a visual representation of all effects (both main and interaction) in the form of bar charts in relation with how they significantly affect the dependent variable. A dashed red line running across any of the bar charts shows the magnitude required for that effect to be statistically significant. It lists each effect in the order of significance. The Pareto chart is very useful in reviewing a large number of factors, and for presenting the results of an experiment to an audience that is not familiar with standard statistical terminologies.

2.2.3. Marginal Means

Marginal means plots were used in this experiment to pictorially show the profile variation of the factors (spindle speed, feed rate, and cooling strategy) on the dependent variables (surface roughness)

2.2.4. Desirability Surface/Contour Plot

The desirability surface/contour plots were used in this experiment to show a 3-D figure of the statistical relationship between the factors (spindle speed, feed rate and cooling strategy) and the dependent variables (cutting force, tool wear, and cutting temperature). The plots are partitioned in areas marked by distinct colors (green, yellow, and red). These colors help in the interpretation of the relationship between the factors and the dependent variable in a given region of the plot. More green color means that the factor is more desirable, and more red means it is less desirable.

2.3. SETTING UP OF COOLING STRATEGIES

One of the aims of this experiment is to investigate the effects of cooling strategies on cutting force components, tool wear and cutting temperature. The cooling strategies that will be investigated are: MQL, LN_2, and combined (MQL+LN_2). Each of these cooling strategies was set up independently for this experiment.

2.3.1. Minimum Quantity Lubrication Set up

MQL is a mixture of mineral oil and air that is sprayed on the cutting zone in the form of mists. For this experiment, an Acculube MQL precision pump applicator was used to spray lubricant mist on the cutting zone. The precision pump applicator uses a

positive displacement system to spray the lubricant, and it can be regulated to control the amount of lubricant applied to the cutting zone and on the tool flutes. For this experiment, shop air supplied at 85 psi to the CNC machine is stepped down at the input to the MQL precision pump applicator to 65 psi. Thus, the air pressure used by the precision pump applicator is 65 psi. It also has a valve that can be used to regulate the volume of air that is mixed with the droplets of oil. Due to the extreme hardness of Inconel 718 super alloy, it is pertinent that sufficient volume of air is used to transport the lubricant. This would be more efficient in cooling the cutting zone and removing chips. To this end, the air valve was increased by turning it counter clock wisely two and a half times. This ensured that sufficient volume of air was available to transport the lubricant to the cutting zone. Furthermore, the volume of oil that gets mixed up with the air to form the lubricant can also be regulated. The precision pump applicator has a valve, which is graduated from 0 to 7, and this valve can be controlled to regulate the amount of oil going to the cutting zone depending on the machining operation involved. For this milling experiment, the precision pump applicator manual was consulted and the recommendation was for the valve to be set at 7, between 0 and 6. Also, the precision pump has a frequency generator which is used to regulate the number of times the lubricant is applied to the cutting zone per second, which is the pump cycle. For this experiment, various pump cycles were investigated to see which was more efficient in milling Inconel 718 without wasting so much lubricant. A pump cycle of 3 strokes per second was chosen for this work. Lastly, a loc-line adjustable nozzle was connected to the precision pump applicator so the lubricant can flow through it to the cutting zone.

2.3.2. Cryogenic Liquid Nitrogen Set up

The use of cryogenic Liquid Nitrogen (LN_2) in milling involves the application of sub zero temperature liquid nitrogen to the cutting zone. This method of cooling is very efficient in removing the enormous amount of heat generated during the milling of Inconel 718 alloy. A 160 liters cylinder with a pressure relief valve of 230 psi containing liquid nitrogen was used for this experiment. Transportation of liquid nitrogen from the cylinder to the milling zone was done using pipe couplings, valves, nozzles, and a flexible cryogenic flow line. The cryogenic flow line had a pressure gauge fitted to it to measure the pressure of liquid nitrogen flowing through it to the cutting zone. The pressure gauge had a 0.25" (6.35 mm) Swagelok pipe fitted to it, which was also connected to a 0.25" (6.35 mm) Tee, and in turn linked up to a 0.25" (6.35 mm) pig tail pipe. This was in order to prevent liquid nitrogen from getting in contact with the pressure gauge so as not to damage it. The temperature of liquid nitrogen in the tank was extremely cold at -196˚C. This extremely cold temperature of liquid nitrogen if used this way, would negatively affect the milling of Inconel 718 alloy. Very cold temperatures have the tendency to increase the hardness of the already difficult to cut metals and this would increase the cutting forces drastically, which will lead to severe wear of the cutting flutes and consequently tool breakage. To this end, it was pertinent to increase the temperature of liquid nitrogen before applying it on the cutting zone. As a result, a 1.5 inches outer diameter and 1.375" (34.93 mm) inner diameter nozzle with an orifice of 1/16" (1.59 mm) was designed to help increase LN_2 temperature from -196˚C. Also, liquid nitrogen was mixed with shop air to help increase the cold air temperature to a more acceptable working temperature to avoid work-hardening of the workpiece. For this experiment a temperature of -15˚C was chosen for the mixture of LN_2 and shop air as the

optimum milling temperature for Inconel 718 super alloy based on published literature data [23]. The challenge therefore, was how to increase the temperature from -196˚C to -15˚C in the output nozzle.

2.4. CALIBRATION OF CRYOGENIC SET UP

The calibration of the cryogenic set up was necessary in order to ensure repeatability in getting a fixed optimum temperature of -15˚C at the output nozzle. To ensure a fixed temperature at the output nozzle, it is pertinent to determine a fixed amount of liquid nitrogen pressure and air pressure combination that will yield the desired temperature. The calibration was done by recording different values of LN_2 and air pressures and their corresponding temperatures at the nozzle outlet. A total number of 11 different combinations of LN_2 pressure, air pressure and their corresponding temperatures were made. To perform the calibration, a multiple regression model was developed using Statistica software 7 from Stat Soft. The multiple regression model has 2 factors namely: LN_2 pressure and shop air pressure, and one dependent variable which is the temperature at the nozzle outlet. The aim of the regression model is to establish a relationship between the factors LN_2 pressure and air pressure and the dependent variable output temperature. Thus, fixed values of LN_2 pressure and shop air pressure can be obtained, which when combined will give a nozzle output temperature of -15˚C. A 0.125" (3.175 mm) diameter ungrounded k-type thermocouple was taped around the nozzle output to record the temperature of LN_2 and air mixture. The multiple regression model is of the form:

$$Y = Bo + B_1X_1 + B_2X_2 + Є \quad \textbf{1}$$

Where Y represents the dependent variable output temperature, X_1 represents LN_2 pressure, and X_2 represents shop air pressure. Bo represents the intercept of the equation, B_1 represents the coefficient of LN_2 pressure, B_2 represents the coefficient of shop air pressure, and Є represents the error. The multiple regression analysis was performed using a significance level of 0.05. To begin calibrating, the cryogenic flow line was turned on for the LN_2 to gush out of the nozzle outlet. To ensure the pressure of LN_2 in the flow line was steady as seen from the gauge, LN_2 was allowed to flow out for about 20 minutes until the whole length of the flow line was completely frozen and ice became visible throughout the length of the flow line. This was important in order to prevent the fluctuation of LN_2 pressure in the flow line. Once the LN_2 pressure in the flow line became constant, shop air was turned on to mix with the LN_2 to form a mixture. Then, different values of LN_2 pressure and air pressure were selected and their output temperature was measured and recorded. The range of values of LN_2 pressure chosen was from 40 psi to 75 psi, while the range of values for shop air pressure chosen was 15 to 45 psi. These ranges of values were chosen arbitrarily, however, consideration was taken to avoid high air pressure so as to prevent excessive whistling noise made by air at high pressure. Firstly, LN_2 pressure at 40 psi was chosen together with air pressure of 15 psi. The temperature measured by the thermocouple was 2.41268 ˚C. Secondly, LN_2 pressure of 50 psi and air pressure of 20 psi were chosen, and the recorded temperature was 1.02068 ˚C. This procedure was repeated until 11 different combinations of LN_2 pressures and air pressures with their corresponding output temperatures were recorded. For each combination of LN_2 and air pressure, the reading of the thermocouple was recorded. Table 3 gives 11 cryogenic temperature calibration data

Table 3. Cryogenic Temperature calibration data

LN_2 Pressure Psi (MPa)	Air Pressure Psi (MPa)	Temperature (˚C)
40 (0.276)	15 (0.103)	2.41268
50 (0.345)	20 (0.138)	1.02068
55 (0.379)	30 (0.207)	-0.33645
60 (0.414)	15 (0.103)	-25.9122
60 (0.414)	30 (0.207)	-13.7055
60 (0.414)	25 (0.172)	-15.8007
65 (0.448)	30 (0.207)	-17.3153
65 (0.448)	35 (0.241)	-15.1913
70 (0.483)	35 (0.241)	-24.6755
70 (0.483)	40 (0.276)	-20.2317
75 (0.517)	45 (0.310)	-24.6572

The above data was entered into Statistica Software 7 and Analysis of Variance (ANOVA) was conducted on the observations to see if the treatment combination mean was significantly different from zero or not. In simple terms, to find out if the results gotten were significant. Table 4 presents the results obtained from Analysis of Variance (ANOVA).

Table 4. ANOVA for Calibration of Cryogenic set-up

Effect	Analysis of Variance; DV: Temperature				
	Sums of Squares	df	Mean Squares	F	P-level
Regress.	1023.510	2	511.7551	49.81684	0.000031
Residual	82.182	8	10.2727		
Total	1105.692				

From the ANOVA table above, it can be seen that the treatment combination has a p-value of 0.000031. This p-value is the probability that the observations made were due to random chance and not because of an actual variation of the effects. This p-value is compared with the significance level ($\alpha = 0.05$), and since the p-value is much less than 0.05 it shows there is sufficient evidence to conclude that the test for the treatment combination means is significant. In other words the result of the calibration is significant at the given significance level of 0.05.

Next, a model was fitted to the observations made by conducting a multiple regression analysis. The aim of the model is to generate an equation which best approximates the relationship between the independent variables (LN_2 and air pressures) and the dependent variable (temperature). A forward step wise multiple regression method was used, and Table 5 shows the results of the multiple regression model.

Table 5. Multiple regression model for calibration data

	Regression Summary for Dependent Variable: Temperature					
	R = 0.96211945 R^2 = 0.92567383 Adjusted R^2 = 0.90709228					
N = 11	F (2,8) = 49.817 P<0.00003 Std. Error of estimate: 3.2051					
	Beta	Std. Err. of Beta	B	Std. Err. of Beta	t(8)	p-level
Intercept			59.01976	7.417012	7.95735	0.000045
LN_2 Pressure	-1.52675	0.176607	-1.61276	0.186555	-8.64493	0.000025
Air Pressure	0.79834	0.176607	0.86543	0.191448	4.52045	0.001949

From the table, the p-values of the intercept, LN_2 pressure, and air pressure are 0.000045, 0.000025, and 0.001949 respectively. They are all less than the significance level of 0.05, and thus, their effect is not due to random chance and so they have a significant effect on temperature. Therefore, the 3 of them can be left in the model equation. Furthermore, the coefficients of the intercept, LN_2 pressure and air pressure are 59.01976, -1.61276, and 0.86543 respectively. Thus, the multiple regression equation becomes:

$$Y = 59.02 - 1.613 X_1 + 0.865 X_2 \quad \textbf{2}$$

Where Y represents temperature, X_1 represents LN_2 pressure and X_2 represents air pressure. The above equation can be used to predict values of shop air, when LN_2 pressure and temperature are known, and also values for LN_2 pressure when shop air pressure and temperature are known. Also, the R^2 value of the model is 0.9257, which is the value that measures the validity of the model. For this calibration, it means that 92.57

percent of the observed values can be accounted for by the model equation**.** Table 6 presents different predicted values of shop air pressure which will give temperatures of -10˚C, -15˚C, and -20˚C when LN_2 pressures are fixed.

Table 6. Pressure predicted values from calibration

Temperature(˚C)	LN_2 Pressure Psi (MPa)	Air Pressure Psi (MPa)
-10˚ C	55 (0.379)	22.77 (0.157)
	60 (0.414)	32.09 (0.221)
	65 (0.448)	41.42 (0.286)
-15˚C	**55 (0.379)**	**16.99 (0.117)**
	60 (0.414)	26.31 (0.181)
	65 (0.448)	35.64 (0.246)
-20˚C	55 (0.379)	11.21 (0.077)
	60 (0.414)	20.53 (0.142)
	65 (0.448)	29.86 (0.206)

These predicted values for shop air were gotten by substituting the fixed values of LN_2 pressures and the desired output temperatures into the model equation, and solving for X_2 which represents air pressure. Therefore, the table above presents calibrated values of various possible combinations of LN_2 pressure and air pressure, and their corresponding output temperature. For this experiment, a combination of LN_2 pressure at 55 psi and air pressure at 16.99 psi was chosen to give the optimum desired cooling temperature of -15˚C.

3. EXPERIMENTAL SET-UP AND PROCEDURE

A picture of the experimental set-up is shown in figure 1.

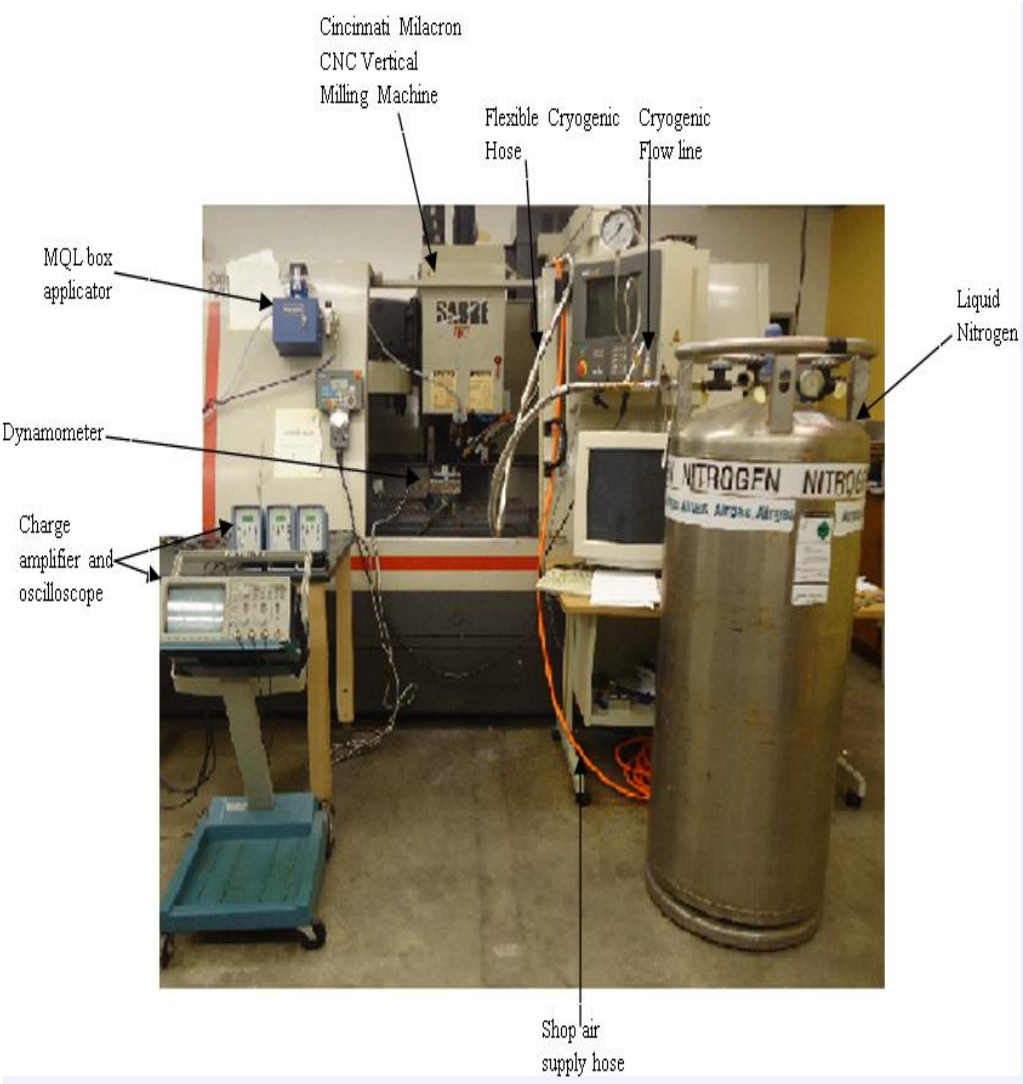

Figure 1. Photograph of complete experimental set-up showing VMC, force data acquisition system, MQL, LN_2 cooling strategies.

The set-up for the cooling strategies investigated was made up of cryogenic liquid nitrogen (LN_2) flow line built in-house at Missouri University of Science and Technology for liquid nitrogen (LN_2) cooling, and Acculube Minimum Quantity Lubricant precision box applicator for MQL cooling. Slot end-milling experiments were conducted on a

Cincinnati Milacron Vertical Machining Center (VMC), Sabre 750 equipped with acramatic 2100 controller. Two rectangular blocks of Inconel 718, AMS 5596 K of dimensions 3 in. (76.2 mm) × 6 in. (152.4 mm) × 1.5 in. (38.1 mm) were used for the slot end-milling experiments. These blocks of Inconel 718 were already previously drilled, counterbored and tapped for other investigations of cutting force components and cutting temperature reported in another paper. A 4-flute uncoated bull-nose solid carbide helical end-mill of 0.5 inch (1.27 mm) diameter, 1 inch length of cut, 3 inches overall length 0.03 inch corner radius was used for all experimental runs. Two sets of machining tests were conducted in this experiment using both blocks of Inconel 718. Each block was designed to contain a maximum of 8 slots, and the slots were separated by a rib of width 0.125 in. First, 9 slots each having a depth and width of 1 in. and 0.5 in. respectively were made in order to investigate the effects of machining parameters and the three cooling strategies on surface roughness and also to obtain optimum machining parameters and cooling strategy that will give the least surface roughness. The machining parameters investigated were: spindle speed at 250 (10), 500 (20), and 750 rpm (30) m/min, feed rates at 1, 2, and 3 ipm. While the cooling strategies investigated were: MQL, LN_2 and combined (MQL+LN_2). An axial depth-of-cut of 0.05 in. was chosen and held constant for all experimental runs. Also, the radial depth of cut was constant at 0.5 in. The machining parameters used were specific to the carbide tool used for this experiment, and were chosen based on contemporary machining standards obtainable in many manufacturing industries after due consultations. Also, before arriving at these parameters, various spindle speeds and feed rates were investigated and many issues were encountered. Speeds of 900, 1000, 1500, and 2000 rpm were first investigated; however,

the cutting forces generated were so high thereby causing tool breakage along the shank with just a little impact on the workpiece. Likewise, feed rates of 6, 9 and 12 ipm were investigated. These also generated extremely high cutting forces and led to tool breakage within a short machining duration. This is because machining Inconel 718 in extremely high speeds and feeds generates an enormously high amount of temperature at the cutting zone and also induces high cutting forces, which results in an extreme wear of the cutting edges, high surface roughness and high residual stresses. This invariably leads to total plastic deformation of the cutting edges, and in very extreme cases tool breakage. Also, various axial depths-of-cut were investigated such as: 0.125 inches, 0.1 inches, and 0.0625 inches. These axial depths-of-cut induced very high cutting forces, which led to complete plastic deformation of the cutting edges and tool breakage. For this experiment, an axial depth-of-cut of 0.05 in. was found to be suitable and was used for all experimental runs conducted. This resulted in a total of 20 passes made for each slot in order to achieve the required depth of 1 inch. For each machining pass, the appropriate speed, feed and cooling strategy were used. A new end-mill was used for each slot bringing the total to 9 end-mills used for the first part of this experiment. For the second part of this experiment, a high spindle speed of 750 rpm and low feed rate of 1 ipm were chosen and used in conducting a comparative evaluation of the 3 cooling strategies, MQL, LN_2, and combined (MQL+LN_2), in order to see which of the cooling strategies optimized the machining process the most, in terms of surface roughness and residual stress reduction. Therefore, an additional 2 end-mills were used bringing the total number of end-mills used for all machining tests to 11.

After machining the slots, a pocket surf profilometer was used to measure the surface roughness of the slots. Surface roughness was measured on the left rib and on the web of each slot. The measurement on the rib was made perpendicular to the feed direction (positive Y-axis), where roughness is more pronounced. Also, surface roughness measurements were taken at 3 different locations (1 inch apart) along the left rib and the web, and the three points were used to perform Analysis of Variance (ANOVA) in order to obtain experimental error. The unit of surface roughness used for this experiment was micro meters (μm). To measure surface roughness, the profilometer probe was made to rest on the surface being measured in such a way that it was on the same level with the surface. After pressing the start button, the probe moves backwards and forwards according to the traverse length that is set and the surface roughness value is measured and displayed on the read-out screen. In this way, surface roughness values were obtained for the left ribs and the webs of all the machined slots at 3 different locations. Additionally, the machining parameters and cooling strategy, which gave the least surface roughness was determined and chosen as the optimum parameters for surface roughness improvement during slot end-milling Inconel 718. Also, a comparative evaluation was made between the 3 cooling strategies to ascertain which of the 3 cooling methods gave the least surface roughness at high speed of 750 rpm (30 m/min) and a low feed rate of 1 ipm (25.4 mm/min).

Also, as mentioned before, Proto Manufacturing was contracted to measure the residual stresses of designated slots. Measurements were made on the left rib of 3 slots to be used for comparative evaluation of the 3 cooling strategies. Both compressive and tensile stresses for each designated slot were determined**.** For most thin-walled machined

parts, compressive stresses are preferred to tensile stresses. The cooling strategy that gave the lowest compressive stresses and the highest tensile stresses were determined. Residual stress measurements were performed using a 2.0 mm round aperture. The collection time for each x-ray diffraction peak was about 30 seconds. Furthermore, the x-ray diffraction residual stress measurements were collected using the multiple exposure technique with a minimum of 22 psi, angles as per SAE HS784. A target was used to diffract from the (311) plane for all locations at a diffraction angle of 152º. A Gaussian function was used to fit the diffraction peaks. The XEC was determined experimentally as per ASTM E1426 to be 22,896 ksi. All residual stress measurements were performed using the Proto LXRD stress analyzer. Figure 2 shows 2-D and 3D schematics of the machined slots.

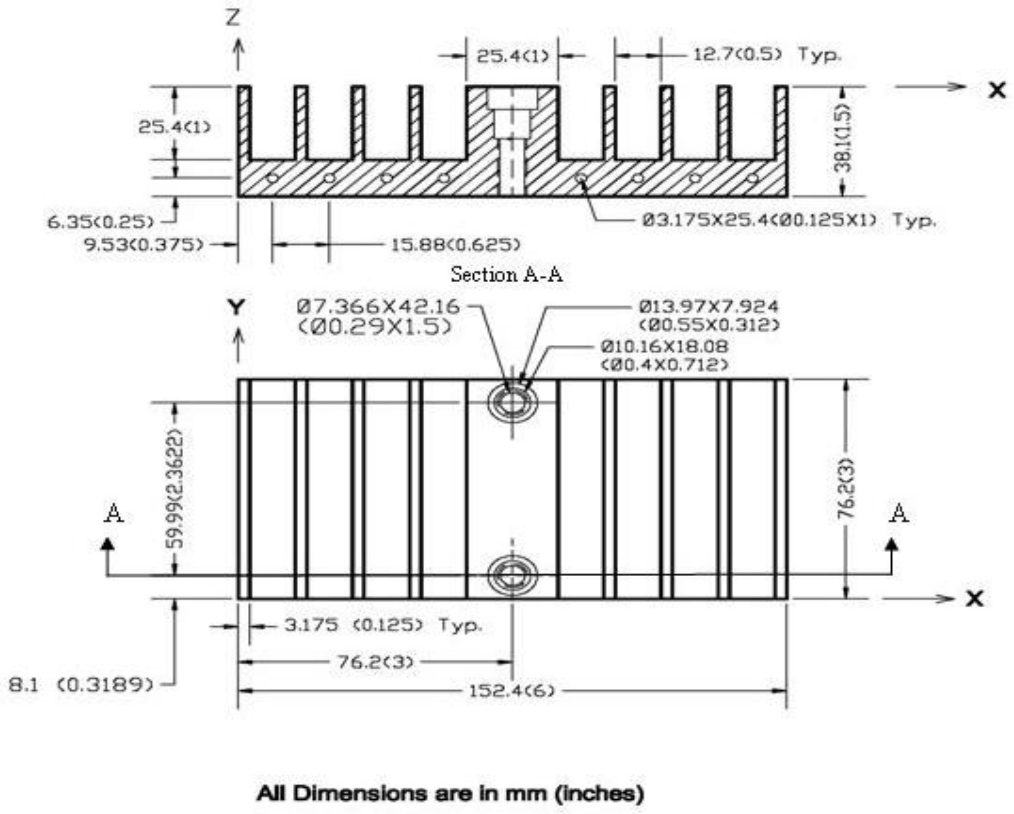

Figure 2.Workpiece design for slot end-milling experiments

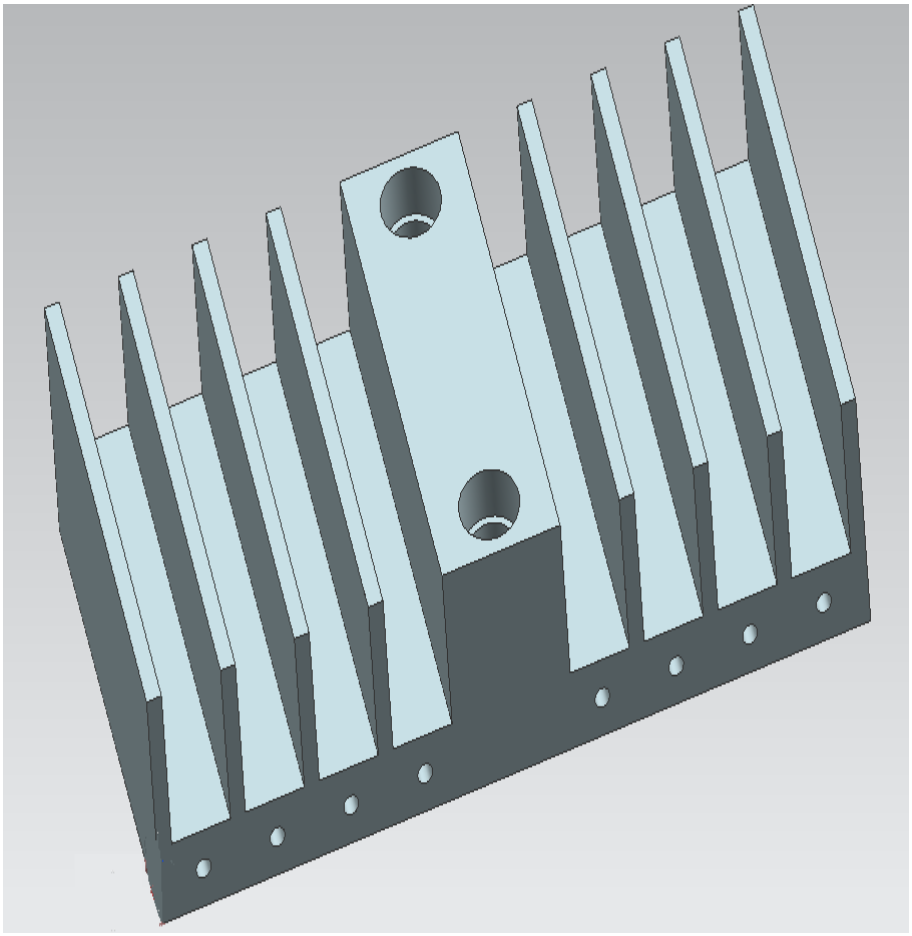

Figure 2.Workpiece design for slot end-milling experiments (Cont.)

3.1. SURFACE ROUGHNESS MEASUREMENT

In this experiment, surface roughness was measured using a portable Brown and Sharpe pocket surf profilometer. This profilometer uses a piezoelectric probe for measurements. A traverse length of 0.195 inches (5 mm) was chosen. A cut-off position of 5 was chosen for this experiment. In addition, the profilometer has 3 evaluation lengths of 0.3 inches (0.8 mm); 0.09 inches (2.4 mm); 0.15 inches (4 mm), and a traverse speed of 0.2 inches (5.08) per second. An evaluation length of 0.15 inches (4 mm) was chosen

for this experiment. Roughness average (Ra) was used for this experiment, which measures roughness by taking the arithmetic average height of roughness irregularities measured from a mean line within the evaluation length.

3.2. RESIDUAL STRESS MEASUREMENT

After machining of the 9 slots**,** Proto manufacturing Taylor MI was contracted for the measurement of residual stresses for comparative evaluation of the 3 cooling strategies. X-ray diffraction method was used to measure residual stresses on the left rib. The X-ray diffraction uses the distance between crystallographic planes, i.e. d-spacing as a strain gage. When the material is in tension, the d-spacing increases and when the material is under compression the d-spacing decreases. The diffraction angle 2θ is measured experimentally and the d-spacing is then calculated using Bragg's law. The presence of residual stresses in the material produces a shift in the X-ray diffraction peak angular position which is directly measured by the detector. The determination of the shift in the Bragg angle is thus interpreted in terms of shifts in the lattice spacing.

Bragg's law, $n\lambda = 2d\sin\theta$ **2**

Where λ is the wavelength of the radiation.

Figure 3 shows the photograph of the residual stress set-up from Proto manufacturing

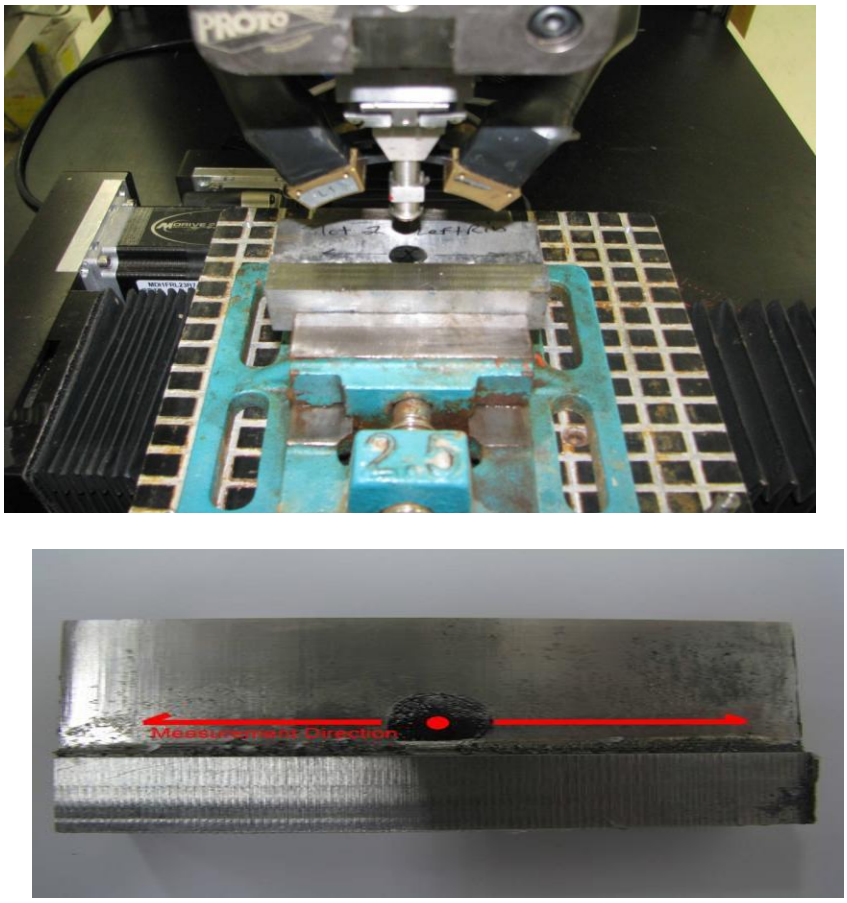

Figure 3: Photograph of Residual Stress Measurement set-up (Proto Manufacturing)

Wire of diameter 0.012 inch (0.30480 mm) was used with on a Hitachi Model 8Q EDM machine to cut off the identified left ribs for measurement.

3.3. MACHINING CODES

The slot end-milling experimental runs were performed at cutting speeds of 250 rpm, 500 rpm, and 750 rpm, feed rates at 1 ipm, 2 ipm and 3 ipm, and cooling strategies were cryogenic cooling at -15^{o}C, and minimum quantity lubrication at constant axial and radial depths of cut of 0.125" (3.175 mm) and 0.5" (12.7 mm) respectively were maintained. The feed direction of the workpiece/table was along the positive y-axis of the workpiece/table applying right-hand rule. A total of 20 machining passes were made for each machined slot, for the 1 inch (25.4 mm) deep slots. The CNC program containing the G & M codes for machining test run #1 (slot #1) in inch unit is given below;

: T1 M6;

N10 G01 X0.375 Y-1 Z1 F50;

N20 G01 Z-0.05 F10; (Pass #1)

N30 S250 M03

N40 G01 Y3.7 F1

N50 G01 Z1 F50

N60 G01 X0.375 Y-1 F50

N70 G01 Z-0.1; (Pass # 2)

N80 G01 Y3.7 F1

N90 G01 Z1 F50

N100 G01 X0.375 Y-1 F50

N110 G01 Z-0.15; PASS # 3

N120 G01 Y3.7 F1

N130: G01 Z1 F50

N140: G01 X0.375 Y-1 F50

N150: G01 Z-0.2 F10; PASS # 4

N160: G01 Y3.7 F1

N170: G01 Z1 F50

N180: G01 X0.375 Y-1 F50

N190: G01 Z-0.25 F10; PASS # 5

N200: G01 Y3.7 F1

N210: G01 Z1 F50

N220: G01 X0.375 Y-1 F50

N230: G01 Z-0.3 F10; PASS # 6

N240: G01 Y3.7 F1

N250: G01 Z1 F50

N260: G01 X0.375 Y-1 F50

N270: G01 Z-0.35 F20; PASS # 7

N280: G01 Y3.7 F1

N290: G01 Z1 F50

N300: G01 X0.375 Y-1 F50

N310 G01 Z-0.4 F10

N320 G01 Y3.7 F1

N330 G01 Z1 F4

N340 G01 X0.375 Y-1 Z-0.45 PASS #9

N350 G01 Y3.7 F1

N360 G01 Z1 F50

N370 G01 X0.375 Y-1 Z-0.5 PASS #10

N380 G01 Y3.7 F1

N390 G01 Z1 F4

N400 M02

4. RESULTS AND DISCUSSIONS

4.1. SURFACE ROUGHNESS

Table 7 and 8 show the measured surface roughness values for the left rib and web respectively for all 9 slots. Surface roughness of the machined left rib and bottom of the slot (web surface) were measured at 3 different points (Ra_1, Ra_2, and Ra_3) along the rib and the web, and these points were used as replications to conduct ANOVA.

Table 7.Measured Surface roughness values on the left rib

Expt. Runs	Treat. Comb.	3 factors at 3 levels			Surface Roughness (Left Rib)			
		Cooling Method	Speed (rpm)	Feed (ipm)	Ra_1 (µm)	Ra_2 (µm)	Ra_3 (µm)	Ra ave (µm)
1	(0,0,0)	MQL	250	1	1.22	1.26	1.70	1.39
2	(0,1,2)	MQL	500	3	0.52	0.60	0.5	0.54
3	(1,0,1)	LN_2	250	2	0.39	0.52	0.60	0.50
4	(2,0,2)	MQL+LN_2	250	3	0.73	0.72	0.89	0.78
5	(0,2,1)	MQL	750	2	0.39	0.58	0.47	0.48
6	(1,1,0)	LN_2	500	1	0.61	0.94	1.72	1.09
7	(1,2,2)	LN_2	750	3	1.86	3.2	3.04	2.7
8	(2,1,1)	MQL+LN_2	500	2	0.41	0.36	0.62	0.46
9	(2,2,0)	MQL+LN_2	750	1	0.48	0.60	2.59	1.22

Table 8. Measured Surface roughness values on the web

Exp. Runs	Treat. Comb.	3 factors at 3 levels			Surface Roughness (Web)			
		Cooling Method	Speed (rpm)	Feed (ipm)	Ra_1 (µm)	Ra_2 (µm)	Ra_3 (µm)	Ra ave (µm)
1	(0,0,0)	MQL	250	1	0.77	0.91	0.84	0.84
2	(0,1,2)	MQL	500	3	0.33	0.21	0.24	0.26
3	(1,0,1)	LN_2	250	2	1.1	1.92	2.96	1.99
4	(2,0,2)	MQL+LN_2	250	3	1.09	1.06	0.79	0.98
5	(0,2,1)	MQL	750	2	0.28	0.25	0.19	0.24
6	(1,1,0)	LN_2	500	1	0.7	0.53	1.09	0.77
7	(1,2,2)	LN_2	750	3	1.48	3.65	4.22	3.12
8	(2,1,1)	MQL+LN_2	500	2	0.55	0.72	0.92	0.73
9	(2,2,0)	MQL+LN_2	750	1	0.38	0.55	0.6	0.51

4.2. ANALYSIS OF VARIANCE (ANOVA)

Table 9 and 10 shows the results of the analysis of variance for surface roughness on the left rib and the web respectively.

Table 9. ANOVA for Surface roughness values on the left rib

Factor	ANOVA; Var. :Ra (Left rib); R-sqr = 0.72351; Adj: 0.60063 3 3-Level factors, 1 block, 27 runs; MS Residual = 0.265237 DV: Ra (Left rib)				
	SS	df	MS	F	p
(1)cooling L+Q	2.29132	2	1.145659	4.319379	0.029365
(2)speed L+Q	5.00780	2	2.503902	9.440241	0.001571
(3)feed L+Q	3.74563	2	1.872813	7.060902	0.005448
1*2	2.43469	1	2.434689	9.179295	0.007204
1*3	2.62205	1	2.622050	9.885686	0.005610
Error	4.77427	18	0.265237		
Total SS	17.26759	26			

Table 10. ANOVA for Surface roughness values on the Web

Factor	ANOVA; Var. :Ra (Web); R-sqr = 0.76951; Adj: 0.66707 3 3-Level factors, 1 block, 27 runs; MS Residual = 0.3474889 DV: Ra (Web)				
	SS	df	MS	F	p
(1)cooling L+Q	11.61210	2	5.806048	16.70859	0.000079
(2)speed L+Q	2.45647	2	1.228235	3.53460	0.050721
(3)feed L+Q	6.08295	2	3.041473	8.75272	0.002212
1*2	3.62702	1	3.627022	10.43781	0.004638
1*3	1.84961	1	1.849606	5.32278	0.033147
Error	6.25480	18	0.347489		
Total SS	27.13699	26			

Table 9 shows that the main effect of cooling, speed, and feed significantly affect surface roughness on the left rib. Furthermore, the 2-factor interactions of cooling and speed, as well as cooling and feed also significantly affect surface roughness on the left rib. This is because their p-values are less than the significance level (0.05).

Table 10 shows that the main effect of cooling and feed significantly affect roughness on the web, while the main effect of speed does not significantly affect roughness on the web. Also the 2-factor interaction of cooling and speed, as well as the 2-factor interaction of cooling and feed significantly affect surface roughness on the web.

4.3. PARETO CHART OF EFFECTS ON THE LEFT RIB AND WEB

Figure 4 shows the Pareto chart of the effects of machining parameters and cooling strategies on surface roughness on the left rib and the web respectively.

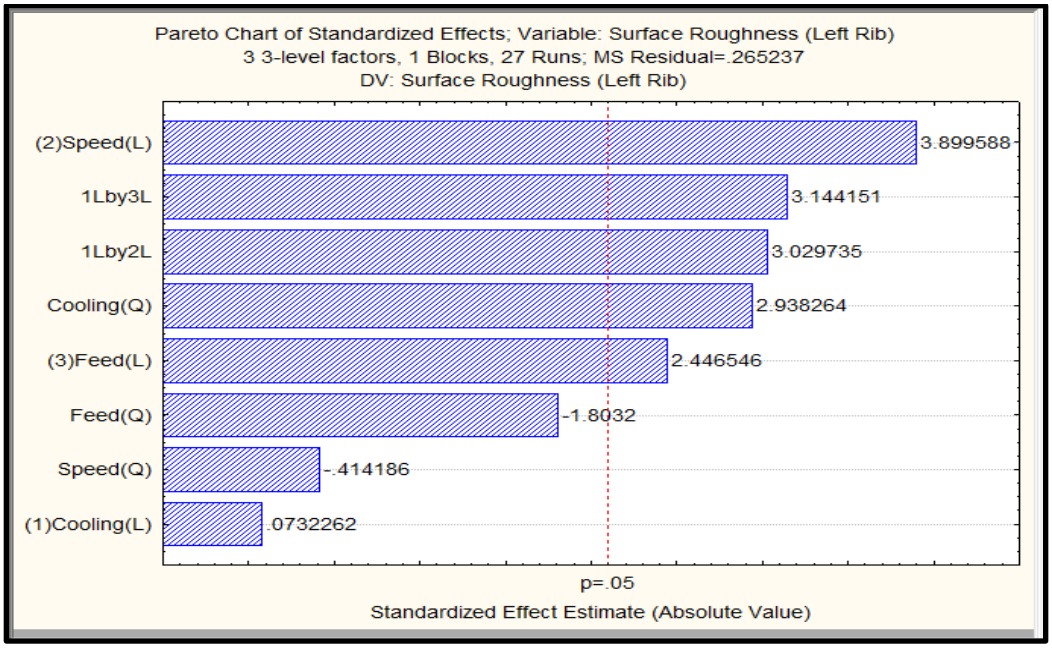

a. Pareto chart of effects on surface roughness on the left rib

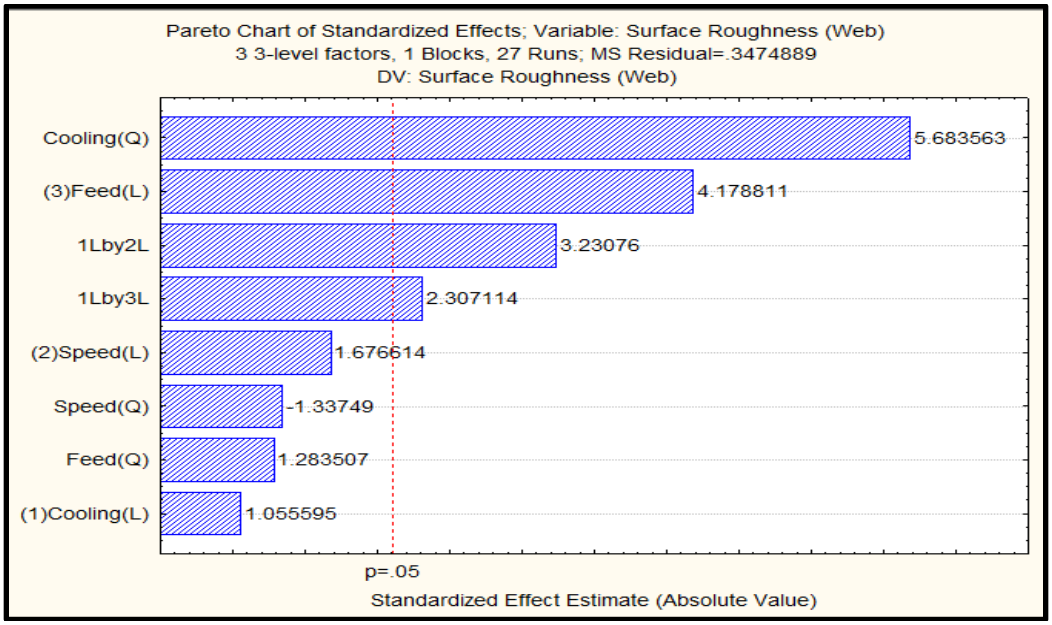

b. Pareto chart of effects on surface roughness on the web

Figure 4. Pareto chart of effects on surface roughness on the left rib and web.

The Pareto chart of figure 4a shows the linear main effect of speed to be the most significant effect on surface roughness on the left rib, followed by the 2-factor interaction of cooling and feed, and the 2-factor interaction of cooling and speed. The quadratic main effect of cooling and the linear main effect of feed are the 4^{th} and 5^{th} significant parameters respectively. All these parameters have increasing effect on surface roughness with their increase. Additionally, figure 4b shows the quadratic main effect of cooling to have the most significant effect on surface roughness on the web, followed by the linear main effect of feed. The 2-factor interaction of cooling and speed together with the 2-factor interaction of cooling and feed are the 3^{rd} and 4^{th} most significant parameters affecting surface roughness on the web. All parameters have increasing effect on surface roughness with their increase.

4.4. MARGINAL MEANS PLOT OF MAIN EFFECTS ON SURFACE ROUGHNESS ON THE LEFT RIB AND THE WEB

Figure 5 shows the marginal means plot for surface roughness on the left rib and web.

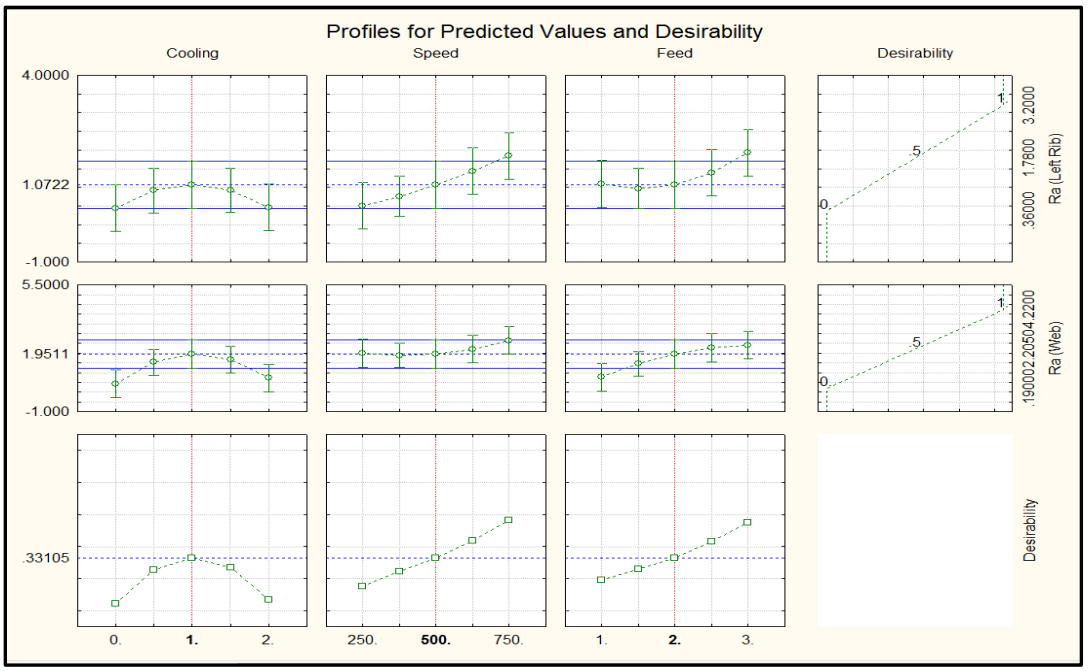

Figure 5. Marginal means plot of main effects on surface roughness on the left rib and the web

The plot shows the variation of the 3 factors on surface roughness on the left rib and the web. They both show similar variation when compared among the 3 factors. The speed and feed curves increase continuously from low value to high value while that of cooling increases from a low value to a high one, before descending again to a low value.

4.4. EFFECTS OF COOLING STRATEGIES ON SURFACE ROUGHNESS ON THE LEFT RIB AND WEB.

From the Pareto charts, the quadratic effect of cooling was the 4th most statistically significant factor affecting surface roughness on the left rib, while the quadratic effect of cooling was the most significant factor affecting surface roughness on the web. Furthermore, figure 5 shows that the quadratic effect of cooling has an increasing effect on the surface roughness on the left rib and the web. Furthermore, figure 5 shows that medium cooling strategy (cryogenic liquid nitrogen) gave the highest surface roughness on the left rib. Figure 5 shows that as the cooling strategy changed from low (MQL) to medium cooling (cryogenic LN_2), surface roughness on the rib and

the web increased to a maximum, and reduced while the cooling strategy was changed from cryogenic to high cooling strategy (MQL+LN_2). The reduction in surface roughness on both the left rib and the web when using MQL and combined MQL+LN_2 can be attributed to the lubricating effect of oil during slot end-milling Inconel 718. Oil improves lubrication by reducing coefficient of friction, and consequently tool wear. This invariably leads to improvement in the surface of a machined part. Conversely, the increase in surface roughness while using cryogenic liquid nitrogen cooling strategy at -15°C may be attributed to the work-hardening effect of the workpiece resulting from the use of extremely low temperatures of liquid nitrogen, together with the lack of lubrication at the tool-chip/tool-workpiece interface. These lead to severe tool wear which severely degrades the surface of the machined surface.

4.5. EFFECTS OF SPINDLE SPEED ON SURFACE ROUGHNESS ON THE LEFT RIB AND WEB.

From the Pareto chart of figure 4a, the linear effect of spindle speed was the most statistically significant effect on surface roughness on the left rib, while figure 4b shows that the main effect of speed was not significant on surface roughness on the web. It also shows that as speed increases, surface roughness on the left rib and web increases. This is evident in the marginal means plot in figure 5, which shows surface roughness on the left rib and web to have increased to a maximum value as the speed increased. This means a change of speed from 250 rpm to 750 rpm in slot end-milling inconel 718 had an adverse effect on surface finish of the machined part. Ulutan and Ozel (2011) conducted a review on machining induced surface integrity in titanium and nickel alloys. They reported also that an increase in machining speed leads to an increase in surface roughness of the machined part. They attributed this to the fact that during high-speed machining of

Inconel 718, the high temperature generated causes built-up layers to be created at the cutting location, which might push the tool away from its original route, thereby increasing the surface roughness. This means that high-speed machining does not improve the machinability of Inconel 718 in terms of surface roughness reduction.

4.6. EFFECTS OF FEED RATE ON SURFACE ROUGHNESS ON THE LEFT RIB AND WEB.

From the Pareto chart in Figure 4a, the linear effect of feed was the least significant effect on the surface roughness of the left rib, while the linear effect of feed was the 2nd most significant effect on surface roughness on the web as shown in the Pareto chart figure 4b. Figure 5 shows that an increase in feed rate increased surface roughness on the left rib and the web. This means that as the feed rate was changed from 1 ipm to 3 ipm, there was an increase in the surface roughness of the rib and the web. A low feed rate of 1 ipm produced the lowest surface roughness both on the rib and the web, while a high feed rate of 3 ipm produced the highest surface roughness on the rib and the web.

4.7. MACHINABILITY IMPROVEMENT BY SURFACE ROUGHNESS REDUCTION

Figure 6 shows a 3D surface desirability and contour plot for surface roughness improvement on the left rib and the web respectively during slot end-milling Inconel 718 alloy.

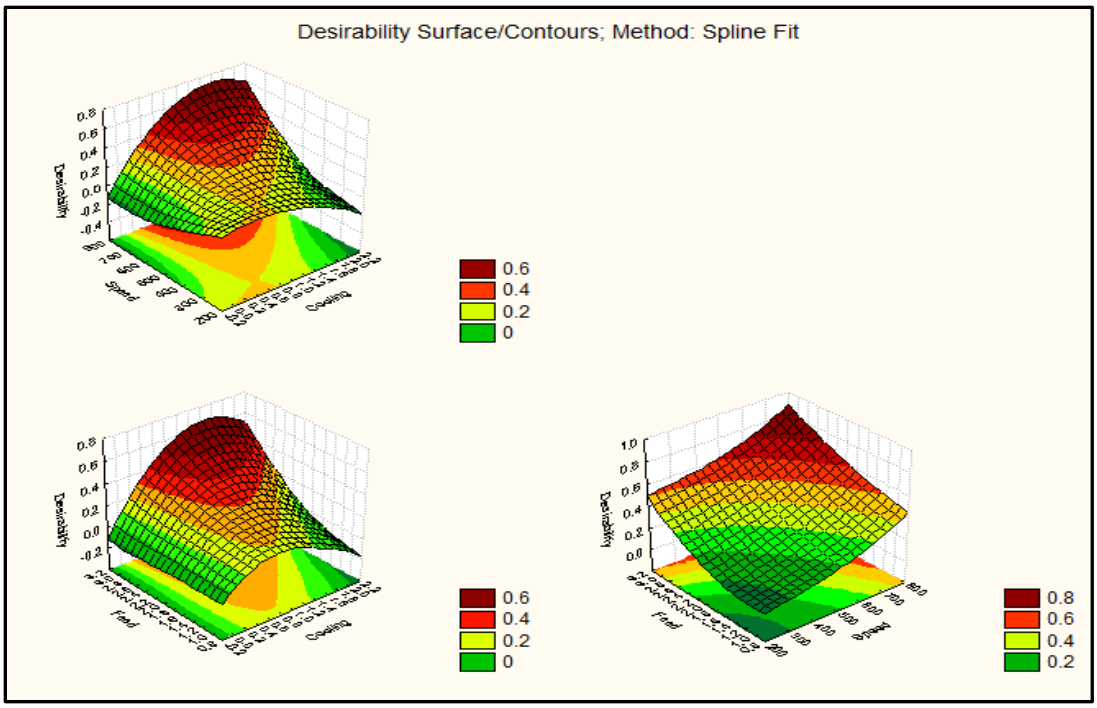

Figure 6. Surface Desirability/contour plot of surface roughness

The 1st plot shows that high speeds and high cooling strategy of combined MQL+LN_2 gave the best surface finish on the left rib and the web. In the 2nd plot of figure 6, high (MQL+LN_2) and low (MQL) cooling strategies, together with medium and high feed rates of 2 ipm and 3 ipm gave the lowest surface roughness on the left rib and the web. Lastly, the 3rd plot of figure 6 shows that a combination of low speed and low feed rate was most desirable in improving the surface integrity of the machined part in the left rib and the web. Therefore, a low spindle speed of 250 rpm and a low feed rate of 1 ipm are the optimum machining parameters that improved surface roughness the most during slot end-milling Inconel 718 alloy.

4.8. SURFACE ROUGHNESS COMPARATIVE INVESTIGATION OF THE 3 COOLING STRATEGIES

A comparative investigation of the 3 cooling strategies of (MQL, LN_2, & MQL+LN_2) was conducted for surface roughness on the left rib and the web using fixed machining parameters (high speed 750 rpm and low feed 1 ipm). Surface roughness was measured at 3 locations 1 inch apart along the left rib and the web and averaged. The values measured for the left rib and the web are given in table 11 and 12 respectively.

Table 11. Table for comparative evaluation of surface roughness on the left rib

Cooling Method	Ra_1 (µm)	Ra_2 (µm)	Ra_3 (µm)	Ra ave (µm)
MQL	1.24	0.82	0.89	0.98
LN2	2.47	3.89	4.01	3.46
MQL+LN2	0.48	0.6	2.59	1.22

Table 12. Table for comparative evaluation of surface roughness on the web

Cooling Method	Ra_1 (µm)	Ra_2 (µm)	Ra_3 (µm)	Ra ave (µm)
MQL	0.24	0.29	0.61	0.38
LN2	1.4	N/F	N/F	N/F
MQL+LN2	0.38	0.55	0.6	0.51

The value of surface roughness measured at 3 different points along the left rib and the web 1 inch apart was averaged and the resulting values were used in plotting a

histogram for each of the 3 cooling strategies. The cell designated as N/F stands for "non-feasible", and this corresponds to the regions in the web where measurement could not be taken as a result of a severely degraded slot. During machining with LN2 cooling strategy, the tool was severely worn as a result of high temperatures generated. As a result, the surface integrity of the slot was greatly impaired. The surface was burnt with large formations of built-up edges that had a bluish coloration. Consequently, it was impossible for the piezoelectric probe of the profilometer to slide forwards and backwards in order to make the surface roughness measurement. Therefore, measurements could not be made on the web of the slot where LN2 cooling strategy was used. Figure 7 is a plotted histogram of surface roughness values on the left rib and on the web for each cooling strategy.

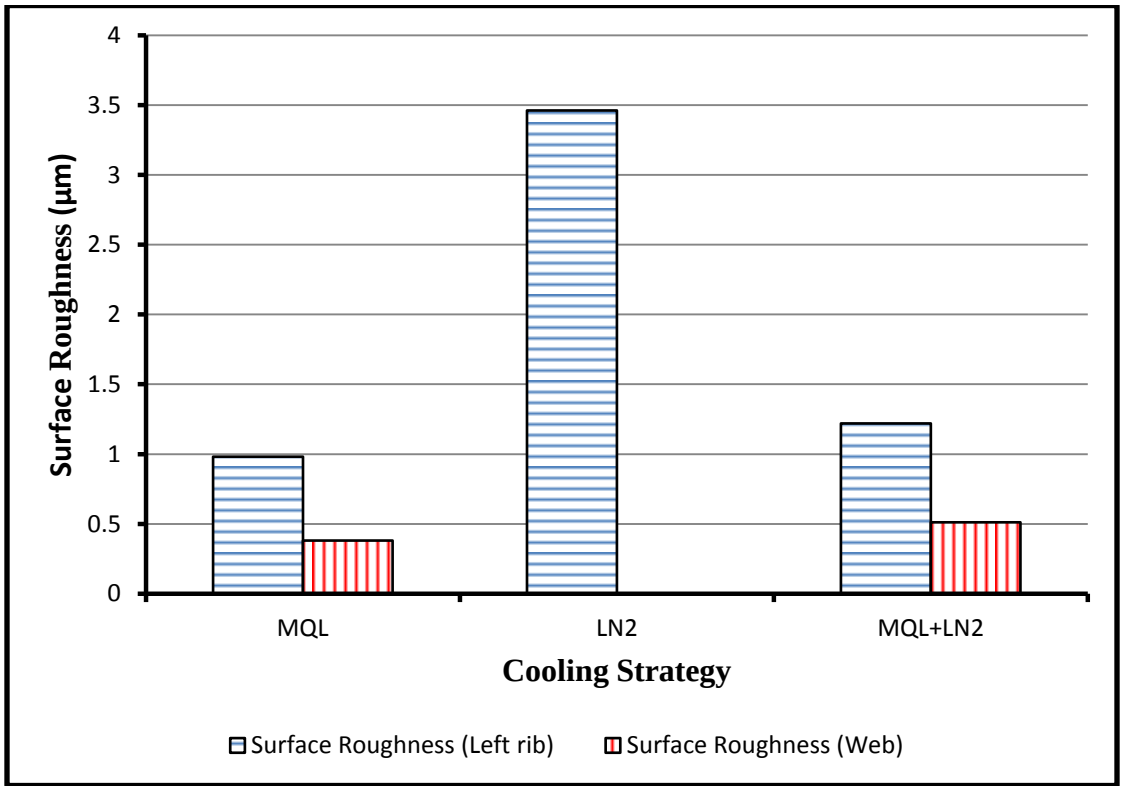

Figure 7. Comparative evaluation of cooling strategies on surface roughness on the left rib and web.

Figure 7 shows the surface roughness values for the left rib and the web. It shows that the surface roughness on the left rib is higher than that on the web for each of the 3 cooling strategies. As explained earlier, surface roughness on the web when using LN2 cooling strategy could not be measured as a result of the inability of the probe of the profilometer to slide on the severely degraded slot. Thus, no value was obtained for that. Furthermore, the plot shows that LN_2 cooling strategy gave the highest surface roughness on the left rib, while MQL gave the least surface roughness, followed by the combination of MQL & LN_2. From the results obtained, it can be deduced that MQL improved surface integrity on the left rib by 71.68 % compared to LN_2 cooling strategy, while combined MQL+LN_2 improved surface integrity by 64.7% compared to LN_2 cooling strategy. Furthermore, MQL improved surface roughness only about approximately 20 % compared to MQL+LN_2 on the left rib. Likewise, MQL improved surface roughness on the web by about 25 % compared to combined MQL+LN_2, while surface roughness values on the web for LN_2 cooling strategy could not be measured because LN_2 produced a very poor surface finish.

4.9. RESIDUAL STRESS

Residual stresses were measured at 1 point each (X = 1.5 inches and Z= 0.75 inches) as shown in figure 8 on the left rib of slots 2 (MQL+LN_2), 7 (MQL), and 8 (LN_2) at 4 different depths of 0 mm, 0.01 mm, 0.02 mm and 0.05 mm to be used for comparative evaluation of the 3 cooling strategies. The slots were machined at a high speed of 750 rpm and a low feed rate of 1 ipm. The results of the measurements are given in tables 13.

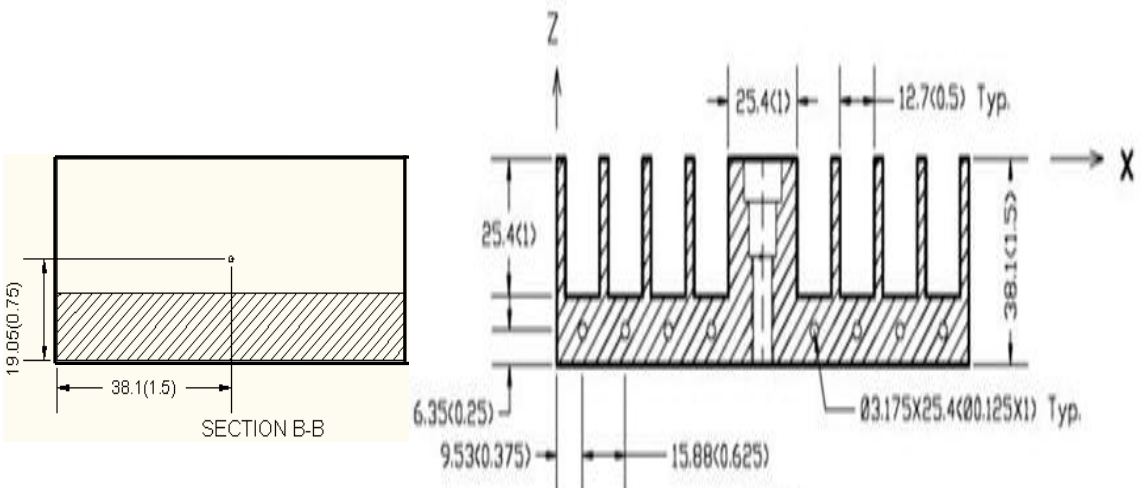

All dimensions are in mm (inches)

Figure 8: Measurement Location for residual stresses

Table 13. Residual stress values for comparative analogy

Depth (mm)	Rib 2 ($MQL+LN_2$) (ksi)		Rib 7 (MQL) (ksi)		Rib 8 (LN_2) (ksi)	
0.00	+45	± 2	-49	±2	+58	±3
0.01	+23	± 1	-73	±1	+69	±3
0.02	+17	± 1	-80	±1	+95	±3
0.05	+37	± 1	-55	±1	+97	±1

The residual stress values were plotted for each depth measured. Figure 9 shows the variation of residual stress with depth.

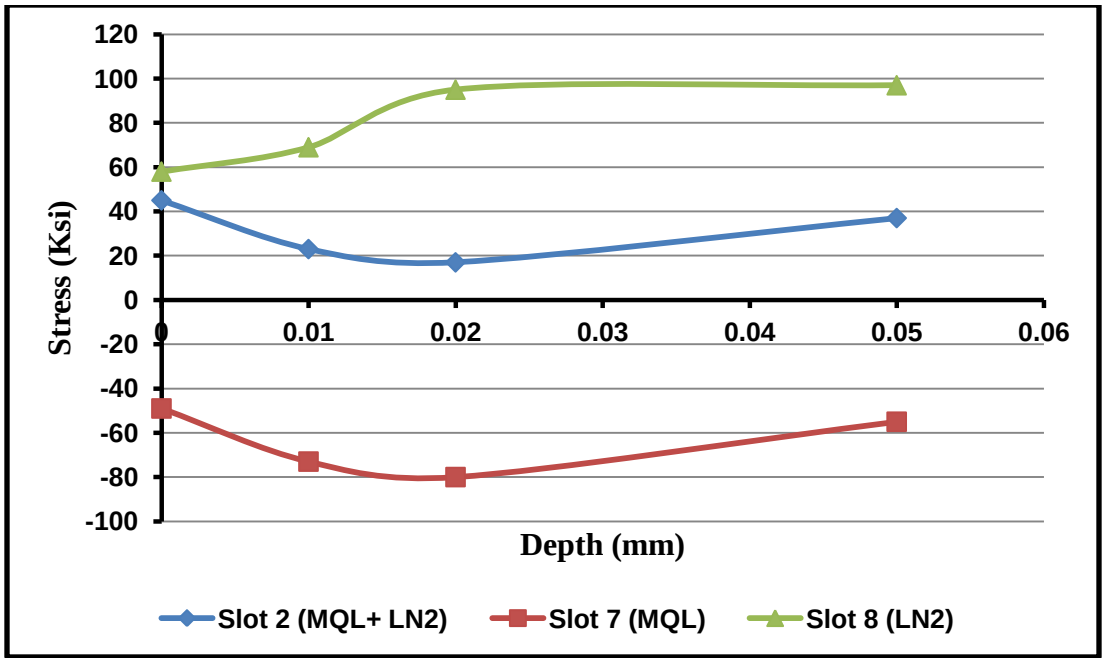

Figure 9. Plot of residual stress versus depth on the left ribs.

The plot shows that MQL cooling strategy gave compressive residual stress values on the surface and at each measured depth. Conversely, combined (MQL+LN_2) and LN_2 cooling strategies gave tensile residual stress values on the surface and at every measured depth. However, LN_2 cooling strategy produced higher tensile surface residual stress values compared to combined (MQL+LN_2). High tensile stresses adversely affect the fatigue life of many engineering components and thus, increase the likelihood of failure. Compressive residual stresses increase the fatigue life of components. Therefore, MQL cooling strategy gave the best effect, in terms of inducing compressive residual stresses. Furthermore, combined (MQL+LN_2) gave the lower tensile stresses compared to LN_2 cooling strategy. The reason combined (MQL+LN_2) and LN_2 cooling strategies gave tensile stresses can be attributed to the effect of increased wear in the flank of the tool, as a result of the work-hardening effect triggered by the extremely cold temperatures of cryogenic liquid nitrogen at -15° C. Cold temperatures of LN_2 work-hardens Inconel 718

workpiece, which leads to an increase in coefficient of friction at the tool-workpiece interface and tool wear. The increased tool wear observed from using both cooling strategies severely degraded the machined surface, thereby inducing tensile residual stresses. Peng et al. (2013) lent credence to this when he investigated surface integrity and the influence of tool wear in high speed machining of Inconel 718. He explained that with increase in tool wear, mechanical forces and heat involved in the cutting operation increased, which leads to more drastic changes in the surface integrity. He further stated that high surface tensile residual stresses and dissolution of reinforcing precipitates and recrystallization of the surface layer were induced by severe tool wear which can significantly affect the fatigue life of the machined part. Additionally, E.O. Ezugwu (2004) reiterated that the use of cryogenic cooling in grinding operations can alter the chemical and physical properties of ground surfaces, thereby inducing tensile residual stresses, as well as surface and subsurface cracks which are detrimental to the fatigue life of machined parts.

5. CONCLUSIONS

This research investigated the effects of machining parameters and cooling strategies on surface roughness and a comparative performance evaluation of 3 cooling strategies (MQL, LN_2 at -15 ˚C and combined (MQL+LN_2) in high-speed end-milling of Inconel 718 alloy. From the results obtained, the following conclusions can be drawn:

1. Results obtained from analysis of variance show that cooling strategy, speed, and feed rates, as well as their 2-factor interactions all significantly affect surface roughness on the left rib. Furthermore, cooling strategy and feed rate significantly affect surface roughness on the web but not speed.

2. Low spindle speed (250 rpm) gave the least surface roughness on the rib and the web, while high spindle speed (750 rpm) gave the highest surface roughness on the rib and the web.

3. Low feed rate of 1 ipm (25.4 mm/min) is the best feed rate for reducing surface roughness on the rib and on the web, while high feed rate 3 ipm (76.2 mm/min) gave the highest surface roughness on the rib and web.

4. Combined (MQL+LN_2) and MQL cooling strategies generates lower surface roughness values on the rib and web compared to LN_2 cooling strategy.

5. From the results of comparative evaluation of surface roughness, MQL and combined MQL+LN_2 improve surface roughness on the left rib by 71.68% and 64.7% respectively compared to LN_2 cooling strategy.

6. MQL improved surface roughness on the left rib by approximately 20% compared to combined (MQL+LN_2).

7. LN_2 produced a highly degraded surface finish on the web during high-speed slot end-milling of Inconel 718 and thus could not be measured. Whereas, MQL and combined (MQL+LN_2) produced a very smooth finish on the web with MQL performing slightly better than combined (MQL+LN_2) by 25%

8. From the comparative evaluation with reference to residual stresses, MQL gave the best effect on residual stresses by inducing compressive stresses for every measured depth compared with combined (MQL+LN_2) and LN_2 cooling strategies which generates tensile residual stresses.

ACKNOWLEDGEMENTS

The financial support from the National Science Foundation (NSF) under grant No. CMMI800871 and the Intelligent Systems Center (ISC) of the Missouri University of Science and technology are gratefully acknowledged. The financial assistance provided in the form of graduate teaching assistantship by the Department of Mechanical and Aerospace Engineering at Missouri University of Science and Technology is also gratefully acknowledged.

REFERENCES

(1) Aramcharoen, A. and Chuan S. K., 2014. "An experimental investigation on cryogenic milling of Inconel 718 and its sustainability assessment", International conference of high performance cutting, 14, 529-534.

(2) Che-Haron, C. H., 2001. "Tool life and surface integrity in the turning of Titanium alloy", journal of Materials Processing Technology, 118, 231-237.

(3) Dudzinski, D., Devillez, A., Moufki, A., Larrouquere, D., Zerrouki, V., Vigneau, J., 2012. "A Review of Developments towards dry and high speed machining of Inconel 718 alloy", International Journal of Machine Tools and Manufacture, 44, 439-456

(4) Ezugwu, E.O., and Wang, Z.M., 1997. "A review of Titanium alloys and their machinability", Journals of Materials processing technology, 262-274.

(5) Ezugwu, E. O., 2004. "High Speed Machining of aero-engine alloys", Journal of the Braz. Soc. of Mech. Sci. & Eng, 26, No 1.

(6) Jiang, X., Li, B., Yang, J., Zuo, X., Y., Li, K., 2012. "An approach for analyzing and controlling residual stress generation during high-speed circular milling", International journal for advanced manufacturing technology DOI 10.1007/s00170-012-4421-8.

(7) Jiann-Cherng, S., Young, A.K., Kong, M., Srivatsa, S., Morehouse, J.B., Liang, S.Y., 2012. "Modelling of residual stresses in milling", International Journal for advanced manufacturing technology, DOI 10.1007/s00170-0124211-3.

(8) Mhamdi, M-B., Bouljelbene M., Bayraktar, E., Zghal, A., 2012. "Surface integrity of titanium alloy Ti-6Al-4V in ball end-milling", International conference on solid state devices and materials sciences, 25, 355-362.

(9) Peng, R.L., Zhou, J., Johansson, S., Billenius, A., Bushlya, V., Stahl, J., 2013. "Surface integrity and the influence of Tool Wear in High-Speed machining of inconel 718, 13th international conference on fracture.

(10) Pinault, J. A., Belassel, M., Brauss, M.E., "X-ray diffraction residual stress measurement in failure analysis", Proto Manufacturing Limited, pp. 485-497.

(11) Rao, B., Dandekar, C. R., Shin, Y. C., 2011. "An experimental and numerical study on the face milling of Ti-6Al-4V alloy", Journal of Materials processing technology, 294- 304.

(12) Sasahara, H., 2005. "The effect on fatigue life of residual stress and surface hardness resulting from different cutting conditions of 0.45 % C Steel", International Journal of machine tools and manufacture, 45, 131-136.

(13) Shokrani, V., Dhokia, S.T., Newman, R., Imani-Asrai, R., Imani-Asrai, 2012. "An initial study of the effect of using liquid nitrogen coolant on the surface roughness of Inconel 718 nickel- based alloy in CNC milling", 45th CIRP conference on manufacturing systems, 3, 121-125.

(14) Sun, J., and Guo Y. B., 2009. "A comprehensive experimental study on surface integrity by end-milling Ti-6Al-4V", Journal of Materials Processing Technology, 209, 4036-4042.

(15) Thamizhmanii, S., Rosli, Hasan, S., 2009. "A study of minimum quantity lubrication on Inconel 718", Archives of materials science and technology, 39, 38-44.

(16) Ulutan, D., and Ozel, T., 2011. "Machining induced surface integrity in titanium and nickel alloys: A review", International Journal of Machine Tools and Manufacture, 51, 250-280.

(17) Umbrello, D., Micari, F., Jawahir, I. S., 2012. "The effects of cryogenic cooling on surface integrity in hard machining: A comparison with dry machining", CIRP Annals-manufacturing technology, 61, 103-106.

(18) Ying-lin, K.E., Gang, L., Ming, Z., Hui-Yue, D., 2009. "Use of Nitrogen gas in High-Speed Milling of Ti-6Al-4V", Transactions of non-ferrous Metals Society of China, 530-534.

(19) Zhang, Z., Chen, J. C., Kirby, E. D., 2007. "Surface roughness optimization in an end-milling operation using the taguchi design method", Journal of materials processing technology, 184, 233-239.

SECTION

2. CONCLUSIONS

From the results of the investigation, the following conclusions can be drawn:

1. The cutting force component F_y (feed force) is the most sensitive to tool wear, followed by the axial cutting force component (F_z), and are recommended for indirect monitoring of tool wear.

2. Cutting speed, interaction of cooling strategy and cutting speed are the significant factors affecting F_y, while cooling strategy, cutting speed, feed rate, and the interaction of cooling strategy and cutting speed are the significant factors affecting F_z.

3. High cutting speed and medium feed rate decrease cutting force components for sharp cutting flutes and moderate tool wear.

4. Cutting speed, feed rate and the interaction of cooling strategy and spindle speed are the significant factors affecting feed force, while cooling strategy, spindle speed, feed rate and interaction of cooling strategy and speed are the significant factors affecting F_z for intermediate or severe tool wear.

5. MQL+LN_2 and MQL cooling at high spindle speed of 750 rpm and a medium feed rate of 2 ipm are the optimum cooling strategy and machining parameters that gave the lowest cutting force components F_x, F_y, and F_z in slot end-milling Inconel 718 and are recommended for improving machinability of Inconel 718 with reference to cutting force components.

6. MQL+LN_2 cooling at low spindle speed (250 rpm) and low feed rate (1 ipm) are the optimum cooling strategy and machining parameters that gave the lowest tool wear, and are recommended for improving the machinability of Inconel 718 with reference to tool wear.

7. Cutting force component F_x was found to be consistently higher than cutting force components F_y and F_z for initial machining lengths, however, F_y always surpassed F_x to become the dominant cutting force component during severe tool wear.

8. Cutting force component F_z rises above F_y and Fx to become the dominant cutting force component during extreme tool wear and just before complete plastic deformation.

9. LN_2 cooling strategy at -15 ˚C gave the lowest workpiece temperature but the highest cutting force components compared to MQL and combined (MQL+LN_2).

10. Low spindle speed of 250 rpm (10 m/min) and high feed rate of 3 ipm (76.2 mm/min) gave the lowest workpiece cutting temperature.

11. High spindle speed of 750 rpm (30 m/min), and low feed rate of 1 ipm (25.4 mm/min) are recommended as optimum machining parameters, taking advantage of the low cutting force components (due to high speed) and low tool wear (due to low feed) for Inconel 718.

12. A comparative evaluation of the three cooling strategies at the recommended optimum machining parameters of 750 rpm (30 m/min) and 1 ipm (25.4 mm/min) shows that MQL generates the lowest cutting force components, followed by combined (MQL+LN_2) with the least being LN_2.

13. Comparative evaluation of cooling strategies shows that MQL and combined (MQL+LN_2) cooling strategies increase tool life by 25% compared to LN_2 cooling strategies.

14. Results obtained from analysis of variance show that cooling strategy, speed, and feed rates, as well as their 2-factor interactions all significantly affect surface roughness on the left rib. Furthermore, cooling strategy and feed rate significantly affect surface roughness on the web but not speed.

15. Low spindle speed (250 rpm) (10 m/min) gave the least surface roughness on the rib and the web, while high spindle speed (750 rpm) (30 m/min) gave the highest surface roughness on the rib and the web.

16. Low feed rate of 1 ipm (25.4 mm/min) is the best feed rate for reducing surface roughness on the rib and on the web, while high feed rate 3 ipm (76.2 mm/min) gave the highest surface roughness on the rib and web.

17. Combined (MQL+LN_2) cooling and MQL cooling strategies generates lower surface roughness values on the rib and web compared to LN_2 cooling strategy.

18. From the results of comparative evaluation of surface roughness, MQL and combined (MQL+LN_2) improve surface roughness on the left rib by 71.68% and 64.7% respectively compared to LN_2 cooling strategy.

19. MQL improved surface roughness on the left rib by approximately 20% compared to combined (MQL+LN_2).

20. LN2 produced a highly degraded surface finish on the web during high-speed slot end-milling of Inconel 718 and thus could not be measured. Whereas MQL and combined (MQL+LN_2) produced a very smooth finish on the web, with MQL performing slightly better than combined (MQL+LN_2) by 25%.

21. From the comparative evaluation with reference to residual stresses, MQL gave the best effect on residual stresses by inducing compressive stresses for every measured depth compared with combined (MQL+LN_2) and LN_2 cooling strategies which generates tensile residual stresses.

VITA

Chukwujekwu Ikwy Nnadi was born in Warri, Delta State, Nigeria. He received his Bachelor of Engineering degree from Nnamdi Azikiwe University Awka, Anambra state, Nigeria in July 2009. He has been enrolled in Mechanical Engineering at Missouri University of Science and Technology since August 2012, and has held a Graduate research assistant position under Dr. A. C. Okafor, and a Graduate Teaching assistantship in the Department of Mechanical and Aerospace Engineering department at Missouri University of Science and Technology. He received his Master's degree in December 2014.